A STUDY OF ACOUSTIC WAVE PROPAGATION WITHIN CURVED DUCTING SYSTEMS

by

Graham Douglas Furnell, B.Sc.(Hons.) (Adelaide)

Thesis submitted for the degree of
Doctor of Philosophy
at the University of Adelaide

Departments of Applied Mathematics
and Mechanical Engineering

March, 1989.

When once we have discovered the physical phenomena which constitute the foundation of sound, our explorations are in great measure transferred to another field lying within the dominion of the principles of Mechanics. Important laws are in this way arrived at, to which the sensations of the ear cannot but conform.

Lord Rayleigh 1878 *Theory of Sound.*

TABLE OF CONTENTS

ABSTRACT

In this thesis, a series of numerical methods are developed for determining the acoustic characteristics of fluid ducting systems which contain one or more bends. The ducting systems considered are assumed to contain a fluid which is essentially static, and to have walls which are either perfectly rigid or perfectly compliant.

The numerical methods are developed by firstly considering straight and uniformly curved ducts. Rectangular cross-sectioned ducts are analysed in some detail using standard analytical techniques. Variational principles are then called upon so that ducts of more general cross-section can be analysed by the Rayleigh-Ritz method. In an example, the acoustic modes within straight and uniformly curved ducts of elliptic cross-section are determined. The interesting observation is made that the acoustic modes within uniformly curved ducts appear to be radially biased versions of the modes within straight ducts. This bias is seen to be away from the centre of curvature of the duct's longitudinal axis for propagating modes, and towards this centre of curvature for non-propagating modes.

Next, the modal scattering characteristics of single sections of straight and uniformly curved duct are studied. A general method, which is based upon the Rayleigh-Ritz analysis used earlier, is presented so that modal scattering matrices for these sections of duct can be calculated. In an example, the modal scattering matrix of a section of uniformly curved, elliptic duct is calculated. Algorithms are then presented which combine the modal scattering matrices of the curved and straight sections in a multi-bend ducting system, to form a modal scattering matrix for the entire system. A method for determining the acoustic field within each section of duct is also presented, and out-of-plane and serpentine bends are considered.

Finally, acoustic wave propagation within non-uniformly curved ducts is considered. Two approaches to this problem are presented. In the first approach, the use of a generalised coordinate transformation is suggested. This transformation maps the curved axis of the duct onto a straight line, thus enabling the acoustic field to be determined by methods commonly used to analyse straight ducts. This approach is used in conjunction with the Galerkin method to calculate the modal scattering matrix of a section of spirally curved, rectangular duct. In the second approach, the non-uniformly curved duct is approximately represented by a series of uniformly curved duct segments. The acoustic characteristics of the duct are then determined with the aid of the previously derived scattering matrix algorithms. The modal scattering matrix of the section of spirally curved, rectangular duct considered earlier is calculated by this method, and comparisons are made. The effectiveness of the second approach is then further illustrated by using it to study the propagation of acoustic waves through sections of parabolically curved, elliptic and circular duct. Through the examples given, it is shown that acoustic waves maintain quasi-modal characteristics within non-uniformly curved ducts. It is also shown that higher order mode coupling effects within curved ducting systems are mainly caused by the presence of duct curvature discontinuities.

The thesis is concluded with a review of the work presented. A list which highlights the achievements of the thesis is also presented, and some suggestions for future research are made.

SIGNED STATEMENT

I declare that this thesis contains no material which has been accepted for the award of any other degree or diploma in any University and that, to the best of my knowledge and belief, contains no material previously published or written by another person, except where due reference is made in the text of the thesis.

I consent to this thesis being made available for photocopying and loan if applicable if accepted for the award of the degree.

G.D. Furnell

ACKNOWLEDGEMENTS

I wish to express my sincere thanks to Drs. D.A. Bies and P.M. Gill for the help and encouragement offered by them as supervisors during the course of this study. Thanks are also due to Dr. G.R. Haack for his assistance as a mentor.

During the period in which this research was carried out, I was fortunate enough to be financially supported in part by a research scholarship from The University of Adelaide, and a D.S.T.O. Research Scientist Cadetship.

CHAPTER 1

— ◇ —

INTRODUCTION

1.1 OPENING COMMENTS

When seeking solutions to the complex practical design problems posed by modern society, todays engineers have at their disposal three standard tools: analytical techniques, numerical methods and experimentation. Analytical techniques provide formulae which yield quick, easily interpreted solutions, but often place undue restrictions upon the physical characteristics of the problem being considered. Through experimentation, complete sets of data corresponding to particular physical situations can be obtained, but economic and test time limitations restrict the performance of large numbers of tests. In contrast to these, due to the increasing power and decreasing cost of available computing facilities, numerical methods enable engineers to consider a wide range of physical situations, and repeatedly obtain accurate results in a quick, cost-efficient manner. Thus, the development of numerical methods is now a topic of considerable importance in engineering science.

Problems which present a formidable challenge to any numerical method are those which are truly three-dimensional in nature. As we live in a three-dimensional world, such problems are often amongst those in most need of solution. Limits on computer memory size, processing time and machine precision must all be considered when developing the numerical methods used to solve them. A problem which typically displays these three-dimensional characteristics is that of studying acoustic wave propagation

within curved ducting systems. From a practical viewpiont, such studies arise when considering a wide variety of engineering situations. For example, it is often desirable to minimise the acoustic transmissivity of duct bends when designing air-conditioning, exhaust and various other ventilation and cooling systems. Alternatively, the determination of the phase velocity of these waves is a problem often considered in the field of underwater acoustics. Further applications include the design and analysis of acoustical delay lines and musical wind instruments. From an academic viewpoint, these studies are important as they represent a logical extension to the theory of acoustic wave propagation within straight ducts.

The principal aim of this thesis is to develop numerical methods for accurately determining the acoustic characteristics of curved ducting systems in a computationally efficient manner.

1.2 PREVIOUS RESEARCH

Historically, the theoretical study of acoustic wave propagation within ducts dates back to at least 1878, when the straight duct problem was considered by Lord Rayleigh [1]. Since then, the straight duct problem has been well researched, mainly because of its equivalence to the electromagnetic waveguide problem. Lord Rayleigh also considered the propagation of long wavelength acoustic waves within curved ducts. However, it was not until 1939 that the first substantial analysis of modal wave propagation within curved ducts was presented. Buchholz [2], using a Bessel function formulation, considered the propagation of electromagnetic [1] waves within sections of uniformly curved, rectangular waveguide. Although this formulation is in principle exact, the order of

[1] At this point, it is worth noting that the problems of acoustic and electromagnetic wave propagation within curved ducts are theoretically equivalent when the cross-section of the duct is rectangular. For other cross-sections however, this is not true.

the Bessel functions must be found by implicitly solving complicated transcendental equations. This (as Buchholz found) invariably places restrictions upon the attainable accuracy of the solution. Such complications are typical of those which arise when applying analytical techniques to the curved duct problem.

Since Buchholz, the problem of acoustic and electromagnetic wave propagation within uniformly curved, rectangular ducts has been extensively studied. Researchers have used a wide variety of methods to alleviate the inherent difficulties associated with this problem. These methods include those based upon: improved algorithms for determining the order of the Bessel functions [3–6], approximate theories for large and small curvature [7–9], high and low frequency limit cases [10,11], analyses that neglect non-propagating modes [12–15], and purely numerical schemes [16–18].

Studies concerning uniformly curved ducts with cross-sections other than rectangular have been considerably less prevalent than those above, and in general are limited to the case of a circular cross-section. Prikhod'ko and Tvutekin [19] briefly described some interesting results obtained by a small curvature, perturbation analysis. By considering wave propagation in the long wavelength limit, Keefe and Benade [20] were able to examine the acoustic properties of bends in musical wind instruments. However, the most substantial results have come from researchers using numerical methods. These are the surface element analysis of El-Raheb and Wagner [21], and the collocation approach of Firth and Fahy [22].

Not surprisingly, analyses of nonuniformly curved ducts have also been fairly scarce in the literature. Nevertheless, a number of interesting techniques have been used to analyse rectangular cross-sectioned ducts. Quine [23], using a numerical procedure based upon the theory of coupled modes, considered the propagation of electromagnetic waves in a sinusoidally curved duct. In an alternative approach, Bahar [24], and later Bahar and Govindarajan [25] showed that such problems could be more efficiently analysed

if the duct was considered to be comprised of a series of uniformly curved, differential segments. Finally, Ahluwalia, Keller and Matkowsky [26] used ray-optical techniques to study the propagation of high frequency, acoustic waves. The case of non-uniformly curved ducts having a cross-section more general than rectangular has been considered by Ting and Miksis [27], who have presented a formulation which is valid for slender ducts.

Upon leaving the topic of previous research in the field of curved duct acoustics, mention should be made of the work of El-Raheb [28, 29], and El-Raheb and Wagner [30]. The significance of these papers is that they seem to be the only publications which consider multi-modal wave propagation within ducting systems which contain more than one bend. In these papers, rectangular cross-sectioned ducting systems which contain sharp bends and bends of constant curvature are considered, however, the methods used are basically different to the ones which will be presented in this thesis.

1.3 OUTLINE OF THESIS

In Chapter 2, acoustic wave propagation within straight and uniformly curved ducts is considered. Due to their geometrical simplicity, ducts of rectangular cross-section are initially analysed, and a number of general observations are made about the nature of the acoustic field within them. The Rayleigh-Ritz method is then used in a numerical scheme which is suitable for analysing ducts of more general cross-section. The effectiveness of this scheme is illustrated by using it to analyse ducts of elliptic cross-section.

In general, the acoustic fields within the ducts considered in Chapter 2 take the form of a superposition of forward and backward travelling wave modes. In Chapter 3, the scattering of these wave modes within ducting systems which contain one or more bends is considered. The analysis begins with the definition of modal scattering matrices for

sections of straight and uniformly curved duct. A general method, which uses the theory of Chapter 2, is presented for calculating these matrices, and the modal scattering matrix of a section of uniformly curved, elliptic duct is calculated in an example. Algorithms are then presented which combine the modal scattering matrices of the curved and straight sections in a multi-bend ducting system, to form a modal scattering matrix for the entire system. A method for determining the acoustic field within each section of duct is also presented, and the effect of out-of-plane and serpentine bends upon the scattered modes is considered.

Acoustic wave propagation within non-uniformly curved ducts is considered in Chapter 4. Initially, two methods are presented for the analysis of rectangular cross-sectioned ducts. In the first method, a generalised coordinate transformation is used to map the interior region of the curved duct onto that of a straight duct. The Galerkin method is then used to obtain an approximate expression for the acoustic field in the form of a finite functional series. In an example, the first method is used to calculate the modal scattering matrix of a section of spirally curved duct. In the second method, the curved duct is approximately represented by a series of uniformly curved duct segments. The acoustic characteristics of the duct are then determined with the aid of the theory presented in Chapter 3. The modal scattering matrix of the section of spirally curved, rectangular duct considered earlier is calculated by this method, and comparisons are made. It is then suggested that the second method be used for the analysis of ducts having a more general cross-section. In a series of illustrative examples, this method is used to study the propagation of acoustic waves through sections of parabolically curved, elliptic and circular duct.

Chapter 5 concludes the thesis with a summary and review of the work presented. A discussion of the achievements of the thesis is also presented, and some suggestions for future research are made.

1.4 INTRODUCTORY THEORY

The physical characteristics of the ducts considered in this thesis are taken to be the same as those assumed by many of the previous researchers. That is, the fluid within the duct is assumed to be essentially static, with homogeneous properties such that sound propagates through it at a constant velocity, v. Also, the duct walls are assumed to have idealised properties corresponding to them being either perfectly rigid or perfectly compliant.

The problem of determining the acoustic field within such ducts can be reduced to that of solving the Helmholtz Wave Equation

$$\nabla^2\Phi + k^2\Phi = 0 \tag{1.1}$$

throughout the duct, subject to either one of the wall conditions

$$\frac{\partial\Phi}{\partial\underline{n}} = 0 \tag{1.2}$$

or

$$\Phi = 0. \tag{1.3}$$

Here Φ is the acoustic potential, $\underline{n}$ a vector normal to the duct wall and k the wavenumber.

Equation (1.1) was obtained by following the usual practice of assuming a harmonic time dependence of the form $\exp(-i\omega t)$ for all variables in the equations of motion of the duct fluid. It follows that k is related to the angular frequency ω by the equation $k = \omega/v$. k is also related to the free-space wavelength of the acoustic disturbance χ by the equation $k = 2\pi/\chi$. The spatial components of the acoustic particle velocity $\underline{q}$ and pressure p are obtained from the acoustic potential via the relations

$$\underline{q} = -\nabla\Phi \tag{1.4}$$

and

$$p = -i\omega\rho_0\Phi, \tag{1.5}$$

where ρ_0 is the mean density of the duct fluid, and it is understood that only the real part of the variables are considered. Typically, the frequency range considered when performing the analyses presented in this thesis will be such that the cross-sectional dimensions of the duct are of the same order of magnitude as the free-space wavelength χ.

For convenience, solutions to equation (1.1) subject to the homogeneous Neumann wall condition (1.2) will be referred to as N-modes. Similarly, solutions to equation (1.1) subject to the homogeneous Dirichlet wall condition (1.3) will be referred to as D-modes. Equation (1.4) shows that the N-mode solutions describe acoustic waves within perfectly rigid ducts — such as those constructed of metal or other impervious material. Equation (1.5) shows that the D-mode solutions describe acoustic waves within perfectly compliant or pressure release ducts — such as those constructed of a thin membraneous material or bounded by a free surface.

CHAPTER 2

— ◇ —

ACOUSTIC WAVE PROPAGATION WITHIN STRAIGHT AND UNIFORMLY CURVED DUCTS

2.1 INTRODUCTION AND PROBLEM FORMULATION

In this chapter, the characteristics of acoustic waves within straight and uniformly curved ducts are examined. It will be shown that general solutions to equations (1.1)–(1.3) within these ducts take the convenient form of a superposition of exponentially modulated modes, with the modes and modulation parameters being determined by solving two-dimensional eigenvalue problems over the duct cross-section. Though solving these eigenvalue problems is not an easy task (especially for uniformly curved ducts), the fact that they are two-dimensional means that the task of determining the acoustic wave field throughout the duct has been considerably simplified. Later, in Chapter 4, it will be seen that there are significant advantages to be gained by exploiting this simplification when considering non-uniformly curved ducts.

2.1.1 Straight ducts

Consider solving equations (1.1)–(1.3) within the straight duct shown in Figure 2.1. The acoustic potential $\Phi^{(s)}$, which specifies the wave field within this duct, is conveniently

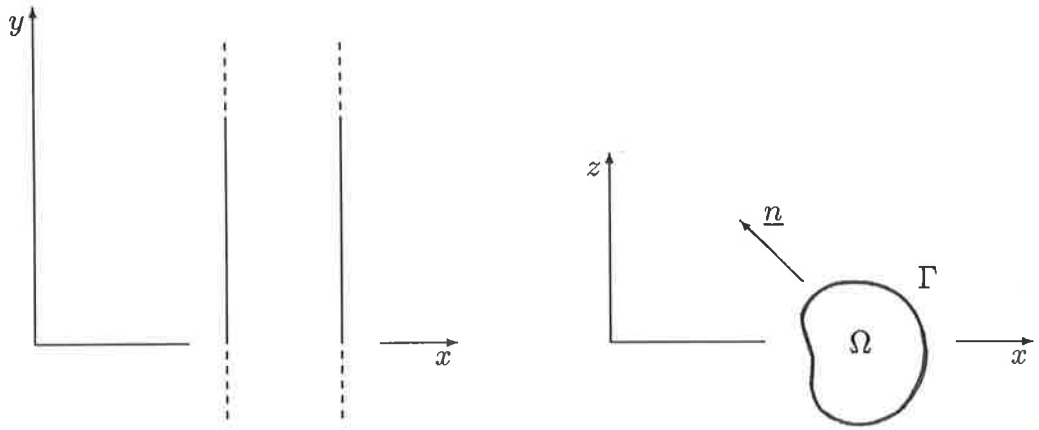

Figure 2.1: *Top and cross-sectional views of a straight duct.*

expressed with respect to the rectangular Cartesian coordinates (x, y, z) shown. Thus $\Phi^{(s)}$ satisfies

$$\frac{\partial^2\Phi^{(s)}}{\partial x^2} + \frac{\partial^2\Phi^{(s)}}{\partial y^2} + \frac{\partial^2\Phi^{(s)}}{\partial z^2} + k^2\Phi^{(s)} = 0 \tag{2.1}$$

throughout the duct. Due to the invariance of the duct cross-section Ω with respect to the y-coordinate, and the separable nature of equation (2.1), $\Phi^{(s)}$ may be written in the form

$$\Phi^{(s)} = \phi(x, z)e^{\pm i\mu y}. \tag{2.2}$$

Substituting equation (2.2) into equations (2.1) and (1.2) or (1.3) yields the following eigenvalue problem for μ^2 and ϕ, namely:

$$\frac{\partial^2\phi}{\partial x^2} + \frac{\partial^2\phi}{\partial z^2} + (k^2 - \mu^2)\phi = 0 \tag{2.3}$$

within Ω, such that

$$\left.\frac{\partial\phi}{\partial\underline{n}}\right|_\Gamma = 0 \tag{2.4}$$

for N-modes, or

$$\phi|_\Gamma = 0 \tag{2.5}$$

for D-modes. Solving equations (2.3) and (2.4) or (2.5) yields a doubly infinite set of eigenvalues μ_{mn}^2 and eigenfunctions ϕ_{mn}; $m, n = 1, 2, 3...$ Finally, the linearity of

equations (1.1)–(1.3) allow a general expression for $\Phi^{(s)}$ to be written as a superposition of modes of the form suggested in equation (2.2). That is

$$\Phi^{(s)}(x,y,z) = \sum_{m=1}^{\infty}\sum_{n=1}^{\infty}\left[\sigma_{mn}e^{i\mu_{mn}y} + \rho_{mn}e^{-i\mu_{mn}y}\right]\phi_{mn}(x,z). \tag{2.6}$$

Here the σ_{mn} and ρ_{mn} are interpreted as being the complex amplitudes of modes associated with waves propagating in the $\pm y$ directions respectively. Hence, a successful analysis of acoustic waves within straight ducts is based upon one's ability to solve equations (2.3)–(2.5), and choose appropriate values of the modal coefficients σ_{mn} and ρ_{mn}.

2.1.2 Uniformly curved ducts

Now consider solving equations (1.1)–(1.3) within the uniformly curved duct shown in Figure 2.2. The acoustic potential $\Phi^{(c)}$, which specifies the wave field within this duct, is conveniently expressed with respect to the cylindrical polar coordinates (r,θ,z) shown.

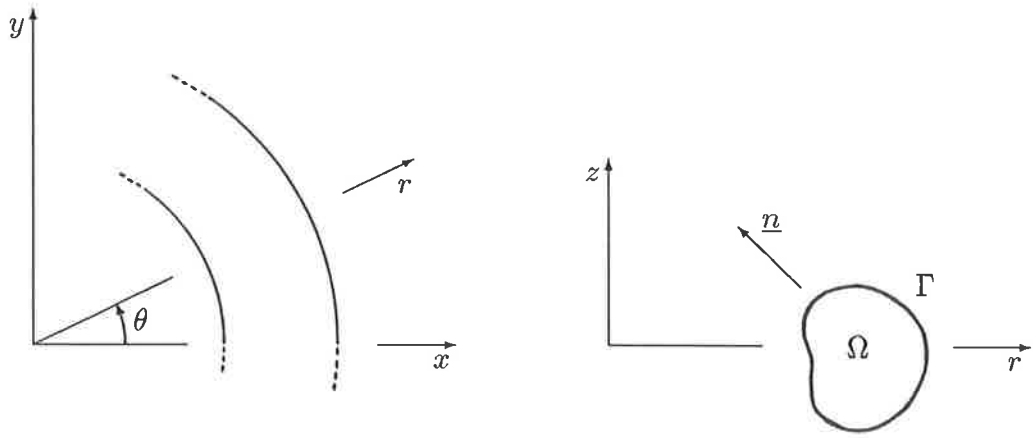

Figure 2.2: *Top and cross-sectional views of a uniformly curved duct.*

Thus $\Phi^{(c)}$ satisfies

$$\frac{\partial^2\Phi^{(c)}}{\partial r^2}+\frac{1}{r}\frac{\partial\Phi^{(c)}}{\partial r}+\frac{1}{r^2}\frac{\partial^2\Phi^{(c)}}{\partial\theta^2}+\frac{\partial^2\Phi^{(c)}}{\partial z^2}+k^2\Phi^{(c)}=0 \tag{2.7}$$

throughout the duct. Due to the invariance of the duct cross-section Ω with respect to the θ-coordinate, and the separable nature of equation (2.7), $\Phi^{(c)}$ may be written in the form

$$\Phi^{(c)}=\psi(r,z)e^{\pm i\nu\theta}. \tag{2.8}$$

Substituting equation (2.8) into equations (2.7) and (1.2) or (1.3) yields the following eigenvalue problem for ν^2 and ψ, namely:

$$\frac{\partial^2\psi}{\partial r^2}+\frac{1}{r}\frac{\partial\psi}{\partial r}+\frac{\partial^2\psi}{\partial z^2}+(k^2-\nu^2/r^2)\psi=0 \tag{2.9}$$

within Ω, such that

$$\left.\frac{\partial\psi}{\partial\underline{n}}\right|_\Gamma=0 \tag{2.10}$$

for N-modes, or

$$\psi|_\Gamma=0 \tag{2.11}$$

for D-modes. Solving equations (2.9) and (2.10) or (2.11) yields a doubly infinite set of eigenvalues ν_{mn}^2 and eigenfunctions $\psi_{mn}(x,z)$; $m,n=1,2,3,\ldots$ Finally, as with the straight duct, the linearity of equations (1.1)–(1.3) allow a general expression for $\Phi^{(c)}$ to be written as a superposition of modes of the form suggested in equation (2.8). That is

$$\Phi^{(c)}(r,\theta,z)=\sum_{m=1}^{\infty}\sum_{n=1}^{\infty}\left[\alpha_{mn}e^{i\nu_{mn}\theta}+\beta_{mn}e^{-i\nu_{mn}\theta}\right]\psi_{mn}(r,z). \tag{2.12}$$

Here the α_{mn} and β_{mn} are interpreted as being the complex amplitudes of modes associated with waves propagating in the $\pm\theta$ directions respectively. Hence, a successful analysis of acoustic waves within uniformly curved ducts is based upon one's ability to solve equations (2.9)–(2.11), and choose appropriate values of the modal coefficients α_{mn} and β_{mn}.

2.1.3 Orthogonality of the modes

A property of the modes which often enables their coefficients to be conveniently determined is that of orthogonality. It follows from equations (2.3)–(2.5) and (2.9)–(2.11) that, subject to appropriate normalisations, the eigenfunctions ϕ_{mn} and ψ_{mn} satisfy the orthogonality relations

$$\iint_{\Omega} \phi_{mn}\phi_{pq}\, dx\, dz = \delta_{mp}\delta_{nq} \tag{2.13}$$

and

$$\iint_{\Omega} \frac{1}{r}\psi_{mn}\psi_{pq}\, dr\, dz = \delta_{mp}\delta_{nq}, \tag{2.14}$$

where

$$\delta_{mn} = \begin{cases} 1 & \text{if } m = n \\ 0 & \text{if } m \neq n. \end{cases} \tag{2.15}$$

As an example of the use of these orthogonality relations, consider acoustic waves propagating in the $+\theta$ direction down a uniformly curved duct when the wave field is specified at the entrance ($\theta = 0$), to the duct. That is, for a given function $F(r, z)$, suppose

$$\Phi^{(c)}(r, 0, z) = \sum_{m=1}^{\infty}\sum_{n=1}^{\infty} \alpha_{mn}\psi_{mn}(r, z) = F(r, z). \tag{2.16}$$

Multiplying through equation (2.16) by $\psi_{pq}(r, z)/r$, integrating over the duct cross-section Ω, and then using equation (2.14) yields

$$\alpha_{pq} = \iint_{\Omega} \frac{1}{r}F\psi_{pq}\, dr\, dz. \tag{2.17}$$

Hence, the acoustic field throughout the duct is expressed in terms of the known entrance function $F(r, z)$.

2.1.4 Energy transmission

In general, the mean (time averaged) power flux associated with a simple time-harmonic acoustic field at any point is given by the mean acoustic intensity vector

$$\underline{J} = \frac{1}{2}\Re\left\{p\underline{q}^*\right\}, \tag{2.18}$$

where the asterisk denotes complex conjugation. Equation (2.18), when combined with equations (1.2)–(1.5), shows that for ducts of the type considered in this thesis, no power will flow into the duct walls. Hence, acoustic energy will be conserved within these ducts, with a net power flow only occurring in a longitudinal direction down the duct. The total mean power flow within the duct is therefore obtained by integrating the longitudinal component of $\underline{J}$ over the duct's cross-section.

We now calculate the total mean power flow associated with a wave field which is propagating in the $+y$ direction down a straight duct. From equation (2.6), the acoustic potential which specifies this wavefield is

$$\Phi^{(s)}(x,y,z) = \sum_{m=1}^{M}\sum_{n=1}^{N}\sigma_{mn}e^{i\mu_{mn}y}\phi_{mn}(x,z) + \sum_{m=M+1}^{\infty}\sum_{n=N+1}^{\infty}\sigma_{mn}e^{-\mu_{mn}y}\phi_{mn}(x,z), \tag{2.19}$$

where non-propagating "evanescent modes" (whose corresponding eigenvalues, μ_{mn}^2, are negative) appear explicitly in the second summation. Non-propagating modes with a positive exponential y-coordinate dependence are excluded from equation (2.19) due to the requirement that each mode should be finite throughout the duct. Using equations (1.4) and (1.5) in conjunction with equation (2.18), the y-component of the mean acoustic intensity vector is found to be

$$J_y = \frac{\omega\rho_0}{2}\Re\left\{i\Phi^{(s)}\frac{\partial\Phi^{(s)^*}}{\partial y}\right\}. \tag{2.20}$$

Substituting equation (2.19) into equation (2.20), integrating the resulting expression over the duct's cross-section and using the orthogonality relation (2.13) finally yields

the total mean acoustic power

$$W^{(s)} = \frac{\omega \rho_0}{2} \sum_{m=1}^{M} \sum_{n=1}^{N} \mu_{mn} |\sigma_{mn}|^2. \tag{2.21}$$

In a similar manner, the total mean acoustic power associated with a wave field which is propagating in the $+\theta$ direction down a uniformly curved duct can be shown to be

$$W^{(c)} = \frac{\omega \rho_0}{2} \sum_{m=1}^{M} \sum_{n=1}^{N} \nu_{mn} |\alpha_{mn}|^2. \tag{2.22}$$

Equations (2.21) and (2.22) define power spectra for wavefields propagating within straight and uniformly curved ducts, with each term in the summations specifying the relative proportion of power allocated to a particular mode. Note that evanescent modes do not contribute to these spectra. Basically, this is because the ducts are assumed to be of infinite extent. However, if one considers the presence of discontinuities within the ducts, evanescent modes can make significant contributions to the transfer of energy between modes in the vicinity of these discontinuities. This transfer of energy occurs in a way which is analogous to the Quantum Mechanical description of the penetration of a barrier potential by a particle.

2.1.5 Variational formulation

An alternative definition of the acoustic modes within straight and uniformly curved ducts follows from the theory of the calculus of variations. According to this theory [31], the eigenvalues and eigenfunctions of equations (2.3)–(2.5) and (2.9)–(2.11) determine the stationary values of the quadratic functionals

$$I^{(s)}(\phi) = \iint_{\Omega} \left[\left(\frac{\partial \phi}{\partial x} \right)^2 + \left(\frac{\partial \phi}{\partial z} \right)^2 - (k^2 - \mu^2)\phi^2 \right] dx\, dz \tag{2.23}$$

and

$$I^{(c)}(\psi) = \iint_{\Omega} r \left[\left(\frac{\partial \psi}{\partial r} \right)^2 + \left(\frac{\partial \psi}{\partial z} \right)^2 - (k^2 - \nu^2/r^2)\psi^2 \right] dr\, dz \tag{2.24}$$

respectively. Posing the eigenvalue problems in this way can be useful as it allows a number of so-called "direct" methods to be used to determine approximate series solutions. In particular, there is the Rayleigh-Ritz method, which will be used in the numerical solution procedure presented in section 2.3.

2.2 ANALYTIC SOLUTIONS

One of the major factors limiting the effective use of analytical techniques for determining the acoustic potential within uniformly curved ducts is the fact that equation (2.9) is only separable in its present form. Therefore, analytic solutions to equations (2.9)–(2.11) can only readily be obtained when the duct cross-section is rectangular, with the walls being defined by equations of the form $r = const.$ and $z = const.$ For this reason, only ducts having a rectangular cross-section of the form shown in Figure 2.3 will be considered in this section. By examining the analytic solutions to equations

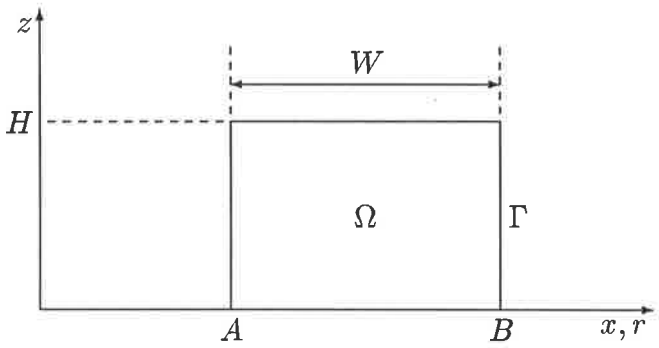

Figure 2.3: *Cross-sectional geometry of the straight and uniformly curved ducts analysed by analytical techniques.*

(2.3)–(2.5) and (2.9)–(2.11) within these ducts, a qualitative appreciation of some general characteristics of acoustic waves within straight and uniformly curved ducts can be obtained. These characteristics will later be observed in the numerical solutions presented in section 2.3.

2.2.1 Exact solutions

Separating variables, one finds that the required solutions to equations (2.3)–(2.5) are

$$\phi(x,z) = X(x)Z(z) \tag{2.25}$$

where for $m, n = 1, 2, 3, \ldots$

$$X(x) = \begin{cases} \cos\left[\frac{(m-1)\pi(x-A)}{W}\right] & \text{for } N\text{-modes} \\ \sin\left[\frac{m\pi(x-A)}{W}\right] & \text{for } D\text{-modes} \end{cases} \tag{2.26}$$

and

$$Z(z) = \begin{cases} \cos\left[\frac{(n-1)\pi z)}{H}\right] & \text{for } N\text{-modes} \\ \sin\left[\frac{n\pi z)}{H}\right] & \text{for } D\text{-modes.} \end{cases} \tag{2.27}$$

Equations (2.26) and (2.27) imply that the straight duct eigenvalues are

$$\mu_{mn}^2 = \begin{cases} k^2 - \left[\frac{(m-1)\pi}{W}\right]^2 - \left[\frac{(n-1)\pi}{H}\right]^2 & \text{for } N\text{-modes} \\ k^2 - \left[\frac{m\pi}{W}\right]^2 - \left[\frac{n\pi}{H}\right]^2 & \text{for } D\text{-modes.} \end{cases} \tag{2.28}$$

Similarly, one finds that the required solutions to equations (2.9)–(2.11) are

$$\psi(r,z) = R(r)Z(z). \tag{2.29}$$

Here, ν^2 and $R(r)$ satisfy the one-dimensional eigenvalue problem:

$$r^2R'' + rR' + (r^2\lambda^2 - \nu^2)R = 0 \tag{2.30}$$

within $[A, B]$, such that

$$R'|_{r=A,B} = 0 \tag{2.31}$$

for N-modes,

$$R|_{r=A,B} = 0 \tag{2.32}$$

for D-modes, and where

$$\lambda^2 = \begin{cases} k^2 - \left[\frac{(n-1)\pi}{H}\right]^2 & \text{for } N\text{-modes} \\ k^2 - \left[\frac{n\pi}{H}\right]^2 & \text{for } D\text{-modes.} \end{cases} \tag{2.33}$$

Equation (2.30) is recognised as being Bessel's equation of order ν, which has solutions of the form

$$R(r) = J_\nu(\lambda r) + (const.)Y_\nu(\lambda r) \tag{2.34}$$

where J_ν and Y_ν are Bessel functions of the first and second kind respectively. Applying the boundary conditions (2.31) and (2.32) to expression (2.34) finally yields

$$R(r) = \begin{cases} J_\nu(\lambda r) - [J'_\nu(\lambda A)/Y'_\nu(\lambda A)]Y_\nu(\lambda r) & \text{for } N\text{-modes} \\ J_\nu(\lambda r) - [J_\nu(\lambda A)/Y_\nu(\lambda A)]Y_\nu(\lambda r) & \text{for } D\text{-modes.} \end{cases} \tag{2.35}$$

The orders of the Bessel functions are infinite in number, and are given by the real and imaginary roots of the characteristic equation $F(\nu) = 0$, where

$$F(\nu) = \begin{cases} J'_\nu(\lambda A)Y'_\nu(\lambda B) - J'_\nu(\lambda B)Y'_\nu(\lambda A) & \text{for } N\text{-modes} \\ J_\nu(\lambda A)Y_\nu(\lambda B) - J_\nu(\lambda B)Y_\nu(\lambda A) & \text{for } D\text{-modes.} \end{cases} \tag{2.36}$$

So it is seen that there are indeed doubly infinite sets of solutions to equations (2.3)–(2.5) and (2.9)–(2.11) within straight and uniformly curved, rectangular ducts. The solutions within straight ducts are easily calculated and interpreted. Equations (2.25)–(2.27) show that the straight duct eigenfunctions take the form of regularly spaced crests and troughs over the duct cross-section, the number of crests and troughs increasing with m and n. Also, equation (2.28) shows that $\mu_{mn}^2 \leq k^2$, and when m and n are such that $\mu_{mn}^2 \leq 0$, equation (2.6) shows that the corresponding straight duct modes will be evanescent. Finally, one can verify the orthogonality relation (2.13) without difficulty using well known properties of trigonometric functions. However, due to the

complicated nature of $R(r)$, the solutions within uniformly curved ducts are not easily calculated or interpreted. In order to obtain a clearer view of the behaviour of $R(r)$, solutions to equations (2.30)–(2.32) will now be re-derived in circumstances where the duct curvature can be considered to be "small".

2.2.2 Slightly curved ducts

Expressing equations (2.30)–(2.32) with respect to the new variable u, defined by the equation

$$r = A + Wu, \tag{2.37}$$

yields the following one-dimensional eigenvalue problem for β^2 and $R(u)$, namely:

$$(1+\epsilon u)^2 R'' + \epsilon(1+\epsilon u)R' + [(1+\epsilon u)^2\alpha^2 - \beta^2]R = 0 \tag{2.38}$$

within $[0,1]$, such that

$$R'|_{u=0,1} = 0 \tag{2.39}$$

for N-modes,

$$R|_{u=0,1} = 0 \tag{2.40}$$

for D-modes, and where

$$\epsilon = W/A, \quad \alpha = W\lambda, \quad \beta = W\nu/A. \tag{2.41}$$

For slightly curved ducts $\epsilon \ll 1$, and when $\epsilon = 0$, equations (2.38)–(2.40) reduce to those describing acoustic waves within straight ducts. Hence, approximate expressions for β^2 and $R(u)$ may be sought in the form of perturbation series expansions with respect to the small parameter ϵ. Therefore let

$$R(u) = R_0(u) + \epsilon R_1(u) + \epsilon^2 R_2(u) + \ldots \tag{2.42}$$

and

$$\beta^2 = \beta_0^2 + \epsilon\beta_1^2 + \epsilon^2\beta_2^2 + \ldots \tag{2.43}$$

Substituting expressions (2.42) and (2.43) into equations (2.38)–(2.40) and equating powers of ϵ yields:

For powers of ϵ^0

$$\begin{aligned} R_0'' + (\alpha^2 - \beta_0^2)R_0 &= 0; \\ R_0'(0) = R_0'(1) &= 0 \quad \text{for } N\text{-modes}, \\ R_0(0) = R_0(1) &= 0 \quad \text{for } D\text{-modes}. \end{aligned} \tag{2.44}$$

For powers of ϵ^1

$$\begin{aligned} R_1'' + (\alpha^2 - \beta_0^2)R_1 = (\beta_1^2 - 2\alpha^2 u)R_0 - R_0' - 2uR_0''; \\ R_1'(0) = R_1'(1) &= 0 \quad \text{for } N\text{-modes}, \\ R_1(0) = R_1(1) &= 0 \quad \text{for } D\text{-modes}. \end{aligned} \tag{2.45}$$

For powers of ϵ^2

$$\begin{aligned} R_2'' + (\alpha^2 - \beta_0^2)R_2 = (\beta_1^2 - 2\alpha^2 u)R_1 - R_1' - 2uR_1'' \\ +(\beta_2^2 - \alpha^2 u^2)R_0 - uR_0' - u^2 R_0''; \\ R_2'(0) = R_2'(1) &= 0 \quad \text{for } N\text{-modes}, \\ R_2(0) = R_2(1) &= 0 \quad \text{for } D\text{-modes}. \end{aligned} \tag{2.46}$$

Though the algebra becomes quite complicated, equations (2.44)–(2.46) can be solved by standard techniques to yield the following expressions for $R_0(u), \ldots R_2(u)$ and $\beta_0^2, \ldots \beta_2^2$. They are:

$$R_0(u) = \begin{cases} \cos(\gamma u) & \text{for } N\text{-modes} \\ \sin(\gamma u) & \text{for } D\text{-modes}, \end{cases} \tag{2.47}$$

$$\beta_0^2 = \alpha^2 - \gamma^2 \tag{2.48}$$

where

$$\gamma = \begin{cases} (m-1)\pi & \text{for } N\text{-modes} \\ m\pi & \text{for } D\text{-modes} \end{cases} \tag{2.49}$$

and $m = 1, 2, 3, \ldots$

For N-modes when $m = 1$, because $R_0(u) = 1$, we have

$$
\begin{aligned}
R_1(u) &= \alpha^2 \left(\frac{u^2}{2} - \frac{u^3}{3} \right), && (2.50)\\
\beta_1^2 &= \alpha^2, && (2.51)\\
R_2(u) &= \frac{\alpha^2}{12} \left(1 + \frac{\alpha^2}{5} \right) u^2 - \frac{\alpha^2}{2} u^3 + \frac{\alpha^2}{12} \left(4 + \frac{\alpha^2}{2} \right) u^4 - \frac{\alpha^4}{15} u^5 + \frac{\alpha^4}{45} u^6, && (2.52)\\
\beta_2^2 &= \frac{\alpha^2}{6} \left(1 + \frac{\alpha^2}{5} \right). && (2.53)
\end{aligned}
$$

Otherwise

$$
\begin{aligned}
R_1(u) &= p_1(u) R_0(u) + q_1(u) R_0'(u), && (2.54)\\
\beta_1^2 &= \beta_0^2, && (2.55)\\
R_2(u) &= p_2(u) R_0(u) + q_2(u) R_0'(u), && (2.56)\\
\beta_2^2 &= \begin{cases} -\frac{\alpha^4}{12\gamma^4}(\gamma^2 + 21) + \frac{\alpha^2}{6\gamma^2}(\gamma^2 + 6) - \frac{\gamma^2}{12} & \text{for } N\text{-modes} \\ -\frac{\alpha^4}{12\gamma^4}(\gamma^2 - 15) + \frac{\alpha^2}{6\gamma^2}(\gamma^2 - 6) - \frac{\gamma^2}{12} & \text{for } D\text{-modes} \end{cases} && (2.57)
\end{aligned}
$$

where

$$
\begin{aligned}
p_1(u) &= -\frac{\alpha^2}{2\gamma^2} u,\\
q_1(u) &= \frac{\beta_0^2}{2\gamma^2}(u^2 - u) + \delta,\\
p_2(u) &= a u^4 + b u^3 + c u^2 + d u,\\
q_2(u) &= e u^3 + f u^2 + g u + h && (2.58)
\end{aligned}
$$

and

$$
\begin{aligned}
a &= -\frac{\beta_0^4}{8\gamma^2},\\
b &= \frac{\beta_0^4}{4\gamma^2},\\
e &= \frac{2}{\gamma^2} a - \frac{\beta_0^2}{6\gamma^2} \left(\frac{7}{2} + \frac{\alpha^2}{\gamma^2} \right),
\end{aligned}
$$

$$
\begin{aligned}
f &= \frac{3}{2\gamma^2}b - \frac{\beta_0^2}{8\gamma^2}\left(5+\frac{\alpha^2}{\gamma^2}\right), \\
c &= -\frac{3}{2}e + \frac{1}{8\gamma^2}\left(4\gamma^2(1-\beta_0^2\delta) - \alpha^2 - \beta_0^4\right), \\
d &= -f + \frac{\beta_0^2}{2}\left(\delta + \frac{1}{2\gamma^2}\right), \\
g &= \frac{1}{\gamma^2}c - \frac{1}{2\gamma^2}\left(\beta_2^2 + \frac{\alpha^2}{2\gamma^2} + \gamma^2\delta\right), \\
h &= \begin{cases} (1/\gamma^2)d & \text{for } N\text{-modes} \\ 0 & \text{for } D\text{-modes,} \end{cases} \\
\delta &= \begin{cases} -\alpha^2/(2\gamma^4) & \text{for } N\text{-modes} \\ 0 & \text{for } D\text{-modes.} \end{cases}
\end{aligned}
\tag{2.59}
$$

Substituting equations (2.47)–(2.59) back into equations (2.42) and (2.43) enables $O(\epsilon^2)$ approximate expressions for $R(u)$ and β^2 to be formed.

Using the perturbation series expansions for β^2, the following approximate expressions for the eigenvalues of equations (2.30)–(2.32) can be obtained. They are:

$$
\nu^2 = A^2\lambda^2\left(1+\tfrac{W}{A}\right) + \tfrac{W^2\lambda^2}{30}(W^2\lambda^2+5) \tag{2.60}
$$

for the fundamental ($m=1$) N-mode,

$$
\begin{aligned}
\nu^2 = {} & A^2\left(\lambda^2 - \left[\tfrac{(m-1)\pi}{W}\right]^2\right)\left(1+\tfrac{W}{A}\right) \\
& -\tfrac{1}{12}\left((m-1)^2\pi^2 - 2\left[\tfrac{W\lambda}{(m-1)\pi}\right]^2[(m-1)^2\pi^2+6] + \left[\tfrac{W\lambda}{(m-1)\pi}\right]^4[(m-1)^2\pi^2+21]\right)
\end{aligned}
\tag{2.61}
$$

for the higher order ($m=2,3,4,\ldots$) N-modes, and

$$
\begin{aligned}
\nu^2 = {} & A^2\left(\lambda^2 - \left[\tfrac{m\pi}{W}\right]^2\right)\left(1+\tfrac{W}{A}\right) \\
& -\tfrac{1}{12}\left(m^2\pi^2 - 2\left[\tfrac{W\lambda}{m\pi}\right]^2[m^2\pi^2-6] + \left[\tfrac{W\lambda}{m\pi}\right]^4[m^2\pi^2-15]\right)
\end{aligned}
\tag{2.62}
$$

for the ($m=1,2,3,\ldots$) D-modes; where the second term in each of these equations is of $O(\epsilon^2)$. Looking at equations (2.60)–(2.62), if the $O(\epsilon^2)$ terms are neglected, one can see

that the straight and curved duct eigenvalues are approximately proportional so that

$$\nu_{mn} \approx A(1 + W/A)^{\frac{1}{2}} \mu_{mn} \approx (A + W/2)\, \mu_{mn}, \tag{2.63}$$

where the μ_{mn} are defined by equation (2.28). Thus, the well known centreline radius approximation for the curved duct propagation constants is obtained. It follows from this observation that there will approximately be a one-to-one correspondence between the modes in the straight and curved ducts. Also, if a straight duct mode propagates and is not near "cut-off" (i.e. $\mu = 0$), then the corresponding curved duct mode will also propagate. These observations are illustrated in Table 2.1, where approximate and exact values of the first six curved duct, N-mode propagation constants are presented when $\lambda = 4\pi$, $W = 1.0$ and $\epsilon = W/A = 0.2, 0.1$. The values of $(A + W/2)\mu$ in Table

$\epsilon = 0.2$			$\epsilon = 0.1$		
$(A + W/2)\mu$	$O(\epsilon^2)$ ν	Exact ν	$(A + W/2)\mu$	$O(\epsilon^2)$ ν	Exact ν
69.11	74.80	72.02	132.0	135.0	134.1
66.92	61.84	65.10	127.8	125.2	126.1
59.85	59.16	59.11	114.2	113.9	113.9
45.72	45.44	45.43	87.28	87.13	87.13
0.000	0.8660i	0.8657i	0.000	0.8660i	0.8659i
51.83i	51.65i	51.65i	98.96i	98.86i	98.86i

Table 2.1: *Approximate and exact values of ν for N-modes when $\lambda = 4\pi$, $W = 1.0$, $\epsilon = 0.2, 0.1$ and $m = 1, \ldots 6$.*

2.1 show that, except for the mode at cut-off, if the m^{th} straight duct mode propagates, then so will the m^{th} curved duct mode. Also, as expected, one can see that ν is more accurately approximated when ϵ is small. However, notice how the $O(\epsilon^2)$ values of ν are

less accurate when the mode number m is small. This characteristic of the perturbation solution means that the greatest errors will be present in the dominant eigenvalues. Further, if λ (and therefore the acoustic frequency ω) is increased, these errors will become more pronounced. Hence, the perturbation solution will not accurately predict the dominant eigenvalues at high frequencies, especially when the duct is more than slightly curved. Here, a frequency is assumed to be "high" when it is such that many modes can propagate within the duct.

Now the perturbation series expansions for $R(u)$ are considered. In general, they are of the form $R(u) = p(u)R_0(u)+q(u)R_0'(u)$, where $R_0(u)$ is a solution of the straight duct eigenvalue problem, and $p(u)$ and $q(u)$ are polynomials whose behaviour is such that $p(u) \to 1$ and $q(u) \to 0$ as $\epsilon \to 0$. Hence, the analysis indicates that the eigenfunctions within the straight and slightly curved ducts will have similar physical characteristics, with the differences being governed by the behaviour of the modulating polynomials $p(u)$ and $q(u)$. Plots showing some typical characteristics of $R(u)$ appear in Figures 2.4–2.6. In Figure 2.4, the plots show how the fundamental $m = 1$, N-mode eigenfunction becomes increasingly biased towards the outer wall of the duct as ϵ, and therefore the curvature of the duct, is increased. Figures 2.5 and 2.6 show how the higher order N-mode eigenfunctions are also biased, but more towards the inner wall of the duct as the mode number m is increased. Notice how the $m = 3$ mode in Figure 2.5 is quite close to cut-off and has essentially no bias. This feature is typical of modes near cut-off, and suggests that in general, propagating modes will be biased towards the outer wall of a curved duct and evanescent modes will be biased towards the inner wall of a curved duct — the degree of bias being greater the further the mode is from cut-off. Unfortunately, due to the limitations of the perturbation solution, it is not possible to provide examples which show greater evidence of the bias just described. However, with the aid of the numerical solution procedure to be presented in the next section, this will be possible.

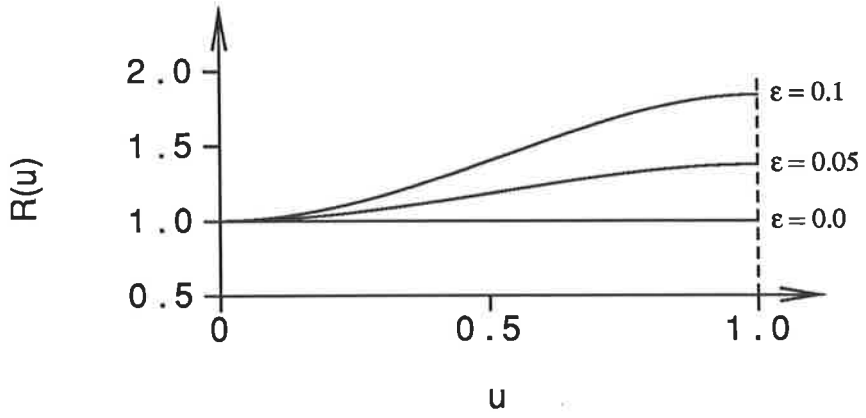

Figure 2.4: *Plots of the m = 1 N-mode eigenfunction;* $\alpha = 2\pi$; $\varepsilon = 0.0, 0.05, 0.1$.

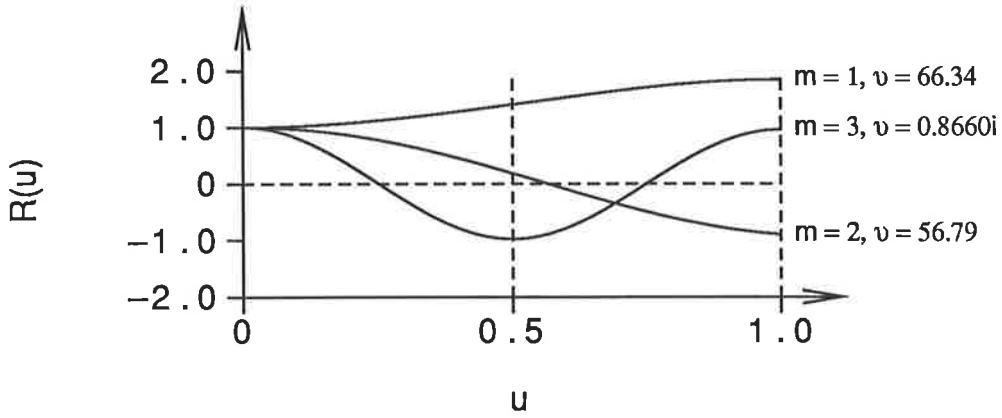

Figure 2.5: *Plots of the m = 1,2,3 N-mode eigenfunctions;* $\alpha = 2\pi$; $\varepsilon = 0.1$.

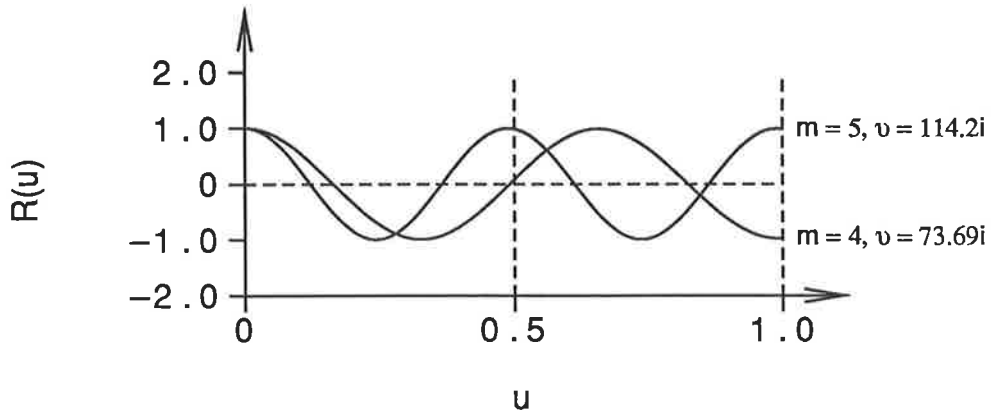

Figure 2.6: *Plots of the m = 4,5 N-mode eigenfunctions;* $\alpha = 2\pi$; $\varepsilon = 0.1$.

2.3 A NUMERICAL SOLUTION

As stated in subsection 2.1.5, the eigenvalues and eigenfunctions of equations (2.3)–(2.5) and (2.9)–(2.11) determine the stationary values of the quadratic functionals (2.23) and (2.24) respectively. Having posed the transverse field eigenvalue problems in this manner, an effective means of approximately generating the eigenvalues and eigenfunctions is via the Rayleigh-Ritz method. Applying this method requires that the approximate eigenfunctions be sought in the form of finite functional series expansions using a set of suitably chosen basis functions. That is, let

$$\phi(x,z) = \sum_{i=1}^{I}\sum_{j=1}^{J} a_{ij} f_{ij}(x,z) \tag{2.64}$$

and

$$\psi(r,z) = \sum_{i=1}^{I}\sum_{j=1}^{J} b_{ij} f_{ij}(r,z). \tag{2.65}$$

The basis functions are chosen to be sufficiently smooth and linearly independent over the duct's cross-sectional domain Ω. They are also chosen so that they satisfy the appropriate boundary conditions on Γ, according to whether N or D-mode solutions are required.

Substituting the series approximations (2.64) and (2.65) into the functionals (2.23) and (2.24) respectively, and seeking stationary values with respect to each of the series coefficients yields the following sets of linear algebraic equations. They are

$$\sum_{k=1}^{I}\sum_{l=1}^{J} K^{(s)}_{ijkl} a_{kl} = \mu^2 \sum_{k=1}^{I}\sum_{l=1}^{J} M^{(s)}_{ijkl} a_{kl} \tag{2.66}$$

and

$$\sum_{k=1}^{I}\sum_{l=1}^{J} K^{(c)}_{ijkl} b_{kl} = \nu^2 \sum_{k=1}^{I}\sum_{l=1}^{J} M^{(c)}_{ijkl} b_{kl} \tag{2.67}$$

where $i = 1,\ldots I$; $j = 1,\ldots J$ and

$$K^{(s)}_{ijkl} = \iint_{\Omega} \left[k^2 f_{ij} f_{kl} - \frac{\partial f_{ij}}{\partial x}\frac{\partial f_{kl}}{\partial x} - \frac{\partial f_{ij}}{\partial z}\frac{\partial f_{kl}}{\partial z} \right] dx\, dz, \tag{2.68}$$

$$M^{(s)}_{ijkl} = \iint_{\Omega} [f_{ij} f_{kl}] \, dx \, dz, \tag{2.69}$$

$$K^{(c)}_{ijkl} = \iint_{\Omega} r \left[k^2 f_{ij} f_{kl} - \frac{\partial f_{ij}}{\partial r} \frac{\partial f_{kl}}{\partial r} - \frac{\partial f_{ij}}{\partial z} \frac{\partial f_{kl}}{\partial z} \right] dr \, dz, \tag{2.70}$$

$$M^{(c)}_{ijkl} = \iint_{\Omega} \frac{1}{r} [f_{ij} f_{kl}] \, dr \, dz. \tag{2.71}$$

Equations (2.66) and (2.67) can be written more compactly as the $(IJ \times IJ)$ generalised matrix eigenvalue problems

$$\mathbf{K}^{(s)} \underline{a} = \mu^2 \mathbf{M}^{(s)} \underline{a} \tag{2.72}$$

and

$$\mathbf{K}^{(c)} \underline{b} = \nu^2 \mathbf{M}^{(c)} \underline{b}. \tag{2.73}$$

Solving equations (2.72) and (2.73) yields two sets of IJ eigenvalues and eigenvectors which approximately specify the dominant eigenvalues and eigenfunctions of equations (2.3)–(2.5) and (2.9)–(2.11).

The approximate solutions provided by the Rayleigh-Ritz method have a number of favourable characteristics. Firstly, the dominant eigenvalues and eigenfunctions are determined with greatest accuracy, with this accuracy being readily improved by increasing I and J. Also, the approximate eigenvalues always converge to the exact eigenvalues from below, a property which enables one to extrapolate more accurately when estimating the exact eigenvalues. Finally, interchanging the indices i, k and j, l in equations (2.68)–(2.71) shows that the matrices $\mathbf{K}^{(s)}$, $\mathbf{M}^{(s)}$, $\mathbf{K}^{(c)}$ and $\mathbf{M}^{(c)}$ are symmetric. These matrices are also real. As a consequence, the eigenvectors of equations (2.72) and (2.73) are M-orthogonal ([32], sect. 10.2). That is

$$\underline{a}^T_{mn} \mathbf{M}^{(s)} \underline{a}_{pq} = \delta_{mp} \delta_{nq} \underline{a}^T_{mn} \mathbf{M}^{(s)} \underline{a}_{mn} \tag{2.74}$$

and

$$\underline{b}^T_{mn} \mathbf{M}^{(c)} \underline{b}_{pq} = \delta_{mp} \delta_{nq} \underline{b}^T_{mn} \mathbf{M}^{(c)} \underline{b}_{mn}, \tag{2.75}$$

where δ_{mn} is as defined by equation (2.15) and the T superscript signifies the matrix operation of transpose. Referring back to the definitions of the matrices $\mathbf{M}^{(s)}$ and $\mathbf{M}^{(c)}$ in equations (2.69) and (2.71), one can see that equations (2.74) and (2.75) imply that (after M-normalising the eigenvectors) the approximate eigenfunctions also satisfy the orthogonality relations (2.13) and (2.14). Hence, the eigenfunctions determined by the Rayleigh-Ritz method can be used in equations such as (2.17) to give an approximate representation of a particular solution within a straight or curved duct.

In the following subsection, the Rayleigh-Ritz method will be used to approximately determine the dominant eigenvalues and eigenfunctions of equations (2.3)–(2.5) and (2.9)–(2.11) when the duct cross-section is elliptic.

2.3.1 A duct of elliptic cross-section

Here a duct of elliptic cross-section, with dimensions as shown in Figure 2.7 is considered. The axes of the ellipse are assumed to be aligned with the (r, z) coordinate axes, with the centre of the cross-section being located a distance c from the z-axis. The equation of the duct wall is therefore

$$\frac{(r-c)^2}{a^2} + \frac{z^2}{b^2} = 1. \tag{2.76}$$

Lowson and Baskaran [33] used the method of separation of variables to determine the acoustic field within a straight duct of elliptic cross-section. However, as mentioned in section 2.2, this method cannot be used when the longitudinal axis of the duct is curved, and some form of approximate analysis must be employed. Elliptic ducts are often studied to determine the effects of imperfect concentricity upon propagation in circular cross-sectioned ducts. They also serve as a useful model of non-circular intake manifolds on jet aircraft. Applying the Rayleigh-Ritz method to this problem therefore offers a good opportunity to illustrate the techniques involved with a useful application.

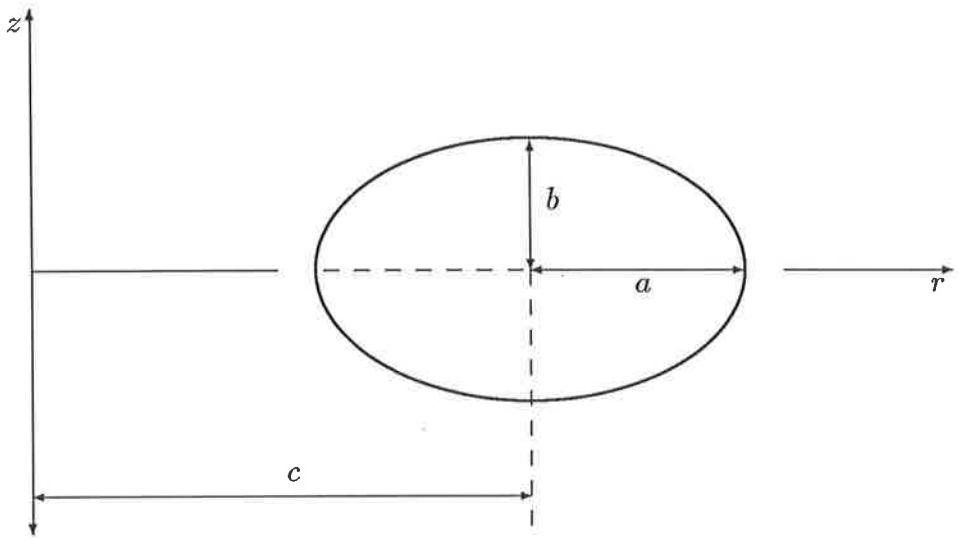

Figure 2.7: *Elliptic duct cross-section.*

When using the Rayleigh-Ritz method, ideally, the exact eigenfunctions of the straight duct problem should be used as basis functions. They are linearly independent and satisfy the required boundary conditions. They also bring an extra degree of accuracy to the formulation which will be used in section 3.2 for calculating the modal scattering matrix of a section of uniformly curved duct. Thus, for rectangular cross-sectioned ducts, the eigenfunctions specified by equations (2.25)–(2.27) should be used. For circular cross-sectioned ducts, the combinations of Bessel and trigonometric functions used by Firth and Fahy [22] should be used. However, as shown by Lowson and Baskaran [33], the exact eigenfunctions for straight, elliptic ducts involve complicated Mathieu functions. In the analysis presented here, the difficulties associated with explicitly using these Mathieu functions are avoided. This is done by applying a coordinate transformation to the cross-sectional domain of the duct. Such an approach has the advantage that it enables simpler trigonometric functions to be used as basis functions.

So, referring to Figure 2.8, a transformation is made from the (r, z) coordinates to the elliptic coordinates (ξ, η). The transformation $(r, z) \rightarrow (\xi, \eta)$ is defined by the pair

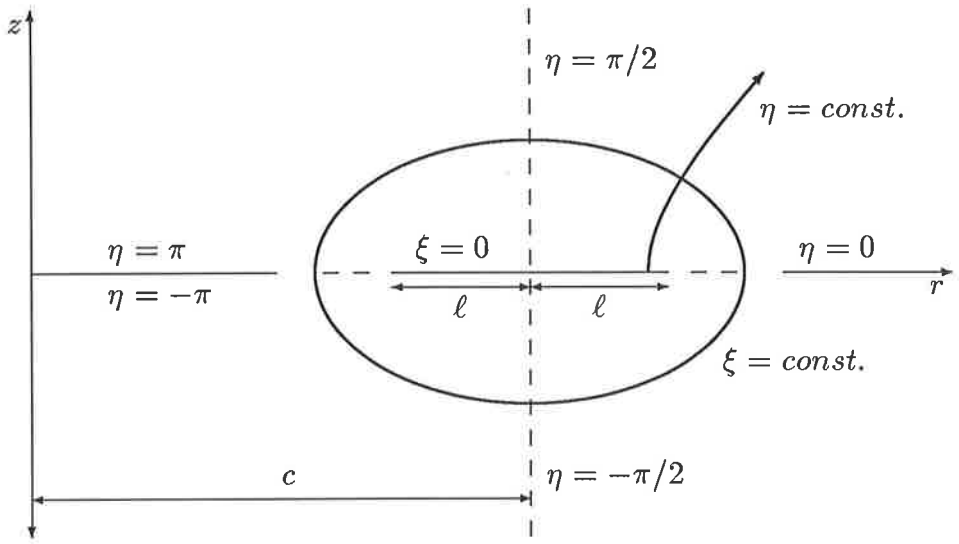

Figure 2.8: *Elliptic coordinate system.*

of equations

$$r = c + \ell \cosh(\xi) \cos(\eta) \tag{2.77}$$

and

$$z = \ell \sinh(\xi) \sin(\eta), \tag{2.78}$$

where $0 \leq \xi \leq \xi_{max}$ and $-\pi < \eta \leq \pi$. The curves $\xi = const.$ and $\eta = const.$ form an orthogonal system of confocal ellipses and hyperbolae, with the duct wall being represented by the ellipse $\xi = \xi_{max}$, which has foci at $(r, z) = (c \pm \ell, 0)$. Substituting equations (2.77) and (2.78) into the equation of the duct wall (2.76) enables the following expressions for ℓ and ξ_{max} in terms of a and b to be determined. They are

$$\ell = \sqrt{a^2 - b^2} \tag{2.79}$$

and

$$\xi_{max} = \ln\left(\frac{a + b}{\ell}\right). \tag{2.80}$$

For equations (2.77)–(2.79) to be valid, the inequality $b < a < c$ must be satisfied. If the cross-section is such that $b > a$, an alternative definition of the transformation equations is required, namely

$$r = c - \ell \sinh(\xi) \sin(\eta) \tag{2.81}$$

and

$$z = \ell \cosh(\xi) \cos(\eta), \tag{2.82}$$

where now $0 \leq \xi \leq \xi_{max}$, $-\pi/2 < \eta \leq 3\pi/2$ and

$$\ell = \sqrt{b^2 - a^2}. \tag{2.83}$$

Equations (2.81) and (2.82) where obtained by effectively rotating the ellipse in Figure 2.8 anticlockwise through an angle of $\pi/2$ radians.

Now, using equations (2.77), (2.78), (2.81) and (2.82), the functionals (2.23) and (2.24) transform to

$$I^{(s)}(\phi) = \int_{\xi=0}^{\xi_{max}} \int_{\eta=\eta_{min}}^{\eta_{max}} \left[\left(\frac{\partial \phi}{\partial \xi} \right)^2 + \left(\frac{\partial \phi}{\partial \eta} \right)^2 - (k^2 - \mu^2) g^2 \phi^2 \right] d\xi \, d\eta \tag{2.84}$$

and

$$I^{(c)}(\psi) = \int_{\xi=0}^{\xi_{max}} \int_{\eta=\eta_{min}}^{\eta_{max}} r \left[\left(\frac{\partial \psi}{\partial \xi} \right)^2 + \left(\frac{\partial \psi}{\partial \eta} \right)^2 - (k^2 - \nu^2/r^2) g^2 \psi^2 \right] d\xi \, d\eta \tag{2.85}$$

where

$$\eta_{min} = \begin{cases} -\pi & \text{if } b < a \\ -\pi/2 & \text{if } b > a, \end{cases} \tag{2.86}$$

$$\eta_{max} = \begin{cases} \pi & \text{if } b < a \\ 3\pi/2 & \text{if } b > a \end{cases} \tag{2.87}$$

and

$$g^2(\xi, \eta) = \ell^2 \left[\cosh^2(\xi) - \cos^2(\eta) \right]; \tag{2.88}$$

g^2 being the Jacobian determinant of the coordinate transformations. Seeking approximate solutions in the form given by equations (2.64) and (2.65), and applying the Rayleigh-Ritz method yields the matrix eigenvalue problems given by equations (2.72) and (2.73), where the matrix elements are

$$K^{(s)}_{ijkl} = \int_{\xi=0}^{\xi_{max}} \int_{\eta=\eta_{min}}^{\eta_{max}} \left[k^2 g^2 f_{ij} f_{kl} - \frac{\partial f_{ij}}{\partial \xi}\frac{\partial f_{kl}}{\partial \xi} - \frac{\partial f_{ij}}{\partial \eta}\frac{\partial f_{kl}}{\partial \eta} \right] d\xi\, d\eta, \tag{2.89}$$

$$M^{(s)}_{ijkl} = \int_{\xi=0}^{\xi_{max}} \int_{\eta=\eta_{min}}^{\eta_{max}} \left[g^2 f_{ij} f_{kl} \right] d\xi\, d\eta, \tag{2.90}$$

$$K^{(c)}_{ijkl} = \int_{\xi=0}^{\xi_{max}} \int_{\eta=\eta_{min}}^{\eta_{max}} r \left[k^2 g^2 f_{ij} f_{kl} - \frac{\partial f_{ij}}{\partial \xi}\frac{\partial f_{kl}}{\partial \xi} - \frac{\partial f_{ij}}{\partial \eta}\frac{\partial f_{kl}}{\partial \eta} \right] d\xi\, d\eta, \tag{2.91}$$

$$M^{(c)}_{ijkl} = \int_{\xi=0}^{\xi_{max}} \int_{\eta=\eta_{min}}^{\eta_{max}} \frac{1}{r} \left[g^2 f_{ij} f_{kl} \right] d\xi\, d\eta. \tag{2.92}$$

The basis functions are chosen so that both $\phi(\xi,\eta)$ and $\psi(\xi,\eta)$ have the following five properties:

1. The boundary condition on the duct wall $\xi = \xi_{max}$ is satisfied. That is

$$\frac{\partial \psi}{\partial \xi}(\xi_{max},\eta) = 0 \quad \text{for } N\text{-modes},$$

$$\psi(\xi_{max},\eta) = 0 \quad \text{for } D\text{-modes}.$$

2. ψ is periodic in η, with period π or 2π.

3. ψ is orthogonally continuous when crossing the interfocal line $z = 0, c-\ell < r < c+\ell$ if $b < a$ or $r = c, -\ell < z < \ell$ if $b > a$. That is

$$\psi(0,\eta) = \psi(0,-\eta).$$

4. The gradient of ψ is orthogonally continuous when crossing the interfocal line $z = 0, c-\ell < r < c+\ell$ if $b < a$ or $r = c, -\ell < z < \ell$ if $b > a$. That is

$$\frac{\partial \psi}{\partial \xi}(0,\eta) = -\frac{\partial \psi}{\partial \xi}(0,-\eta).$$

5. ψ has either an even or odd symmetry about the r-axis. That is about $\eta = 0$ if $b < a$ or $\eta = \pi/2$ if $b > a$.

The following basis functions satisfy these requirements. They are

$$f_{ij}(\xi, \eta) = \cos(A_{ij}\xi + B_j)\cos(C_j\eta + D_j) \tag{2.93}$$

such that:

- If $b < a$ and ψ is even about the r-axis

$$A_{ij} = \begin{cases} \frac{(i-1)\pi}{\xi_{max}} & \text{for } N\text{-modes} \\ \frac{(2i-1)\pi}{2\xi_{max}} & \text{for } D\text{-modes,} \end{cases}$$

$$B_j = 0, \quad C_j = j - 1, \quad D_j = 0. \tag{2.94}$$

- If $b < a$ and ψ is odd about the r-axis

$$A_{ij} = \begin{cases} \frac{(2i-1)\pi}{2\xi_{max}} & \text{for } N\text{-modes} \\ \frac{i\pi}{\xi_{max}} & \text{for } D\text{-modes,} \end{cases}$$

$$B_j = -\pi/2, \quad C_j = j, \quad D_j = -\pi/2. \tag{2.95}$$

- If $b > a$

$$C_j = \begin{cases} j - 1 & \text{if } \psi \text{ is even about the } r\text{-axis} \\ j & \text{if } \psi \text{ is odd about the } r\text{-axis} \end{cases}$$

and if $j = 1, 3, 5, \ldots$

$$A_{ij} = \begin{cases} \frac{(i-1)\pi}{\xi_{max}} & \text{for } N\text{-modes} \\ \frac{(2i-1)\pi}{2\xi_{max}} & \text{for } D\text{-modes,} \end{cases}$$

$$B_j = 0, \quad D_j = 0,$$

else if $j = 2, 4, 6, \ldots$

$$A_{ij} = \begin{cases} \frac{(2i-1)\pi}{2\xi_{max}} & \text{for } N\text{-modes} \\ \frac{i\pi}{\xi_{max}} & \text{for } D\text{-modes,} \end{cases}$$

$$B_j = -\pi/2, \quad D_j = -\pi/2. \tag{2.96}$$

When using these basis functions, The elements of the matrices $\mathbf{K}^{(s)}$, $\mathbf{M}^{(s)}$ and $\mathbf{K}^{(c)}$ can be evaluated analytically. However, this is not possible for the elements of the matrix $\mathbf{M}^{(c)}$ due to the presence of the r^{-1} term in the integrand. In practice, this problem can be overcome by means similar to those employed by Firth and Fahy ([22], sect. 3.1), whereby r^{-1} is represented as a binomial series

$$\begin{aligned} r^{-1} &= \begin{cases} c^{-1}[1+(\ell/c)\cosh(\xi)\cos(\eta)]^{-1} & \text{if } b<a \\ c^{-1}[1-(\ell/c)\sinh(\xi)\sin(\eta)]^{-1} & \text{if } b>a \end{cases} \\ &= \begin{cases} c^{-1}\sum_{n=0}^{\infty}[(-\ell/c)\cosh(\xi)\cos(\eta)]^{n} & \text{if } b<a \\ c^{-1}\sum_{n=0}^{\infty}[(\ell/c)\sinh(\xi)\sin(\eta)]^{n} & \text{if } b>a. \end{cases} \end{aligned} \tag{2.97}$$

Each term in the series provides integrals which can be evaluated analytically by recursion, the series being truncated when sufficient accuracy is achieved. Upon obtaining solutions to the matrix eigenvalue problems (2.72) and (2.73), approximations to ϕ and ψ can be evaluated for given values of ξ and η. Values of ϕ and ψ in the original (r,z)-plane can therefore be obtained after numerically inverting the transformation equations (2.77) and (2.78) (or (2.81) and (2.82)).

The results of calculations of various straight and curved duct, N and D-mode eigenfunctions are now presented. For the cases considered, it will be assumed that, unless otherwise specified, the free-space acoustic wavelength $\chi = 1.0$ — meaning that all other length dimensions will be expressed as multiples of this wavelength. Tables 2.2 and 2.3 show values obtained for the first six even and odd, curved duct, N-mode eigenvalues when $a = 0.8$, $b = 0.5$, $c = 2.0$ and $I = J = 4, 6, 8, 10, 12$. One can see the convergence of the approximate eigenvalues from below, indicating that the $I = J = 12$ estimates of ν^2 are accurate to at least four significant figures. In Figures 2.9 and 2.10, contour plots of the first six straight and curved duct, even and odd N-mode eigenfunctions are shown when $a = 0.8$, $b = 0.5$, $c = 2.0$ and $I = J = 12$. In these figures, the straight duct mode contours appear in the left column, and the curved duct mode contours appear in the right column. Each mode contour is plotted on the duct

I, J	ν^2					
4	0.22458E+3	0.11588E+3	0.60555E+2	−0.29577E+1	−0.32792E+2	−0.13161E+3
6	0.22511E+3	0.11858E+3	0.64644E+2	0.85634E+1	−0.30248E+2	−0.83792E+2
8	0.22511E+3	0.11860E+3	0.64684E+2	0.87833E+1	−0.30206E+2	−0.72998E+2
10	0.22511E+3	0.11860E+3	0.64684E+2	0.87845E+1	−0.30206E+2	−0.72898E+2
12	0.22511E+3	0.11860E+3	0.64684E+2	0.87846E+1	−0.30206E+2	−0.72898E+2

Table 2.2: *Convergence of the curved duct, even N-mode eigenvalues when* $a = 0.8$, $b = 0.5$ *and* $c = 2.0$.

I, J	ν^2					
4	0.11858E+3	0.50527E+2	−0.20145E+2	−0.14017E+3	−0.22456E+3	−0.37185E+3
6	0.11863E+3	0.51168E+2	−0.10873E+2	−0.92426E+2	−0.19565E+3	−0.22378E+3
8	0.11863E+3	0.51180E+2	−0.10692E+2	−0.88881E+2	−0.18726E+3	−0.22372E+3
10	0.11863E+3	0.51180E+2	−0.10691E+2	−0.88830E+2	−0.18660E+3	−0.22371E+3
12	0.11863E+3	0.51180E+2	−0.10691E+2	−0.88830E+2	−0.18658E+3	−0.22371E+3

Table 2.3: *Convergence of the curved duct, odd N-mode eigenvalues when* $a = 0.8$, $b = 0.5$ *and* $c = 2.0$.

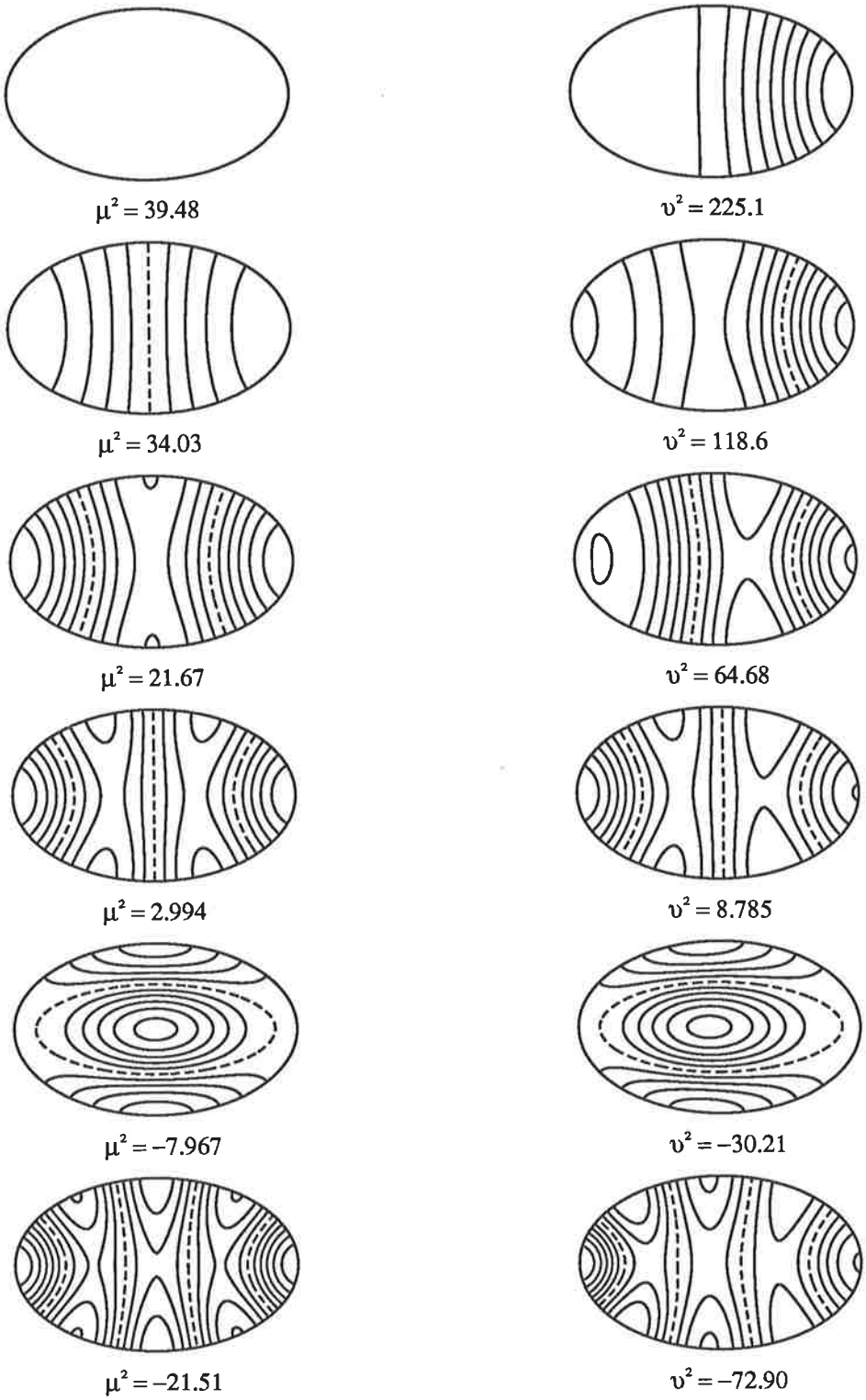

Figure 2.9: *Even N-mode eigenfunction contours in straight and curved elliptic ducts; a = 0.8, b = 0.5, c = 2.0.*

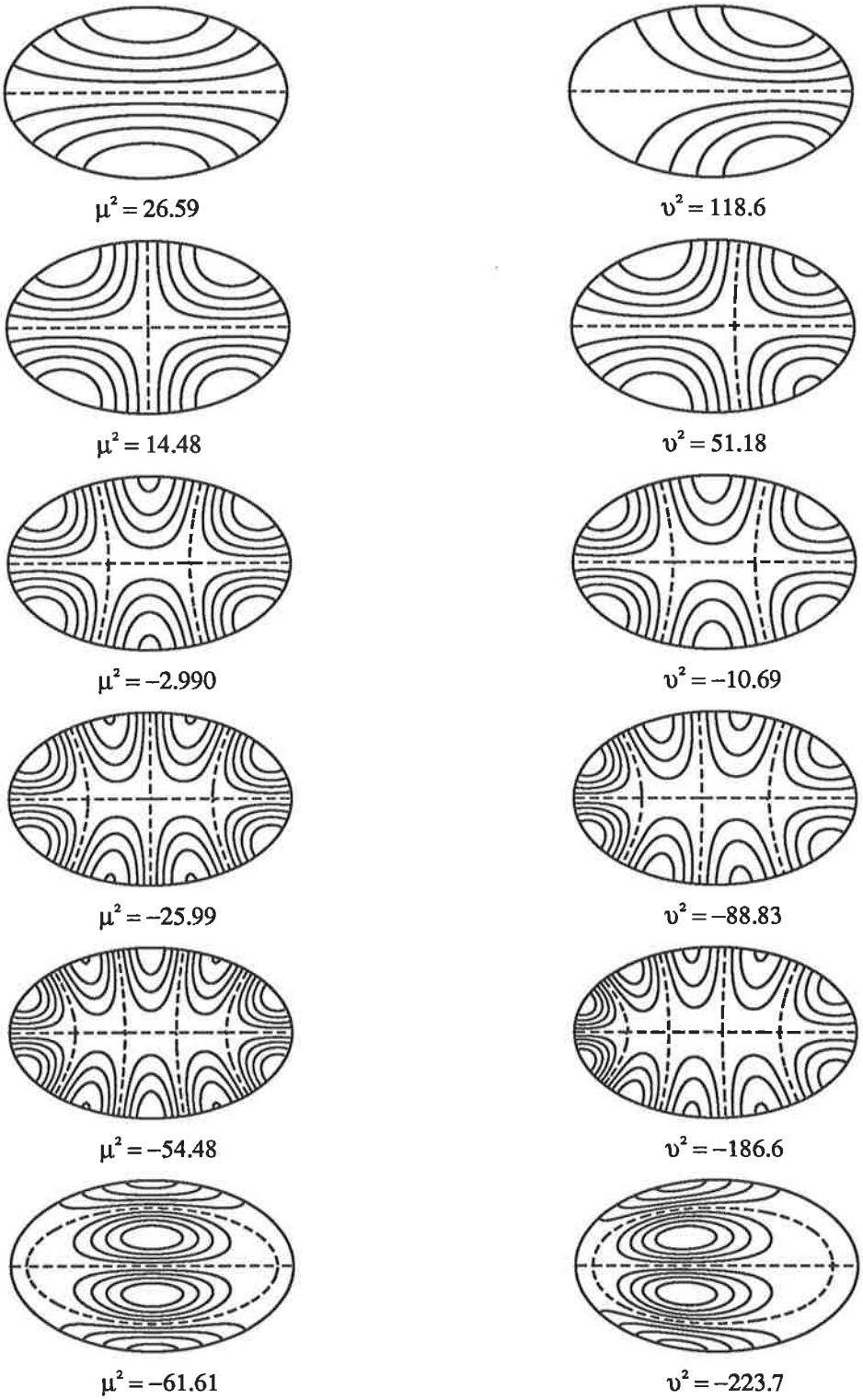

Figure 2.10: *Odd N-mode eigenfunction contours in straight and curved elliptic ducts; a = 0.8, b = 0.5, c = 2.0.*

cross-section, which is viewed from the same standpoint taken in Figure 2.7 (hence, the axis of rotation of the curved duct is to the left of the plot). The dashed contour lines represent a zero value of the eigenfunction, and below each plot is an estimate of the accompanying eigenvalue. An examination of the contour plots shows clearly how the eigenfunctions are biased in a radial sense when the longitudinal axis of the duct is curved. In agreement with the observations made in subsection 2.3.1, this bias is towards the outer wall of the duct when $\nu^2 > 0$ and towards the inner wall of the duct when $\nu^2 < 0$. The bias is minimal when $\nu^2 \approx 0$, and is greater for modes further from cut-off. Looking at the contour plot of the 5^{th} odd eigenfunction in Figure 2.10, one can see that it has a more oscillatory profile than the other eigenfunctions. It is therefore natural to expect that, for a given number of terms in the series approximations, it would not be as accurately represented as the others. The effects of this inaccuracy are illustrated in Table 2.3, where the eigenvalue estimates associated with this eigenfunction are seen to converge at a slightly slower rate than those associated with the other eigenfunctions.

Figures 2.11–2.16 show contour plots of various other straight and curved duct, N and D-mode eigenfunctions, where the biasing of the curved duct eigenfunctions can again be observed. Figures 2.13–2.16 are interesting as they show how the eigenfunctions are often more dramatically biased when the duct's cross-sectional dimensions are such that $b > a$. Finally, the contour plots in Figures 2.17 and 2.18 give a good illustration of how the radial bias of a particular curved duct eigenfunction varies with χ (and therefore the value of ν), and c (and therefore the curvature of the duct). The centreline radius of curvature of the duct is $c = 2.0$ in Figure 2.17 and $c = 4.0$ in Figure 2.18, with the values of χ being the same in both figures. The plots in these figures exhibit the same typical biasing characteristics as those previously observed in Figures 2.9 – 2.16, and show clearly how the degree of bias is minimal when $\nu \approx 0$ — where the contours closely resemble those of the corresponding straight duct eigenfunction (top-left plot in Figure 2.12). A comparison between plots with the same χ value in

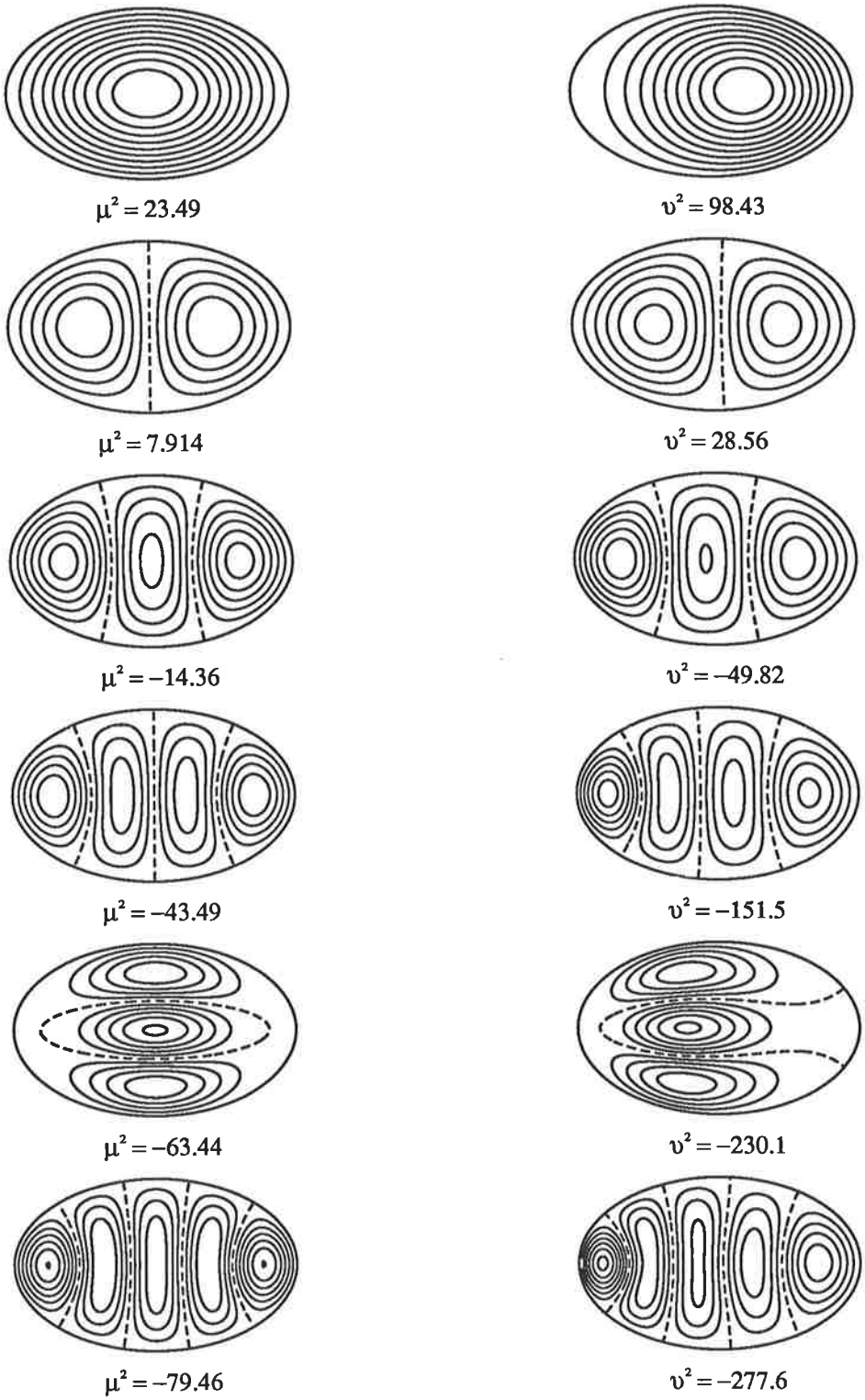

Figure 2.11: *Even D-mode eigenfunction contours in straight and curved elliptic ducts; a = 0.8, b = 0.5, c = 2.0.*

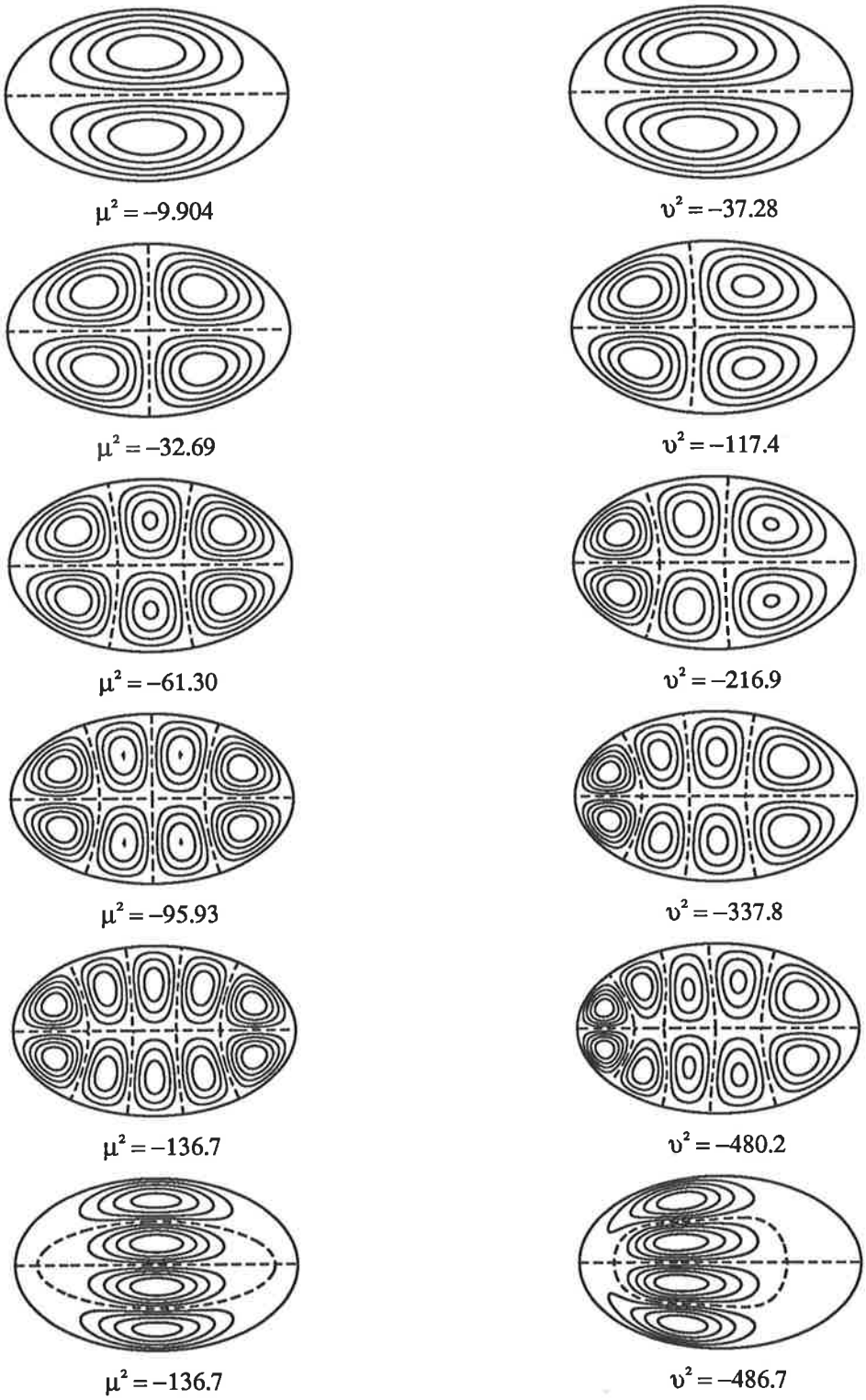

Figure 2.12: *Odd D-mode eigenfunction contours in straight and curved elliptic ducts; a = 0.8, b = 0.5, c = 2.0.*

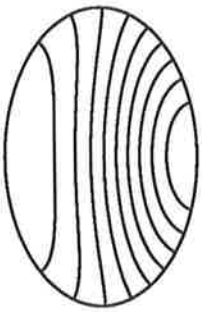

$\upsilon^2 = 179.5$

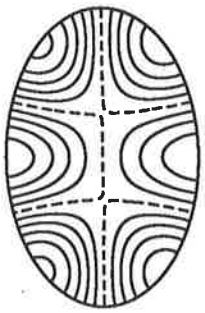

$\upsilon^2 = -11.79$

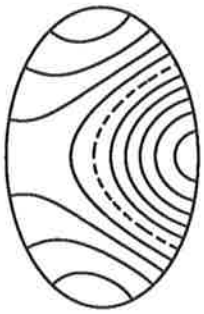

$\upsilon^2 = 102.0$

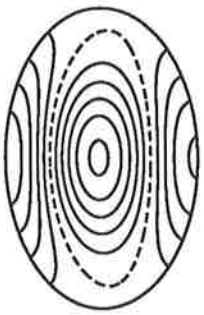

$\upsilon^2 = -30.62$

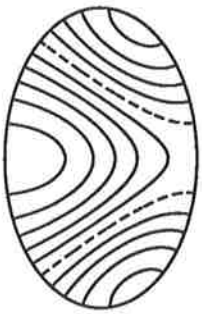

$\upsilon^2 = 78.14$

$\upsilon^2 = -82.79$

Figure 2.13: *Even N-mode eigenfunction contours in a curved elliptic duct; a = 0.5, b = 0.8, c = 2.0.*

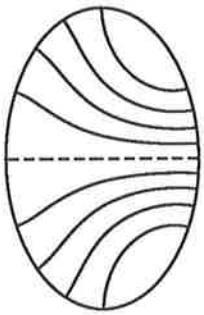

$\upsilon^2 = 143.7$

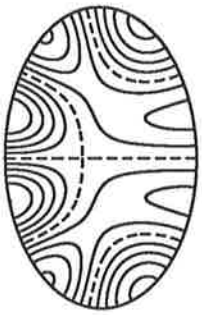

$\upsilon^2 = -96.08$

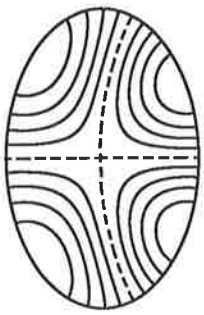

$\upsilon^2 = 54.33$

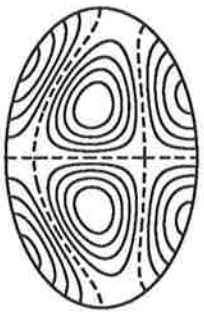

$\upsilon^2 = -117.7$

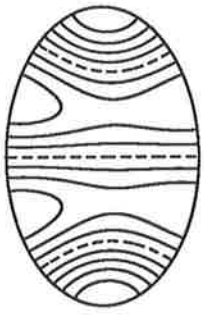

$\upsilon^2 = 11.14$

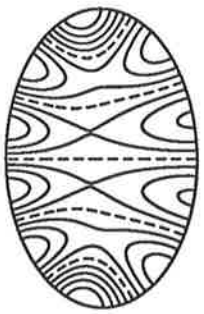

$\upsilon^2 = -197.0$

Figure 2.14: *Odd N-mode eigenfunction contours in a curved elliptic duct; a = 0.5, b = 0.8, c = 2.0.*

$\upsilon^2 = 94.08$

$\upsilon^2 = -228.0$

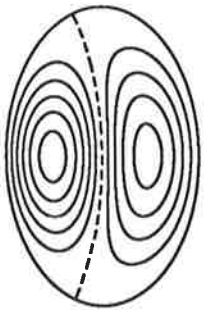

$\upsilon^2 = -37.36$

$\upsilon^2 = -245.9$

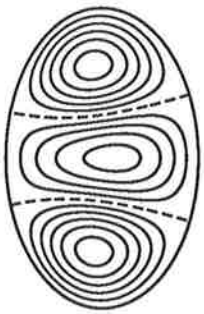

$\upsilon^2 = -56.21$

$\upsilon^2 = -312.1$

Figure 2.15: *Even D-mode eigenfunction contours in a curved elliptic duct; a = 0.5, b = 0.8, c = 2.0.*

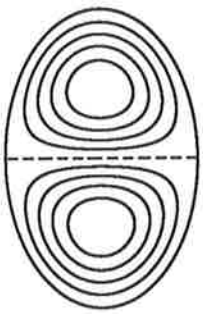

$\upsilon^2 = 31.49$

$\upsilon^2 = -346.1$

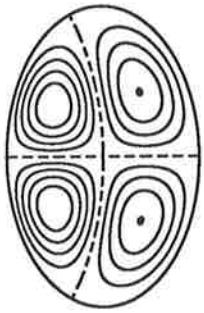

$\upsilon^2 = -123.9$

$\upsilon^2 = -378.4$

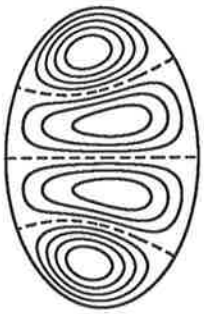

$\upsilon^2 = -170.7$

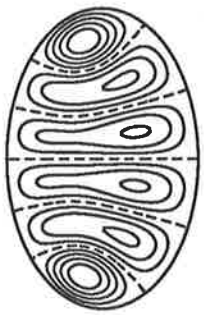

$\upsilon^2 = -479.3$

Figure 2.16: *Odd D-mode eigenfunction contours in a curved elliptic duct; a = 0.5, b = 0.8, c = 2.0.*

$\chi = 0.7, \upsilon^2 = 120.5$

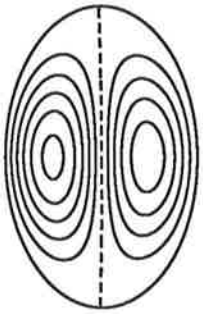

$\chi = 0.9, \upsilon^2 = -2.199$

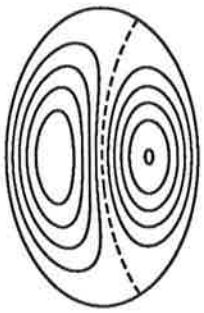

$\chi = 8.0, \upsilon^2 = 47.27$

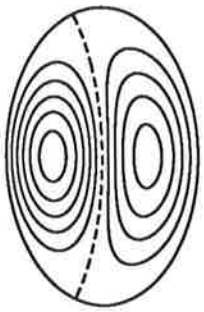

$\chi = 1.0, \upsilon^2 = -37.36$

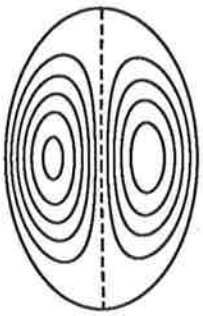

$\chi = 0.89, \upsilon^2 = 1.993$

$\chi = 2.0, \upsilon^2 = -149.1$

Figure 2.17: *Contours of the second, curved duct, even D-mode eigenfunction when a = 0.5, b = 0.8, c = 2.0 and* χ *= 0.7, 0.8, 0.89, 0.9, 1.0, 2.0.*

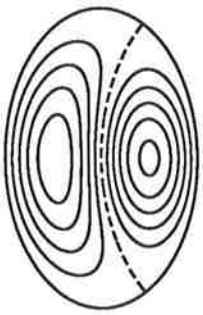

$\chi = 0.7, \upsilon^2 = 494.2$

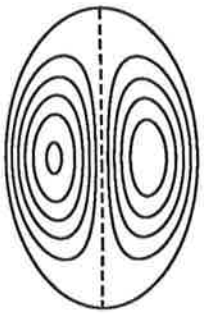

$\chi = 0.9, \upsilon^2 = -9.920$

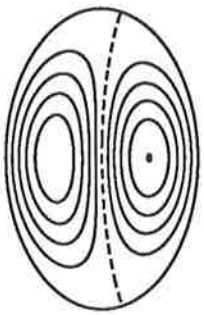

$\chi = 0.8, \upsilon^2 = 194.8$

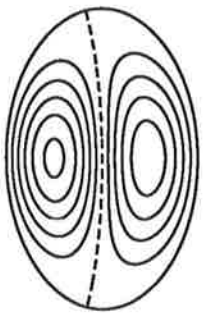

$\chi = 1.0, \upsilon^2 = -156.2$

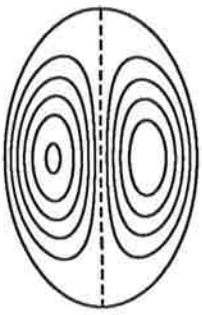

$\chi = 0.89, \upsilon^2 = 7.488$

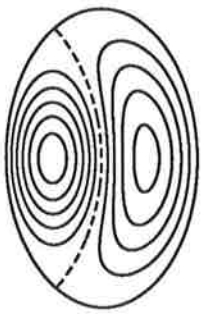

$\chi = 2.0, \upsilon^2 = -622.9$

Figure 2.18: *Contours of the second, curved duct, even D-mode eigenfunction when a = 0.5, b = 0.8, c = 4.0 and* χ *= 0.7, 0.8, 0.89, 0.9, 1.0, 2.0.*

both figures shows that the degree of bias becomes less when the curvature of the duct is reduced.

2.4 SUMMARY

In this chapter, the general solutions to equations (1.1)–(1.3) within straight and uniformly curved ducts have been studied. It was shown that the respective solutions are obtained by solving a two-dimensional eigenvalue problem over the duct's cross-section and then representing the acoustic potential as a modal series. The eigenfunctions were shown to be orthogonal, and alternative variational statements of the eigenvalue problems were given. The transmission of energy within these ducts was also considered.

Analytic expressions for the acoustic potential within rectangular cross-sectioned ducts were presented. It was found from these expressions that the curved duct modes could be considered to be radially biased versions of the straight duct modes. Also, except when near cut-off, if a straight duct mode was a propagating mode, then so was the corresponding curved duct mode. The degree of bias was enhanced by increasing the curvature of the duct, and the bias was shown to be towards the outer wall of the duct for propagating modes and towards the inner wall of the duct for evanescent modes.

Due to the difficulty in applying analytical techniques to the straight and curved duct eigenvalue problems when the duct's cross-section is non-rectangular, a general procedure for numerically solving these problems was presented. The procedure utilised the alternative variational statements of the modal eigenvalue problems presented in subsection 2.1.5, and was based upon the Rayleigh-Ritz method. The procedure was applied to the case of an elliptic cross-sectioned duct, and the results of calculations were presented. The modes within the straight and curved elliptic ducts were found to display the same general characteristics as those previously observed in the rectangular duct

modes. In particular, from the observations of radial biasing of the curved duct modes, the following general conclusions are drawn. Namely, that within uniformly curved ducts, a sound source will more readily excite the dominant (and therefore propagating) modes when it is located near the duct's outer wall. Also, the modal structure of the resulting sound field will be more faithfully preserved under these conditions. These effects will become more pronounced if the curvature of the duct is increased, and if the acoustic frequency is increased so that many modes are above cut-off.

CHAPTER 3

— ◇ —

MODAL SCATTERING WITHIN MULTI-BEND DUCTING SYSTEMS

3.1 INTRODUCTION

In Chapter 2, general solutions to equations (1.1)–(1.3) within straight and uniformly curved ducts were presented. These solutions took the form of a superposition of forward and backward travelling wave modes, with particular solutions being determined by an appropriate choice of the coefficients in the modal series. Therefore, once the modes were calculated, an arbitrary acoustic field within a straight or uniformly curved duct could be completely specified by a discrete set of numerical quantities; namely, the values of the modal coefficients.

Theoretically, an infinite number of modal coefficients are required to exactly specify an arbitrary acoustic field. However, practically, sufficient accuracy can be obtained by only considering finite numbers of these coefficients. To be specific, only the coefficients of the dominant modes (i.e. modes whose associated eigenvalues μ^2, ν^2 are largest) need be considered. There are two reasons for this. Firstly, the eigenfunctions which define the modes form a complete set of functions on the cross-sectional domain of the duct. The modal series is therefore a convergent series, and in general, the coefficients of the dominant modes will have the greatest magnitude. Secondly, the modes whose associated eigenvalues are negative do not propagate along the duct, but are exponentially attenuated, with the attenuation being greater when the eigenvalues are more negative.

As the dominant modes will either propagate or be the least attenuated modes, they will be the most significant contributors to the acoustic field within the duct. Hence, one can legitimately truncate the modal series. As a result, it follows that the acoustic field within a ducting system which contains several straight and uniformly curved sections can be adequately determined if one knows the values of the dominant modal coefficients within each section. Of course, the more modes that are considered to be "dominant", the more accurately the acoustic field will be specified. In its broadest sense, the purpose of this chapter is to develop methods for determining the values of given modal coefficients when considering a variety of multi-bend duct configerations.

In this chapter, when developing the methods used to determine the modal coefficients within the curved and straight sections of a multi-bend ducting system, each section is interpreted as being an individual scatterer of straight duct modes. This interpretation is based upon the fact that the acoustic field at the ends of any duct section can be legitimately expressed as a superposition of straight duct modes. The coefficients of the scattered modes are related to the coefficients of the modes within the duct section in such a way that the acoustic potential and its gradient are continuous. Equations (1.4) and (1.5) show that this ensures that the acoustic pressure and fluid particle velocity are continuous. It follows from the intrinsic linear characteristics of the acoustic field that the coefficients of the scattered modes at both ends of a duct section are related to each other (and to the coefficients of the modes within the duct section) by sets of linear algebraic equations. Thus, a modal scattering matrix for each duct section can be introduced. The acoustic characteristics of the ducting system can then be obtained by considering the system to be a cascade of modal scatterers. There are a number of advantages to be gained by using this scattering matrix approach. For example, the approach enables each duct section to be individually analysed, with the continuity requirements for the acoustic potential being automatically satisfied when performing calculations. From a computational viewpoint, the scattering matrix formu-

lation is well suited for the analysis of ducting systems which contain large numbers of curved and straight sections. Also, the scattering matrix itself provides useful information about the acoustic performance of a section of duct.

The relevant theory for performing a scattering matrix analysis of a multi-bend ducting system is now presented. The presentation begins in the next section, where a general method for numerically determining the modal transmission and reflection matrices of a single duct bend is described. These matrices directly specify the modal scattering matrix for the bend, and are therefore of fundamental importance in the ensuing formulation.

3.2 MODAL SCATTERING FROM A SINGLE DUCT BEND

The problem of describing the propagation of acoustic waves through the simple, single bend ducting system shown in Figure 3.1 is considered. In Figure 3.1, Σ_1 and Σ_3 represent two infinitely long sections of straight duct, and Σ_2 represents a section of uniformly curved, joining duct. General solutions to equations (1.1)–(1.3) within Σ_1, Σ_2 and Σ_3 are most conveniently obtained if they are associated with the coordinates (x, y, z), (r, θ, z) and (x', y', z) respectively. Here the z-axis is normal to the (x, y)-plane and points out of the page, the polar coordinates (r, θ) are as defined in subsection 2.1.2, and the (x', y') axes are obtained by rotating the (x, y) axes through an angle of $\theta = \theta_{max}$, where θ_{max} is the angular extent of Σ_2. Following the theory presented in subsections 2.1.1 and 2.1.2, suitable truncated expressions for the acoustic potential within Σ_1, Σ_2 and Σ_3 are

$$\Phi_1(x, y, z) = \sum_{m=1}^{K} \sum_{n=1}^{K} \left[\sigma_{mn} e^{i\mu_{mn} y} + \rho_{mn} e^{-i\mu_{mn} y}\right] \phi_{mn}(x, z), \tag{3.1}$$

$$\Phi_2(r, \theta, z) = \sum_{m=1}^{K} \sum_{n=1}^{K} \left[\alpha_{mn} e^{i\nu_{mn}\theta} + \beta_{mn} e^{-i\nu_{mn}\theta}\right] \psi_{mn}(r, z) \tag{3.2}$$

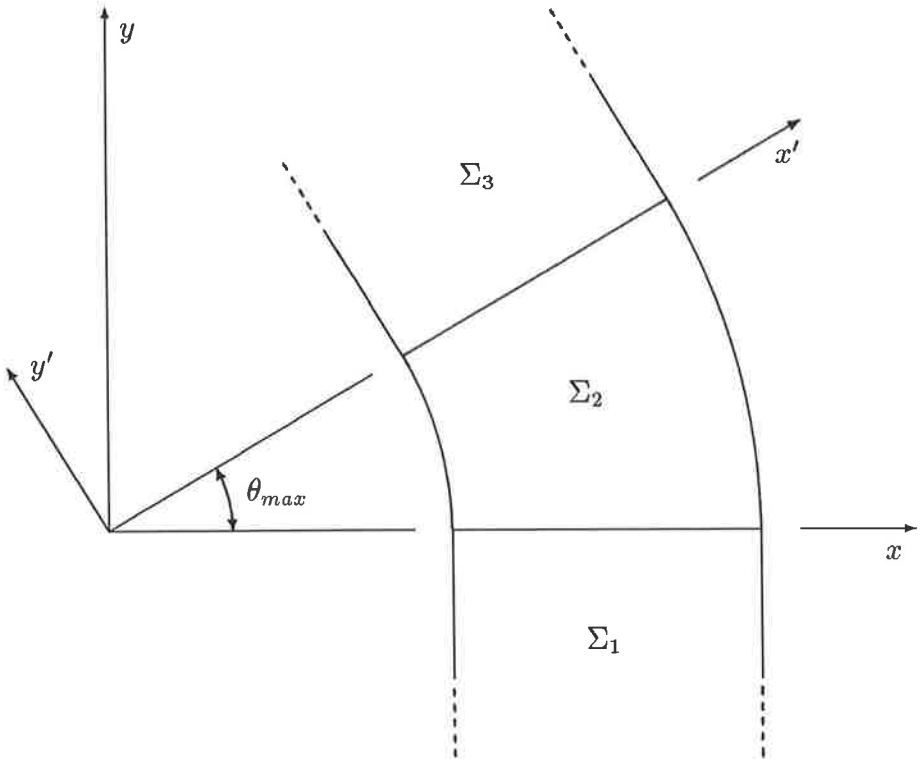

Figure 3.1: *Top view of a simple, single bend ducting system.*

and

$$\Phi_3(x', y', z) = \sum_{m=1}^{K} \sum_{n=1}^{K} \tau_{mn} e^{i\mu_{mn} y'} \phi_{mn}(x', z) \tag{3.3}$$

respectively. In equations (3.1)–(3.3); σ_{mn}, ρ_{mn} and τ_{mn} are the coefficients of modes incident upon, reflected from and transmitted through Σ_2; and α_{mn} and β_{mn} are the coefficients of modes associated with a standing wave field within Σ_2. The simplifying assumption that modes are only incident upon Σ_2 from Σ_1 is made in light of the principle of superposition which applies to modes throughout the ducting system.

Physically, Σ_2 can be thought of as a two-port junction [34], which linearly scatters an incident modal coefficient distribution into modal coefficient distributions transmitted through and reflected from it. The nature of this scattering process is governed by the

fact that the acoustic pressure and fluid particle velocity must be continuous throughout the ducting system. In terms of the potential function formulation, these conditions are satisfied if Φ and the axial component of $\nabla\Phi$ are continuous when crossing the junctions between the straight and curved duct sections. Hence, as a first step towards deriving expressions for the transmission and reflection matrices, the following four continuity equations are proposed. They are:

$$[\Phi_1]_{x=r,y=0} = [\Phi_2]_{\theta=0} \tag{3.4}$$

and

$$[\Phi_3]_{x'=r,y'=0} = [\Phi_2]_{\theta=\theta_{max}}, \tag{3.5}$$

ensuring continuity of Φ; and

$$\left[\frac{\partial\Phi_1}{\partial y}\right]_{x=r,y=0} = \frac{1}{r}\left[\frac{\partial\Phi_2}{\partial\theta}\right]_{\theta=0} \tag{3.6}$$

and

$$\left[\frac{\partial\Phi_3}{\partial y'}\right]_{x'=r,y'=0} = \frac{1}{r}\left[\frac{\partial\Phi_2}{\partial\theta}\right]_{\theta=\theta_{max}}, \tag{3.7}$$

ensuring continuity of the axial component of $\nabla\Phi$.

At this point it is convenient to represent the expressions for Φ_1, Φ_2 and Φ_3 given in equations (3.1)–(3.3) using matrix notation, with the modes appearing in the approximate form obtained from the numerical solution procedure presented in section 2.3. We therefore write

$$\Phi_1(x,y,z) = \underline{f}^T(x,z)\mathbf{A}\left[\mathbf{E}(y)\underline{\sigma} + \mathbf{E}^{-1}(y)\underline{\rho}\right], \tag{3.8}$$

$$\Phi_2(r,\theta,z) = \underline{f}^T(r,z)\mathbf{B}\left[\mathbf{F}(\theta)\underline{\alpha} + \mathbf{F}^{-1}(\theta)\underline{\beta}\right] \tag{3.9}$$

and

$$\Phi_3(x',y',z) = \underline{f}^T(x',z)\mathbf{A}\mathbf{E}(y')\underline{\tau}, \tag{3.10}$$

where for $m,n = 1,\ldots K$

$$\mathbf{E}(y) = diag\left[e^{i\mu_{mn}y}\right] \tag{3.11}$$

and

$$\mathbf{F}(\theta) = diag\left[e^{i\nu_{mn}\theta}\right]. \tag{3.12}$$

Also, for $i = 1, \ldots I$ and $j = 1, \ldots J$ such that $IJ \geq K^2$, $\underline{f}(x,z)$ and $\underline{f}(r,z)$ are column vectors containing the set of basis functions $\{f_{ij}\}$ appearing in equations (2.64) and (2.65). $\mathbf{A}$ and $\mathbf{B}$ are $(IJ \times K^2)$ matrices whose columns are the dominant eigenvectors of equations (2.72) and (2.73) respectively; and $\underline{\alpha}$, $\underline{\beta}$, $\underline{\sigma}$, $\underline{\rho}$ and $\underline{\tau}$ are column vectors containing the corresponding modal coefficients. The μ_{mn} and ν_{mn} in equations (3.11) and (3.12) are the square roots of the dominant eigenvalues of equations (2.72) and (2.73) respectively.

Substitute expressions (3.8)–(3.10) into the continuity equations (3.4)–(3.7). Then pre-multiplying through each equation by $\underline{f}(r,z)$, and integrating over the duct cross-section yields the following set of coupled matrix equations for the modal coefficient vectors:

$$\mathbf{A}\left[\underline{\sigma} + \underline{\rho}\right] = \mathbf{B}\left[\underline{\alpha} + \underline{\beta}\right], \tag{3.13}$$

$$\mathbf{A}\underline{\tau} = \mathbf{B}\left[\mathbf{F}\underline{\alpha} + \mathbf{F}^{-1}\underline{\beta}\right], \tag{3.14}$$

$$\mathbf{M}^{(s)}\mathbf{A}\mathbf{U}\left[\underline{\sigma} - \underline{\rho}\right] = \mathbf{M}^{(c)}\mathbf{B}\mathbf{V}\left[\underline{\alpha} - \underline{\beta}\right] \tag{3.15}$$

and

$$\mathbf{M}^{(s)}\mathbf{A}\mathbf{U}\underline{\tau} = \mathbf{M}^{(c)}\mathbf{B}\mathbf{V}\left[\mathbf{F}\underline{\alpha} - \mathbf{F}^{-1}\underline{\beta}\right]; \tag{3.16}$$

where for $m, n = 1, \ldots K$

$$\mathbf{U} = diag\left[\mu_{mn}\right], \tag{3.17}$$

$$\mathbf{V} = diag\left[\nu_{mn}\right], \tag{3.18}$$

$$\mathbf{F} = diag\left[e^{i\nu_{mn}\theta_{max}}\right] \tag{3.19}$$

and $\mathbf{M}^{(s)}$ and $\mathbf{M}^{(c)}$ are as defined in equations (2.69) and (2.71).

The vectors $\underline{\alpha}$ and $\underline{\beta}$ can be eliminated from equations (3.13)–(3.16) to yield

$$\mathbf{C}\underline{\sigma} + \mathbf{D}\underline{\rho} = \mathbf{F}^{-1}\mathbf{C}\underline{\tau} \tag{3.20}$$

and

$$\mathbf{D}\underline{\sigma} + \mathbf{C}\underline{\rho} = \mathbf{F}\mathbf{D}\underline{\tau}, \tag{3.21}$$

where

$$\mathbf{C} = \mathbf{B}^T\mathbf{M}^{(c)}\mathbf{A} + \mathbf{V}^{-1}\mathbf{B}^T\mathbf{M}^{(s)}\mathbf{A}\mathbf{U} \tag{3.22}$$

and

$$\mathbf{D} = \mathbf{B}^T\mathbf{M}^{(c)}\mathbf{A} - \mathbf{V}^{-1}\mathbf{B}^T\mathbf{M}^{(s)}\mathbf{A}\mathbf{U}. \tag{3.23}$$

Here it should be noted that equation (2.75) has been used, where it is assumed that the eigenvectors are M-normalised. That is

$$\mathbf{B}^T\mathbf{M}^{(c)}\mathbf{B} = \mathbf{I} \tag{3.24}$$

where $\mathbf{I}$ is the $(IJ \times IJ)$ identity matrix. From equations (3.20) and (3.21), the vectors $\underline{\rho}$ and $\underline{\tau}$ can each be eliminated in turn to yield

$$\underline{\tau} = \mathbf{T}\underline{\sigma} \tag{3.25}$$

and

$$\underline{\rho} = \mathbf{R}\underline{\sigma} \tag{3.26}$$

respectively, where

$$\mathbf{T} = \left[\mathbf{C} - \mathbf{F}\mathbf{D}\mathbf{C}^{-1}\mathbf{F}\mathbf{D}\right]^{-1}\mathbf{F}\left[\mathbf{C} - \mathbf{D}\mathbf{C}^{-1}\mathbf{D}\right] \tag{3.27}$$

and

$$\mathbf{R} = \left[\mathbf{C} - \mathbf{F}\mathbf{D}\mathbf{C}^{-1}\mathbf{F}\mathbf{D}\right]^{-1}\left[\mathbf{F}\mathbf{D}\mathbf{C}^{-1}\mathbf{F}\mathbf{C} - \mathbf{D}\right]. \tag{3.28}$$

$\mathbf{T}$ and $\mathbf{R}$ are recognised as being transmission and reflection matrices which specify how the incident straight duct modal coefficients will be scattered from the section of curved duct.

3.2.1 A duct of elliptic cross-section

As the form of equations (3.1)–(3.3) does not depend upon the choice of coordinates used to specify the duct's cross-section, the approximate eigenfunctions calculated in subsection 2.3.1 can be used in their (ξ, η) dependent form to evaluate the modal transmission and reflection matrices for sections of curved elliptic duct. The orthogonality relations for $\phi_{mn}(\xi, \eta)$ and $\psi_{mn}(\xi, \eta)$ are obtained by using equations (2.77) and (2.78) (or (2.81) and (2.82)) to transform equations (2.13) and (2.14) from the (r, z)-plane to the (ξ, η)-plane. This yields

$$\int_{\xi=0}^{\xi_{max}} \int_{\eta=\eta_{min}}^{\eta_{max}} \phi_{mn}\phi_{pq}g^2 \, d\xi \, d\eta = \delta_{mp}\delta_{nq} \tag{3.29}$$

and

$$\int_{\xi=0}^{\xi_{max}} \int_{\eta=\eta_{min}}^{\eta_{max}} \frac{1}{r}\psi_{mn}\psi_{pq}g^2 \, d\xi \, d\eta = \delta_{mp}\delta_{nq}, \tag{3.30}$$

where $g^2(\xi, \eta)$ and $r(\xi, \eta)$ are as defined in equations (2.88) and (2.77) (or (2.81)) respectively, and appropriate normalisations are assumed to have been applied. The set of coupled matrix equations (3.13)–(3.16) are therefore obtained by pre-multiplying the continuity equations through by $g^2(\xi, \eta)\underline{f}(\xi, \eta)$, and integrating them over the limits $\xi \epsilon [0, \xi_{max}]$ and $\eta \epsilon [\eta_{min}, \eta_{max}]$. It follows that the matrices $\mathbf{M}^{(s)}$ and $\mathbf{M}^{(c)}$ whose elements are defined by equations (2.90) and (2.92) can be used in equations (3.22), (3.23), (3.27) and (3.28) to yield approximate expressions for $\mathbf{T}$ and $\mathbf{R}$.

In the following numerical example, $\mathbf{T}$ and $\mathbf{R}$ matrices have been calculated for the modal coefficients associated with the straight duct eigenfunctions plotted in Figures 2.9 and 2.10 when Σ_2 has an angular extent of $\theta_{max} = \pi/2$. Tables 3.1–3.4 show the absolute values of the elements of these $\mathbf{T}$ and $\mathbf{R}$ matrices as the number of terms in the Rayleigh-Ritz modal approximations are increased. In the required calculations, $K = 6$ was used (i.e. 36 modes were assumed to be dominant). Only elements in the top-left (6×6) submatrices of the transmission and reflection matrices are presented in

0.88523E+0	0.24484E+0	0.31697E+0	0.65513E−1	0.18320E−2	0.50297E−2
0.88479E+0	0.24585E+0	0.31763E+0	0.65327E−1	0.18262E−2	0.50331E−2
0.88479E+0	0.24585E+0	0.31763E+0	0.65325E−1	0.18262E−2	0.50155E−2
0.88479E+0	0.24585E+0	0.31763E+0	0.65324E−1	0.18265E−2	0.50147E−2
0.26370E+0	0.69638E+0	0.56391E+0	0.12219E+0	0.36497E−2	0.12385E−1
0.26478E+0	0.69530E+0	0.56510E+0	0.12212E+0	0.36291E−2	0.11867E−1
0.26478E+0	0.69530E+0	0.56511E+0	0.12212E+0	0.36289E−2	0.11807E−1
0.26479E+0	0.69530E+0	0.56511E+0	0.12212E+0	0.36288E−2	0.11807E−1
0.42796E+0	0.70692E+0	0.62866E+0	0.15449E+0	0.59412E−2	0.15682E−1
0.42876E+0	0.70826E+0	0.63028E+0	0.15050E+0	0.58887E−2	0.16448E−1
0.42876E+0	0.70826E+0	0.63029E+0	0.15047E+0	0.58886E−2	0.16397E−1
0.42876E+0	0.70826E+0	0.63030E+0	0.15047E+0	0.58890E−2	0.16395E−1
0.24045E+0	0.41639E+0	0.41996E+0	0.92747E+0	0.59114E−2	0.88530E−1
0.23723E+0	0.41174E+0	0.40486E+0	0.93026E+0	0.59007E−2	0.89249E−1
0.23721E+0	0.41172E+0	0.40478E+0	0.93028E+0	0.59005E−2	0.89033E−1
0.23720E+0	0.41171E+0	0.40478E+0	0.93028E+0	0.59009E−2	0.89029E−1
0.40721E−2	0.75320E−2	0.97808E−2	0.35800E−2	0.24088E−3	0.35712E−3
0.40651E−2	0.75005E−2	0.97111E−2	0.36174E−2	0.24107E−3	0.36522E−3
0.40652E−2	0.75002E−2	0.97107E−2	0.36173E−2	0.24107E−3	0.36454E−3
0.40667E−2	0.74994E−2	0.97104E−2	0.36174E−2	0.24106E−3	0.36453E−3
0.58967E−2	0.13481E−1	0.13617E−1	0.28279E−1	0.18836E−3	0.26820E−2
0.67813E−2	0.14851E−1	0.16420E−1	0.33121E−1	0.22112E−3	0.31771E−2
0.67940E−2	0.14850E−1	0.16455E−1	0.33213E−1	0.22183E−3	0.31786E−2
0.67952E−2	0.14850E−1	0.16452E−1	0.33211E−1	0.22184E−3	0.31782E−2

Table 3.1: *Absolute values of even N-mode $\mathbf{T}$ matrix elements for a uniform bend in an elliptic duct when $\chi = 1.0$, $a = 0.8$, $b = 0.5$, $c = 2.0$, $\theta_{max} = \pi/2$, $K = 6$ and $I = J = 6, 8, 10, 12$.*

0.24162E−2	0.77795E−2	0.44274E−2	0.90847E−2	0.12272E−2	0.96090E−3
0.23709E−2	0.76459E−2	0.42536E−2	0.87955E−2	0.12233E−2	0.99918E−3
0.23715E−2	0.76467E−2	0.42540E−2	0.87936E−2	0.12232E−2	0.99978E−3
0.23729E−2	0.76489E−2	0.42561E−2	0.87927E−2	0.12229E−2	0.99856E−3
0.83788E−2	0.12307E−1	0.14096E−1	0.12254E−1	0.64867E−2	0.53631E−2
0.82378E−2	0.12254E−1	0.13661E−1	0.12044E−1	0.64633E−2	0.53427E−2
0.82363E−2	0.12253E−1	0.13656E−1	0.12043E−1	0.64633E−2	0.53008E−2
0.82354E−2	0.12252E−1	0.13654E−1	0.12043E−1	0.64638E−2	0.52990E−2
0.59776E−2	0.17671E−1	0.16888E−1	0.43111E−1	0.13540E−2	0.67438E−2
0.57425E−2	0.17115E−1	0.16256E−1	0.42525E−1	0.13422E−2	0.74213E−2
0.57426E−2	0.17115E−1	0.16254E−1	0.42521E−1	0.13419E−2	0.74386E−2
0.57434E−2	0.17116E−1	0.16255E−1	0.42520E−1	0.13416E−2	0.74375E−2
0.33343E−1	0.41760E−1	0.11719E+0	0.49307E−1	0.60233E−2	0.89104E−1
0.31938E−1	0.40611E−1	0.11440E+0	0.47617E−1	0.59407E−2	0.89713E−1
0.31931E−1	0.40603E−1	0.11438E+0	0.47602E−1	0.59401E−2	0.89479E−1
0.31933E−1	0.40603E−1	0.11438E+0	0.47601E−1	0.59405E−2	0.89475E−1
0.27278E−2	0.13387E−1	0.22291E−2	0.36477E−2	0.25559E−3	0.14127E−3
0.27229E−2	0.13359E−1	0.22132E−2	0.36417E−2	0.19017E−3	0.76945E−4
0.27229E−2	0.13359E−1	0.22130E−2	0.36415E−2	0.18939E−3	0.75971E−4
0.27232E−2	0.13358E−1	0.22127E−2	0.36419E−2	0.18895E−3	0.76186E−4
0.11265E−2	0.58379E−2	0.58558E−2	0.28462E−1	0.74512E−4	0.30698E−2
0.13432E−2	0.66838E−2	0.74075E−2	0.33294E−1	0.46767E−4	0.36348E−2
0.13543E−2	0.66669E−2	0.74648E−2	0.33380E−1	0.46223E−4	0.37414E−2
0.13554E−2	0.66665E−2	0.74653E−2	0.33378E−1	0.46097E−4	0.37414E−2

Table 3.2: *Absolute values of even N-mode* $\mathbf{R}$ *matrix elements for a uniform bend in an elliptic duct when* $\chi = 1.0$, $a = 0.8$, $b = 0.5$, $c = 2.0$, $\theta_{max} = \pi/2$, $K = 6$ *and* $I = J = 6, 8, 10, 12$.

0.98918E+0	0.12568E+0	0.99104E−2	0.49287E−2	0.59712E−3	0.22436E−3
0.98911E+0	0.12608E+0	0.99045E−2	0.48075E−2	0.21237E−3	0.59470E−3
0.98911E+0	0.12608E+0	0.99045E−2	0.48057E−2	0.21057E−3	0.59458E−3
0.98911E+0	0.12608E+0	0.99045E−2	0.48057E−2	0.21032E−3	0.59482E−3
0.17029E+0	0.98915E+0	0.58156E−1	0.86621E−2	0.40433E−2	0.24507E−2
0.17083E+0	0.98908E+0	0.58005E−1	0.82000E−2	0.32244E−2	0.40168E−2
0.17083E+0	0.98908E+0	0.58004E−1	0.81936E−2	0.32129E−2	0.40166E−2
0.17083E+0	0.98908E+0	0.58004E−1	0.81936E−2	0.32125E−2	0.40161E−2
0.29166E−1	0.12632E+0	0.11994E−1	0.22109E−2	0.52684E−3	0.63327E−3
0.29533E−1	0.12765E+0	0.12232E−1	0.21965E−2	0.79877E−3	0.52953E−3
0.29534E−1	0.12766E+0	0.12234E−1	0.21958E−2	0.79721E−3	0.52954E−3
0.29536E−1	0.12766E+0	0.12234E−1	0.21958E−2	0.79708E−3	0.52948E−3
0.49620E−2	0.64361E−2	0.75633E−3	0.16954E−3	0.27829E−4	0.50431E−4
0.48621E−2	0.61217E−2	0.74502E−3	0.16526E−3	0.58361E−4	0.26404E−4
0.48607E−2	0.61148E−2	0.74478E−3	0.16520E−3	0.58187E−4	0.26374E−4
0.48603E−2	0.61184E−2	0.74478E−3	0.16517E−3	0.58186E−4	0.26386E−4
0.39209E−3	0.19595E−2	0.11755E−3	0.18151E−4	0.80483E−5	0.48419E−5
0.14867E−3	0.16553E−2	0.18624E−3	0.40116E−4	0.86073E−5	0.67199E−5
0.14555E−3	0.16538E−2	0.18658E−3	0.40152E−4	0.86505E−5	0.67132E−5
0.14903E−3	0.16578E−2	0.18682E−3	0.40205E−4	0.86502E−5	0.67295E−5
0.14187E−3	0.11437E−2	0.13606E−3	0.31675E−4	0.46625E−5	0.49030E−5
0.39073E−3	0.19476E−2	0.11667E−3	0.17149E−4	0.63465E−5	0.79472E−5
0.39046E−3	0.19469E−2	0.11663E−3	0.17129E−4	0.63220E−5	0.79439E−5
0.39116E−3	0.19482E−2	0.11671E−3	0.17145E−4	0.63253E−5	0.79484E−5

Table 3.3: *Absolute values of odd N-mode* $\mathbf{T}$ *matrix elements for a uniform bend in an elliptic duct when* $\chi = 1.0$, $a = 0.8$, $b = 0.5$, $c = 2.0$, $\theta_{max} = \pi/2$, $K = 6$ *and* $I = J = 6, 8, 10, 12$.

0.21002E−2	0.94232E−2	0.65470E−2	0.41225E−2	0.22138E−3	0.51439E−3
0.20999E−2	0.94095E−2	0.65361E−2	0.40481E−2	0.52850E−3	0.21942E−3
0.21000E−2	0.94094E−2	0.65361E−2	0.40471E−2	0.52484E−3	0.21931E−3
0.20999E−2	0.94096E−2	0.65360E−2	0.40470E−2	0.52498E−3	0.21956E−3
0.12768E−1	0.76814E−2	0.58701E−1	0.92950E−2	0.41081E−2	0.24006E−2
0.12749E−1	0.77241E−2	0.58555E−1	0.88157E−2	0.31793E−2	0.40817E−2
0.12749E−1	0.77243E−2	0.58554E−1	0.88089E−2	0.31680E−2	0.40815E−2
0.12749E−1	0.77247E−2	0.58554E−1	0.88090E−2	0.31675E−2	0.40810E−2
0.19267E−1	0.12750E+0	0.16329E−1	0.94894E−2	0.16791E−3	0.18015E−2
0.19489E−1	0.12886E+0	0.17266E−1	0.64196E−2	0.17917E−3	0.16662E−3
0.19490E−1	0.12887E+0	0.17274E−1	0.63740E−2	0.17571E−3	0.16598E−3
0.19490E−1	0.12887E+0	0.17275E−1	0.63737E−2	0.17601E−3	0.16737E−3
0.41503E−2	0.69064E−2	0.32462E−2	0.12718E−2	0.32039E−3	0.72603E−2
0.40941E−2	0.65812E−2	0.21779E−2	0.25971E−3	0.35447E−2	0.30019E−3
0.40935E−2	0.65743E−2	0.21610E−2	0.22782E−3	0.33514E−2	0.29871E−3
0.40929E−2	0.65776E−2	0.21618E−2	0.22770E−3	0.33516E−2	0.30041E−3
0.14537E−3	0.19909E−2	0.37465E−4	0.20897E−3	0.12998E−4	0.39763E−4
0.36691E−3	0.16324E−2	0.41970E−4	0.24361E−2	0.68736E−3	0.31041E−4
0.36682E−3	0.16305E−2	0.41363E−4	0.23129E−2	0.84978E−3	0.32373E−4
0.36622E−3	0.16349E−2	0.41085E−4	0.23106E−2	0.84922E−3	0.29829E−4
0.32526E−3	0.11203E−2	0.38706E−3	0.45600E−2	0.38290E−4	0.59740E−3
0.14425E−3	0.19791E−2	0.36708E−4	0.19472E−3	0.30100E−4	0.24924E−4
0.14387E−3	0.19784E−2	0.36556E−4	0.19449E−3	0.29576E−4	0.25117E−4
0.14507E−3	0.19797E−2	0.36834E−4	0.19437E−3	0.30159E−4	0.25601E−4

Table 3.4: *Absolute values of odd N-mode* $\mathbf{R}$ *matrix elements for a uniform bend in an elliptic duct when* $\chi = 1.0$, $a = 0.8$, $b = 0.5$, $c = 2.0$, $\theta_{max} = \pi/2$, $K = 6$ *and* $I = J = 6, 8, 10, 12$.

Tables 3.1–3.4. Looking down a given block of 4 numbers in these tables, one can see the convergence of an element's absolute value as I and J are increased in the manner $I = J = 6, 8, 10, 12$. A point of interest is the accuracy of $\mathbf{T}$ and $\mathbf{R}$ with respect to energy conservation. Theoretically (subsect. 2.1.4), due to the idealised wall conditions, acoustic energy will be conserved within the ducting system. Hence, the net acoustic energy flux through the ends of Σ_2 will be zero. A consequence of this condition is that (see reference [35]) the elements of $\mathbf{T}$ and $\mathbf{R}$ satisfy the reciprocity relations given in references [35–37], namely

$$\mu_i T_{ij} = \mu_j T_{ji} \tag{3.31}$$

and

$$\mu_i R_{ij} = \mu_j R_{ji}, \tag{3.32}$$

where μ_i is the propagation constant associated with the i^{th} dominant straight duct mode. Therefore, an indication of the accuracy of $\mathbf{T}$ and $\mathbf{R}$ with respect to energy conservation is given by the magnitudes of the relative errors

$$\kappa_{ij} = \left| \frac{\mu_i T_{ij}}{\mu_j T_{ji}} - 1 \right| \tag{3.33}$$

and

$$\zeta_{ij} = \left| \frac{\mu_i R_{ij}}{\mu_j R_{ji}} - 1 \right|. \tag{3.34}$$

In practice, it is found that κ_{ij} and ζ_{ij} are always zero (to within the precision used on the computer). Hence, numerically, energy is conserved in the calculations, even though the solution is not exact. This result is due to the fact that the eigenfunctions determined by the Rayleigh-Ritz method are orthogonal.

3.3 MODAL SCATTERING FROM TWO OR MORE DUCT BENDS

Consider a ducting system which has been subdivided into a series of straight and uniformly curved segments, as shown in Figure 3.2. Supposing that there are N segments,

the ducting system can be equivalently interpreted as being the cascade of modal scatterers shown in Figure 3.3. Waves traversing the junctions between neighbouring segments are represented by a superposition of M straight duct modes, whose coefficients are contained in the $(M \times 1)$ column vectors $\underline{a}_n$ and $\underline{b}_n$ $(n = 0, \ldots N)$. The intrinsic linear characteristics of the system enable the modal coefficient vectors of waves incident upon the n^{th} segment, to be related to those of waves scattered from it via the introduction of a $(2M \times 2M)$ partitioned matrix $\mathbf{S}^{(n)}$, such that

$$\begin{bmatrix} \underline{a}_n \\ \underline{b}_{n-1} \end{bmatrix} = \begin{bmatrix} \mathbf{S}_{11}^{(n)} & \mathbf{S}_{12}^{(n)} \\ \mathbf{S}_{21}^{(n)} & \mathbf{S}_{22}^{(n)} \end{bmatrix} \begin{bmatrix} \underline{a}_{n-1} \\ \underline{b}_n \end{bmatrix}. \tag{3.35}$$

$\mathbf{S}^{(n)}$ is referred to as the modal scattering matrix of the n^{th} segment.

Typically, the submatrices of $\mathbf{S}^{(n)}$ are found by calculating $(M \times M)$ modal transmission and reflection matrices for the segment. It follows from the definition of $\mathbf{S}^{(n)}$ in equation (3.35), and the symmetrical curvature of each segment that

$$\mathbf{S}_{11}^{(n)} = \mathbf{S}_{22}^{(n)} = \mathbf{T} \tag{3.36}$$

and

$$\mathbf{S}_{12}^{(n)} = \mathbf{S}_{21}^{(n)} = \mathbf{R}. \tag{3.37}$$

For a straight segment of length L,

$$\mathbf{R} = \mathbf{0} \tag{3.38}$$

and

$$\mathbf{T} = diag\left[e^{i\mu_m L}\right], \tag{3.39}$$

where μ_m $\{m = 1, \ldots M\}$ is the propagation constant associated with the m^{th} dominant straight duct mode. One can see that the matrix elements in equation (3.39) simply specify the appropriate phase shifts which will occur as modes propagate through the straight segment. For a uniformly curved segment, $\mathbf{T}$ and $\mathbf{R}$ can be calculated by one of the specific methods appearing in the papers [16, 22, 38], or by the general method

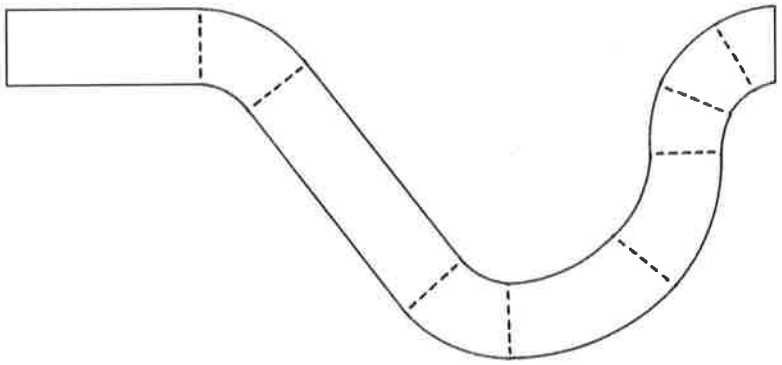

Figure 3.2: *A typical ducting system and its subdivision into a series of straight and uniformly curved segments.*

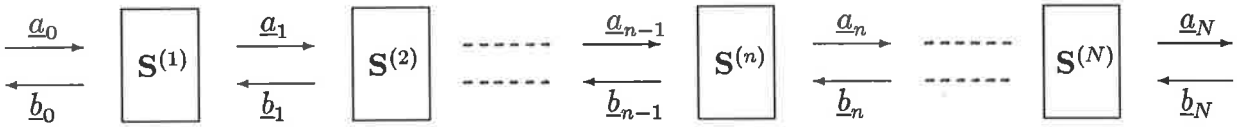

Figure 3.3: *Diagrammatic representation of a series of N straight and uniformly curved duct segments as a cascade of modal scatterers.*

presented in section 3.2. Here it should be noted that for uniformly curved segments, equations (3.36) and (3.37) are only exact if the duct cross-section has a vertical line of symmetry (e.g. rectangular, elliptic). The matrices $\mathbf{S}_{11}^{(n)}$, $\mathbf{S}_{22}^{(n)}$ and $\mathbf{S}_{12}^{(n)}$, $\mathbf{S}_{21}^{(n)}$ will not be the same if the duct cross-section does not have this symmetry. For such cases, these matrices must be calculated by considering the transmission and reflection of modes from both ends of the segment.

In the next two subsections, algorithms are derived which combine the modal scattering matrices of the segments to form a modal scattering matrix for the cascade $\mathbf{S}^{(cas)}$, such that

$$\begin{bmatrix} \underline{a}_N \\ \underline{b}_0 \end{bmatrix} = \begin{bmatrix} \mathbf{S}_{11}^{(cas)} & \mathbf{S}_{12}^{(cas)} \\ \mathbf{S}_{21}^{(cas)} & \mathbf{S}_{22}^{(cas)} \end{bmatrix} \begin{bmatrix} \underline{a}_0 \\ \underline{b}_N \end{bmatrix}. \tag{3.40}$$

3.3.1 Transfer matrix algorithm

Consider the n^{th} segment in the cascade shown in Figure 3.3. From equation (3.35), we have explicitly

$$\underline{a}_n = \mathbf{S}_{11}^{(n)} \underline{a}_{n-1} + \mathbf{S}_{12}^{(n)} \underline{b}_n \tag{3.41}$$

and

$$\underline{b}_{n-1} = \mathbf{S}_{21}^{(n)} \underline{a}_{n-1} + \mathbf{S}_{22}^{(n)} \underline{b}_n. \tag{3.42}$$

Equations (3.41) and (3.42) can be combined and reassembled to form the partitioned matrix equation

$$\begin{bmatrix} \underline{a}_n \\ \underline{b}_n \end{bmatrix} = \begin{bmatrix} \mathbf{Q}_{11}^{(n)} & \mathbf{Q}_{12}^{(n)} \\ \mathbf{Q}_{21}^{(n)} & \mathbf{Q}_{22}^{(n)} \end{bmatrix} \begin{bmatrix} \underline{a}_{n-1} \\ \underline{b}_{n-1} \end{bmatrix}, \tag{3.43}$$

where

$$\mathbf{Q}_{22}^{(n)} = \left(\mathbf{S}_{22}^{(n)}\right)^{-1}, \tag{3.44}$$

$$\mathbf{Q}_{21}^{(n)} = -\mathbf{Q}_{22}^{(n)} \mathbf{S}_{21}^{(n)}, \tag{3.45}$$

$$\mathbf{Q}_{12}^{(n)} = \mathbf{S}_{12}^{(n)} \mathbf{Q}_{22}^{(n)} \tag{3.46}$$

and

$$\mathbf{Q}_{11}^{(n)} = \mathbf{S}_{11}^{(n)} - \mathbf{Q}_{12}^{(n)}\mathbf{S}_{21}^{(n)}. \tag{3.47}$$

The partitioned matrix $\mathbf{Q}^{(n)}$, is referred to as the modal transfer matrix of the n^{th} segment as it relates modal coefficient vectors on the right (output) side of the segment to those on its left (input) side. The modal transfer matrix of the entire cascade is therefore obtained by multiplying the modal transfer matrices of the segments together. Hence

$$\begin{bmatrix} \underline{a}_N \\ \underline{b}_N \end{bmatrix} = \begin{bmatrix} \mathbf{Q}_{11}^{(cas)} & \mathbf{Q}_{12}^{(cas)} \\ \mathbf{Q}_{21}^{(cas)} & \mathbf{Q}_{22}^{(cas)} \end{bmatrix} \begin{bmatrix} \underline{a}_0 \\ \underline{b}_0 \end{bmatrix}, \tag{3.48}$$

where

$$\mathbf{Q}^{(cas)} = \mathbf{Q}^{(N)}\mathbf{Q}^{(N-1)} \ldots \mathbf{Q}^{(1)}. \tag{3.49}$$

Having calculated $\mathbf{Q}^{(cas)}$, the modal scattering matrix of the cascade is obtained by effectively inverting equations (3.44)–(3.47) to obtain

$$\mathbf{S}_{22}^{(cas)} = \left(\mathbf{Q}_{22}^{(cas)}\right)^{-1}, \tag{3.50}$$

$$\mathbf{S}_{21}^{(cas)} = -\mathbf{S}_{22}^{(cas)}\mathbf{Q}_{21}^{(cas)}, \tag{3.51}$$

$$\mathbf{S}_{12}^{(cas)} = \mathbf{Q}_{12}^{(cas)}\mathbf{S}_{22}^{(cas)} \tag{3.52}$$

and

$$\mathbf{S}_{11}^{(cas)} = \mathbf{Q}_{11}^{(cas)} - \mathbf{S}_{12}^{(cas)}\mathbf{Q}_{21}^{(cas)}. \tag{3.53}$$

The transfer matrix algorithm is numerically efficient as only one matrix inversion and three matrix multiplications are required to calculate each $\mathbf{Q}^{(n)}$. However, the algorithm has shortcomings when it is assumed that evanescent modes are excited at the junctions between neighbouring segments. This point is best illustrated by considering the modal transfer matrix of the n^{th} segment if it is taken to be straight and of length L. Substituting equations (3.36)–(3.39) into equations (3.44)–(3.47) we have

$$\mathbf{Q}_{11}^{(n)} = diag\left[e^{i\mu_m L}\right], \tag{3.54}$$

$$\mathbf{Q}_{22}^{(n)} = diag\left[e^{-i\mu_m L}\right] \tag{3.55}$$

and

$$\mathbf{Q}_{12}^{(n)} = \mathbf{Q}_{21}^{(n)} = \mathbf{0}. \tag{3.56}$$

When μ_m is imaginary, positive exponential matrix elements are generated. These elements will predictably cause numerical instability and overflow problems when implementing the algorithm on a computer.

3.3.2 Iterative scattering matrix algorithm

Firstly, consider a two segment cascade. Setting $n = 1, 2$ in equation (3.35) yields

$$\underline{a}_1 = \mathbf{S}_{11}^{(1)}\underline{a}_0 + \mathbf{S}_{12}^{(1)}\underline{b}_1, \tag{3.57}$$

$$\underline{b}_0 = \mathbf{S}_{21}^{(1)}\underline{a}_0 + \mathbf{S}_{22}^{(1)}\underline{b}_1, \tag{3.58}$$

$$\underline{a}_2 = \mathbf{S}_{11}^{(2)}\underline{a}_1 + \mathbf{S}_{12}^{(2)}\underline{b}_2 \tag{3.59}$$

and

$$\underline{b}_1 = \mathbf{S}_{21}^{(2)}\underline{a}_1 + \mathbf{S}_{22}^{(2)}\underline{b}_2. \tag{3.60}$$

Eliminating the modal coefficient vectors $\underline{a}_1$ and $\underline{b}_1$ from equations (3.57)–(3.60), and reassembling the resulting pair of equations yields the partitioned matrix equation

$$\begin{bmatrix} \underline{a}_2 \\ \underline{b}_0 \end{bmatrix} = \begin{bmatrix} \mathbf{S}_{11}^{(cas)} & \mathbf{S}_{12}^{(cas)} \\ \mathbf{S}_{21}^{(cas)} & \mathbf{S}_{22}^{(cas)} \end{bmatrix} \begin{bmatrix} \underline{a}_0 \\ \underline{b}_2 \end{bmatrix}, \tag{3.61}$$

where

$$\mathbf{S}_{11}^{(cas)} = \mathbf{S}_{11}^{(2)}\mathbf{E}\mathbf{S}_{11}^{(1)}, \tag{3.62}$$

$$\mathbf{S}_{12}^{(cas)} = \mathbf{S}_{12}^{(2)} + \mathbf{S}_{11}^{(2)}\mathbf{S}_{12}^{(1)}\mathbf{F}\mathbf{S}_{22}^{(2)}, \tag{3.63}$$

$$\mathbf{S}_{21}^{(cas)} = \mathbf{S}_{21}^{(1)} + \mathbf{S}_{22}^{(1)}\mathbf{S}_{21}^{(2)}\mathbf{E}\mathbf{S}_{11}^{(1)}, \tag{3.64}$$

$$\mathbf{S}_{22}^{(cas)} = \mathbf{S}_{22}^{(1)}\mathbf{F}\mathbf{S}_{22}^{(2)}, \tag{3.65}$$

$$\mathbf{E} = \left(\mathbf{I} - \mathbf{S}_{12}^{(1)}\mathbf{S}_{21}^{(2)}\right)^{-1} \tag{3.66}$$

and

$$\mathbf{F} = \left(\mathbf{I} - \mathbf{S}_{21}^{(2)}\mathbf{S}_{12}^{(1)}\right)^{-1} \tag{3.67}$$

where $\mathbf{I}$ is the $(M \times M)$ identity matrix. Of course, $\mathbf{S}^{(cas)}$ is the modal scattering matrix of the two segment cascade. If a third segment is now added to the cascade, the modal scattering matrix for this new cascade can be found by setting $\mathbf{S}^{(1)}$ = the old $\mathbf{S}^{(cas)}$ and $\mathbf{S}^{(2)} = \mathbf{S}^{(3)}$ in equations (3.62)–(3.67). This iterative process can be continued until all of the segments in an N segment cascade have been considered.

The iterative scattering matrix algorithm requires two matrix inversions and twelve matrix multiplications per iteration, and is therefore not as efficient as the transfer matrix algorithm. However, it does have the advantage that any number of evanescent modes can be included in the calculations. For example, consider a cascade consisting of two straight segments of lengths $L1$ and $L2$. Substituting equations (3.36)–(3.39) into equations (3.62)–(3.67) yields

$$\mathbf{S}_{11}^{(cas)} = \mathbf{S}_{22}^{(cas)} = diag\left[e^{i\mu_m(L1+L2)}\right] \tag{3.68}$$

and

$$\mathbf{S}_{12}^{(cas)} = \mathbf{S}_{21}^{(cas)} = \mathbf{0}. \tag{3.69}$$

Therefore, when μ_m is imaginary, only negative exponential matrix elements are generated. Not only does this ensure that the algorithm is numerically stable, but also it localises the effects of fringing caused by the generation of evanescent modes at the junctions between neighbouring segments.

3.3.3 Calculating Φ within a duct segment

General expressions for the coefficients of the modes within each segment can be determined while the scattering matrices are being combined. One means of performing

these calculations is as follows.

Let $\mathbf{S}^{(it:n)}$ be the modal scattering matrix obtained after the n^{th} iteration ($n = 0, 1, \ldots$) of the iterative scattering matrix algorithm. Then

$$\begin{bmatrix} \underline{a}_{n+1} \\ \underline{b}_0 \end{bmatrix} = \mathbf{S}^{(it:n)} \begin{bmatrix} \underline{a}_0 \\ \underline{b}_{n+1} \end{bmatrix}. \tag{3.70}$$

If the modal transfer matrix $\mathbf{Q}^{(it:n)}$ is calculated from $\mathbf{S}^{(it:n)}$ in the manner prescribed by equations (3.44)–(3.47), then

$$\begin{bmatrix} \underline{a}_{n+1} \\ \underline{b}_{n+1} \end{bmatrix} = \mathbf{Q}^{(it:n)} \begin{bmatrix} \underline{a}_0 \\ \underline{b}_0 \end{bmatrix}. \tag{3.71}$$

Now, from equation (3.40) we have

$$\begin{bmatrix} \underline{a}_0 \\ \underline{b}_0 \end{bmatrix} = \begin{bmatrix} \mathbf{I} & \mathbf{0} \\ \mathbf{S}_{21}^{(cas)} & \mathbf{S}_{22}^{(cas)} \end{bmatrix} \begin{bmatrix} \underline{a}_0 \\ \underline{b}_N \end{bmatrix} \tag{3.72}$$

where $\mathbf{I}$ and $\mathbf{0}$ are the $(M \times M)$ identity and zero matrices respectively. Therefore, combining equations (3.71) and (3.72) yields

$$\begin{bmatrix} \underline{a}_{n+1} \\ \underline{b}_{n+1} \end{bmatrix} = \mathbf{Q}^{(it:n)} \begin{bmatrix} \mathbf{I} & \mathbf{0} \\ \mathbf{S}_{21}^{(cas)} & \mathbf{S}_{22}^{(cas)} \end{bmatrix} \begin{bmatrix} \underline{a}_0 \\ \underline{b}_N \end{bmatrix}. \tag{3.73}$$

If the ducting system is anechoically terminated, $\underline{b}_N = \underline{0}$, and equation (3.73) yields explicitly

$$\underline{a}_{n+1} = \left[\mathbf{Q}_{11}^{(it:n)} + \mathbf{Q}_{12}^{(it:n)}\mathbf{S}_{21}^{(cas)}\right] \underline{a}_0 \tag{3.74}$$

and

$$\underline{b}_{n+1} = \left[\mathbf{Q}_{21}^{(it:n)} + \mathbf{Q}_{22}^{(it:n)}\mathbf{S}_{21}^{(cas)}\right] \underline{a}_0. \tag{3.75}$$

In equation (3.73), the modal coefficient vectors of waves traversing the junction between the $(n+1)^{th}$ and $(n+2)^{th}$ segments are expressed in terms of the modal coefficient vectors of waves incident upon the cascade. If the $(n+2)^{th}$ segment is

straight, then $\underline{a}_{n+1}$ and $\underline{b}_{n+1}$ directly specify the coefficients of the modes which define Φ throughout that segment. If the $(n+2)^{th}$ segment is curved, then as $\underline{a}_{n+1}$ and $\underline{b}_{n+1}$ specify Φ at one end of this segment, enforcing the requirement that Φ and its gradient be continuous at that end enables general expressions for the coefficients of the curved duct modes within that segment to be determined. To give a specific illustration of this matching technique, it is applied to the formulation presented in section 3.2. In that formulation, the straight duct modal coefficient vectors $\underline{\sigma}$ and $\underline{\rho}$ play equivalent roles to $\underline{a}_{n+1}$ and $\underline{b}_{n+1}$. Applying the appropriate continuity conditions for Φ and its gradient at the junction ($\theta = 0$) yields equations (3.13) and (3.15). These equations can be solved for the curved duct modal coefficient vectors $\underline{\alpha}$ and $\underline{\beta}$ to yield

$$\begin{bmatrix} \underline{\alpha} \\ \underline{\beta} \end{bmatrix} = \frac{1}{2} \begin{bmatrix} \mathbf{C} & \mathbf{D} \\ \mathbf{D} & \mathbf{C} \end{bmatrix} \begin{bmatrix} \underline{a}_{n+1} \\ \underline{b}_{n+1} \end{bmatrix}. \tag{3.76}$$

Here, the matrices $\mathbf{C}$ and $\mathbf{D}$ are as defined in equations (3.22) and (3.23). Hence, using equation (3.76) in conjunction with equation (3.73), a general expression for Φ within the curved segment is obtained.

3.3.4 Out-of-plane and serpentine bends

When calculating the modal scattering matrix of each bend in a curved ducting system, it is convenient to do so using a coordinate system in which the bend assumes a standard orientation (e.g. the "left-handed" orientation assumed in section 3.2). If the ducting system is planar and contains bends which are all actually orientated in this way, then the algorithms presented in subsections 3.3.1–3.3.3 can be used directly on the resulting scattering matrix cascade without problem. However, if the ducting system contains a bend (or bends) which has a different plane or direction of curvature to the bend preceding it, then an extra "acoustic potential reorientation" scattering matrix must be introduced into the cascade. This $\mathbf{S}^{(apr)}$ matrix is located in the cascade directly

before the modal scattering matrix of the bend, and operates on the straight duct modal coefficient vectors at this point. It transforms these vectors so that the acoustic potential is reorientated in such a way that it allows the bend to be considered as if it had the standard orientation.

A mathematical derivation of the $\mathbf{S}^{(apr)}$ matrix for an out-of-plane bend is now given with the aid of Figure 3.4, which shows a view of the entrance to the bend, as seen from the preceding duct segment. Here, the x'-axis lies in the plane of curvature of the bend's centreline, the x-axis lies in the plane of curvature of the previous bend's centreline and the y-axis points into the page, with $y = 0$ specifying the entrance to the bend. The

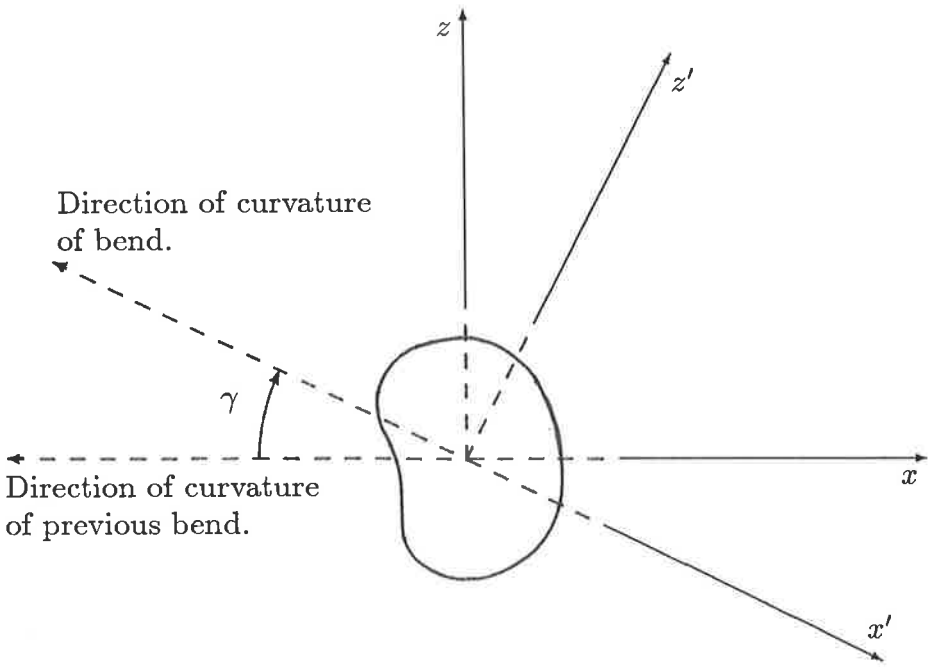

Figure 3.4: *Cross-sectional view of the entrance to an out-of-plane bend showing the direction of curvature of the bend inclined at an angle γ to the direction of curvature of the previous bend.*

(x, z) coordinates are related to the (x', z') coordinates via the equation

$$\begin{bmatrix} x \\ z \end{bmatrix} = \begin{bmatrix} \cos\gamma & \sin\gamma \\ -\sin\gamma & \cos\gamma \end{bmatrix} \begin{bmatrix} x' \\ z' \end{bmatrix}. \tag{3.77}$$

Assuming that the standard bend orientation is left-handed, $\gamma = 0$ implies that the bend has the same left-hand orientation as the previous bend, $\gamma = \pi$ implies that the bend has a right-hand orientation, $\gamma = \pi/2$ implies that the bend is orientated so that it curves vertically upward, and so on.

Now, let Ω and Ω' define the duct's cross-sectional domain on the (x, z) and (x', z') coordinate planes respectively. Also, let μ_n $(n = 1, \ldots M)$ be the propagation constant associated with the n^{th} dominant straight duct mode, with ϕ_n and ϕ_n' being the corresponding acoustic eigenfunctions on Ω and Ω' respectively. The acoustic potential on Ω is given by

$$\Phi = \left[\sum_{n=1}^{M} \left[a_n e^{i\mu_n y} + b_n e^{-i\mu_n y}\right] \phi_n(x, z)\right]_{y=0}. \tag{3.78}$$

Similarly, the acoustic potential on Ω' is given by

$$\Phi' = \left[\sum_{n=1}^{M} \left[a_n' e^{i\mu_n y} + b_n' e^{-i\mu_n y}\right] \phi_n'(x', z')\right]_{y=0}. \tag{3.79}$$

For Φ and Φ' to specify the same acoustic pressure and particle velocity fields, we must have

$$[\Phi(x, y, z)]_{y=0} = [\Phi'(x', y, z')]_{y=0} \tag{3.80}$$

and

$$\left[\frac{\partial \Phi}{\partial y}(x, y, z)\right]_{y=0} = \left[\frac{\partial \Phi'}{\partial y}(x', y, z')\right]_{y=0}, \tag{3.81}$$

where it is assumed that equation (3.77) is satisfied by the (x, z) and (x', z') coordinates. Substituting equations (3.78) and (3.79) into equations (3.80) and (3.81) yields

$$\sum_{n=1}^{M} [a_n + b_n] \phi_n(x, z) = \sum_{n=1}^{M} \left[a_n' + b_n'\right] \phi_n'(x', z') \tag{3.82}$$

and

$$\sum_{n=1}^{M} \mu_n [a_n - b_n] \phi_n(x, z) = \sum_{n=1}^{M} \mu_n \left[a_n' - b_n'\right] \phi_n'(x', z'). \tag{3.83}$$

Multiplying through equations (3.82) and (3.83) by $\phi'_m(x', z')$ $(m = 1, \ldots M)$, integrating the resulting equations over Ω', and using the orthogonality of the modes yields the pair of matrix equations

$$\mathbf{H}\,(\underline{a} + \underline{b}) = \underline{a}' + \underline{b}' \tag{3.84}$$

and

$$\mathbf{HU}\,(\underline{a} - \underline{b}) = \mathbf{U}\,(\underline{a}' - \underline{b}')\,, \tag{3.85}$$

where

$$H_{mn} = \iint_{\Omega'} \phi'_m(x', z')\phi_n(x, z)\, dx'\, dz' \tag{3.86}$$

and

$$U_{mn} = diag\,[\mu_m]\,. \tag{3.87}$$

Rearranging equations (3.84) and (3.85), the partitioned transfer matrix $\mathbf{Q}^{(apr)}$ is defined such that

$$\begin{bmatrix} \underline{a}' \\ \underline{b}' \end{bmatrix} = \begin{bmatrix} \mathbf{Q}_{11}^{(apr)} & \mathbf{Q}_{12}^{(apr)} \\ \mathbf{Q}_{21}^{(apr)} & \mathbf{Q}_{22}^{(apr)} \end{bmatrix} \begin{bmatrix} \underline{a} \\ \underline{b} \end{bmatrix}, \tag{3.88}$$

where

$$\mathbf{Q}_{11}^{(apr)} = \mathbf{Q}_{22}^{(apr)} = \frac{1}{2}\left[\mathbf{H} + \mathbf{U}^{-1}\mathbf{HU}\right] \tag{3.89}$$

and

$$\mathbf{Q}_{12}^{(apr)} = \mathbf{Q}_{21}^{(apr)} = \frac{1}{2}\left[\mathbf{H} - \mathbf{U}^{-1}\mathbf{HU}\right]. \tag{3.90}$$

Note that if there is a $\mu_m = 0$, then equations (3.89) and (3.90) are not valid. When this occurs, the rows of $\mathbf{Q}^{(apr)}$ which specify a'_m and b'_m are obtained by setting $b'_m = b_m$ and using equation (3.84) to yield $a'_m = H_{mn}(a_n + b_n) - b_m$, where the repeated indices indicate a summation. Finally, the $\mathbf{S}^{(apr)}$ matrix is obtained from $\mathbf{Q}^{(apr)}$ in an analogous manner to that prescribed by equations (3.50)–(3.53). Hence, one can see that the introduction of an $\mathbf{S}^{(apr)}$ matrix into a scattering matrix cascade will have the effect of implicitly ensuring that the acoustic potential is reorientated in the required manner at that point.

Practically, there are some important points to be considered when using the $\mathbf{S}^{(apr)}$ matrices. Firstly, it is important to observe that one may no longer have the freedom to assume that Φ is comprised only of modes with special symmetries (e.g. odd, even), as these symmetries may not apply to Φ within an out-of-plane bend. Also, if one wishes to determine Φ within an out-of-plane or oppositely curved bend, the transformed modal coefficient vectors should be the ones used to specify Φ at the bend's entrance. The acoustic field obtained within the bend will therefore be the one experienced by an observer who sees the bend orientated in its standard sense. Finally, if the duct cross-section has no rotational symmetry, then the straight duct eigenmodes will be unambiguously defined such that $\phi_n(x,z) = \phi_n'(x',z')$. Under these circumstances, equations (3.86), (3.89) and (3.90) show that $\mathbf{S}^{(apr)}$ will reduce to the $(2M \times 2M)$ identity matrix.

3.4 SUMMARY

In this chapter, methods were developed for the study of acoustic wave propagation within ducting systems which contain one or more bends of constant curvature. Initially, propagation within a simple, single bend ducting system was considered. A general method, which utilised the numerical solution procedure of Chapter 2, was presented for calculating modal transmission and reflection matrices for the bend. In an example, a 90^0 bend in a duct of elliptic cross-section was considered, and the accuracy of the transmission and reflection matrices was shown to improve as the numerical solution procedure was refined. Also, it was noted that the transmission and reflection matrices satisfied reciprocity relations, thereby showing that the calculations were consistent with energy conservation principles.

After completing the analysis of the simple, single bend ducting system, it was proposed that complicated multi-bend ducting systems should be analysed by subdividing

them into a series of purely curved and straight sections. By calculating modal transmission and reflection matrices (and therefore a modal scattering matrix) for each section, a sytem was analysed by considering it to be a cascade of modal scatterers. A transfer matrix algorithm and an iterative scattering matrix algorithm were presented which both enabled the modal scattering matrix of a cascade of modal scatterers to be calculated. It was noted that the iterative scattering matrix algorithm had the advantage that it enabled evanescent modes to be readily included in the calculations. A method for determining the acoustic potential within any element of a cascade was then presented, and finally, out-of-plane and serpentine duct bends were considered.

Hence, the necessary methods were developed to enable one to successfully determine the acoustic characteristics of a wide variety of uniformly curved, multi-bend ducting systems. The scattering cascade approach to this problem has a number of favourable characteristics. Firstly, it allows the acoustic characteristics of a ducting system to be determined from the independent analyses of each of its constituent components. Thus a single, large, complicated problem is broken down into a series of smaller, less complicated problems — namely, the determination of each component's modal scattering matrix. As these matrices provide a compact and complete description of the acoustic characteristics of each component, an analysis can be implemented which only makes modest demands on computer memory. Also, the effects of adding extra components onto a previously analysed ducting system can be determined without the performance of major recalculations. Finally, if the same component occurs more than once within a ducting system, it need only be analysed once. A good example of how these principles can be used to simplify the solution of a curved duct problem is as follows. Suppose one wishes to investigate how the modal scattering matrix $\mathbf{S}$, of a section of uniformly curved duct varies with the length of the duct's centreline axis. Ordinarily, one would need to repeatedly calculate $\mathbf{S}$ from its definition for a series of centreline lengths. However, the problem is more efficiently solved by calculating $\triangle\mathbf{S}$, where $\triangle\mathbf{S}$ is the modal

scattering matrix of a small section of the duct, and using $\Delta\mathbf{S}$ repeatedly in the iterative scattering matrix algorithm — outputting $\mathbf{S}^{(cas)}$ after each iteration. This type of "duct segment" approach will be used to great advantage in the next chapter, where the idea of representing a non-uniformly curved duct bend by a series of uniformly curved duct segments will be presented.

CHAPTER 4

— ◇ —

ACOUSTIC WAVE PROPAGATION WITHIN NON-UNIFORMLY CURVED DUCTS

4.1 INTRODUCTION

It was seen in Chapter 2 that the task of determining solutions to equations (1.1)–(1.3) within uniformly curved ducts was complicated by the fact that in general, only the longitudinal θ-coordinate variations of Φ could be expressed via a separable factor. This meant that a two-dimensional analysis was required to determine the transverse coordinate variations of Φ within the duct. Hence, if the uniformly curved duct problem is compared with a problem in which Φ takes a fully separable form, this complication can be considered to roughly square the amount of effort (numerical or analytical) required to obtain a solution. Needless to say, the fact that the coordinate variations of Φ generally remain completely coupled within non-uniformly curved ducts adds a greater degree of difficulty to the problems considered in this chapter.

In sections 4.2 and 4.3, two different numerical methods for solving equations (1.1)–(1.3) within non-uniformly curved ducts will be presented. Rectangular cross-sectioned ducts are considered when presenting these methods because they enable the dimensionality of the problem to be reduced without altering the basic principles behind the methods. Also, when developing these methods, an emphasis is placed upon their ability to determine a modal scattering matrix for the bend. This is done so that the methods can be readily assimilated into the multi-bend analysis procedure of Chapter 3. In the

first method, a generalised coordinate transformation is used to map the longitudinal axis of the duct onto a straight line. This has the effect of simplifying the duct wall conditions to be satisfied by Φ. The Galerkin method is then used to determine a functional series representation for Φ within the duct. In an example, the method is used to analyse a section of spirally curved duct. The second method uses the fact that the curvature of any non-uniformly curved duct remains essentially constant within small intervals along its length. The duct can therefore be geometrically approximated by a series of uniformly curved duct segments, joined end to end. Hence, by using the theory of Chapters 2 and 3, the acoustic characteristics of this "multi-bend ducting system" can be determined. The same section of spirally curved duct considered earlier is analysed in an example, and comparisons are made.

In section 4.4, the second method is extended so that ducts of arbitrary cross-section can be studied. The power of the method is demonstrated by using it to study the propagation of acoustic waves within sections of parabolically curved, elliptic and circular duct.

4.2 RECTANGULAR CROSS-SECTIONED DUCTS — A NUMERICAL SOLUTION WHICH USES A GENERALISED COORDINATE TRANSFORMATION AND THE GALERKIN METHOD

Here, in a formulation which is similar in context to the one presented in section 3.2, a study is made of the propagation of acoustic waves through a single, non-uniformly curved duct bend. The duct is assumed to have a rectangular cross-section, with height H in the z-axis direction (assumed to point out of the page), and lying on the (x, y)-plane in the manner shown in Figure 4.1. The inner wall of the bend is taken to follow the curve defined by the polar equation $r = R(\theta)$, where $0 \leq \theta \leq \theta_{max}$ and R is a continuous, monotonic function of θ. If $\underline{n}(\theta)$ is a unit vector, normal to this curve, and

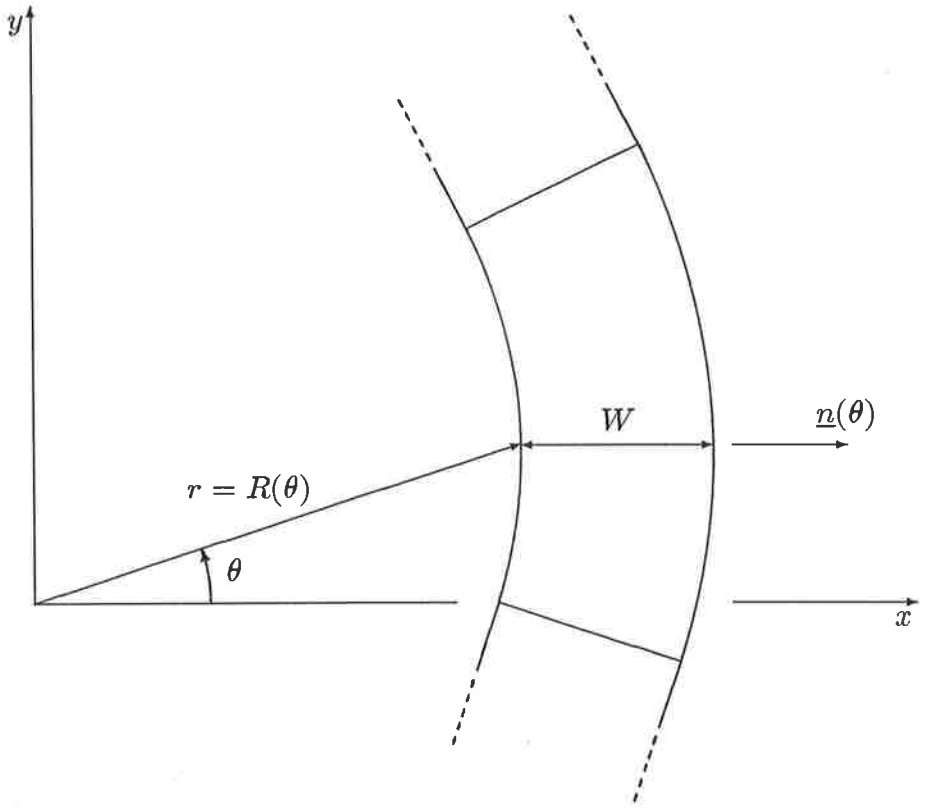

Figure 4.1: *Top view of a non-uniformly curved duct bend.*

points away from its centre of curvature, then the outer wall will be a distance W from the inner wall (as measured along $\underline{n}(\theta)$), and will also be normal to $\underline{n}(\theta)$.

The required solutions to equations (1.1)–(1.3) are most conveniently obtained by subdividing the duct into the regions Σ_1, Σ_2 and Σ_3; as shown in Figure 4.2. Figure 4.2 also shows the definition of (x', y') and (x'', y'') coordinate axes. It follows from the theory presented in subsections 2.1.1 and 2.2.1 that with respect to these coordinates, acceptable general solutions to equations (1.1)–(1.3) within Σ_1 and Σ_3 are

$$\Phi_1(x', y') = \sum_{m=1}^{M} \left[\sigma_m e^{i\mu_m y'} + \rho_m e^{-i\mu_m y'}\right] \phi_m(x') \tag{4.1}$$

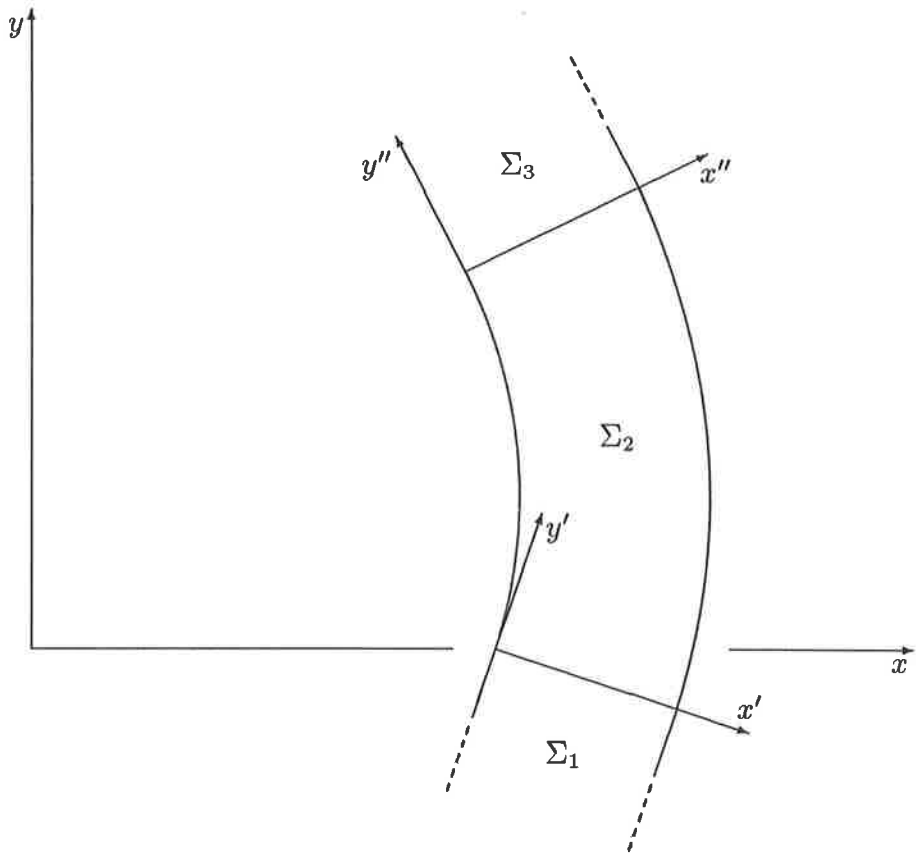

Figure 4.2: *Subdivision of the simple, single bend ducting system.*

and

$$\Phi_3(x'', y'') = \sum_{m=1}^{M} \tau_m e^{i\mu_m y''} \phi_m(x'') \tag{4.2}$$

respectively, where

$$\phi_m(x) = \begin{bmatrix} \cos\left[\frac{(m-1)\pi x}{W}\right] & \text{for } N\text{-modes} \\ \sin\left[\frac{m\pi x}{W}\right] & \text{for } D\text{-modes,} \end{bmatrix} \tag{4.3}$$

$$\mu_m^2 = \begin{bmatrix} \lambda^2 - \left[\frac{(m-1)\pi}{W}\right]^2 & \text{for } N\text{-modes} \\ \lambda^2 - \left[\frac{m\pi}{W}\right]^2 & \text{for } D\text{-modes,} \end{bmatrix} \tag{4.4}$$

and λ^2 is as defined by equation (2.33). Note that for convenience, the z-coordinate dependence of the solutions has been suppressed, as it can be adequately specified through the choice of λ^2. The coefficients σ_m, ρ_m and τ_m are complex constants which

specify the phase and amplitude of modes incident upon, reflected from and transmitted through Σ_2.

The simple form of the solutions Φ_1 and Φ_3 results from the fact that they are expressed with respect to coordinates whose axes are aligned with the boundaries of regions Σ_1 and Σ_3. In the following subsection, these principles are used to define a coordinate system which will simplify the task of determining a solution within Σ_2.

4.2.1 Natural coordinates for the duct bend

Referring back to Figure 4.1, one can see that points (x_0, y_0) on the inner wall of the duct bend can be represented parametrically by the vector equation

$$\begin{bmatrix} x_0 \\ y_0 \end{bmatrix} = R(\theta) \begin{bmatrix} \cos(\theta) \\ \sin(\theta) \end{bmatrix}. \tag{4.5}$$

Further, points within the duct bend can be reached by firstly choosing an appropriate point on the bend's inner wall, and then moving from that point a given distance ξ in the direction of the local normal vector $\underline{n}(\theta)$. Hence, any point (x, y) within Σ_2 can be specified by making an appropriate choice of the parameters ξ and θ (where $0 \leq \xi \leq W$ and $0 \leq \theta \leq \theta_{max}$), and using the vector equation

$$\begin{bmatrix} x \\ y \end{bmatrix} = R(\theta) \begin{bmatrix} \cos(\theta) \\ \sin(\theta) \end{bmatrix} + \xi \underline{n}(\theta). \tag{4.6}$$

Now, it follows from equation (4.5) that

$$\underline{n}(\theta) = \frac{1}{\sqrt{R^2 + R'^2}} \begin{bmatrix} R\cos(\theta) + R'\sin(\theta) \\ R\sin(\theta) - R'\cos(\theta) \end{bmatrix}, \tag{4.7}$$

where the primes signify differentiation with respect to θ. Hence, equation (4.6) yields explicitly

$$x = R\cos(\theta) + \frac{\xi}{\sqrt{R^2 + R'^2}} [R\cos(\theta) + R'\sin(\theta)] \tag{4.8}$$

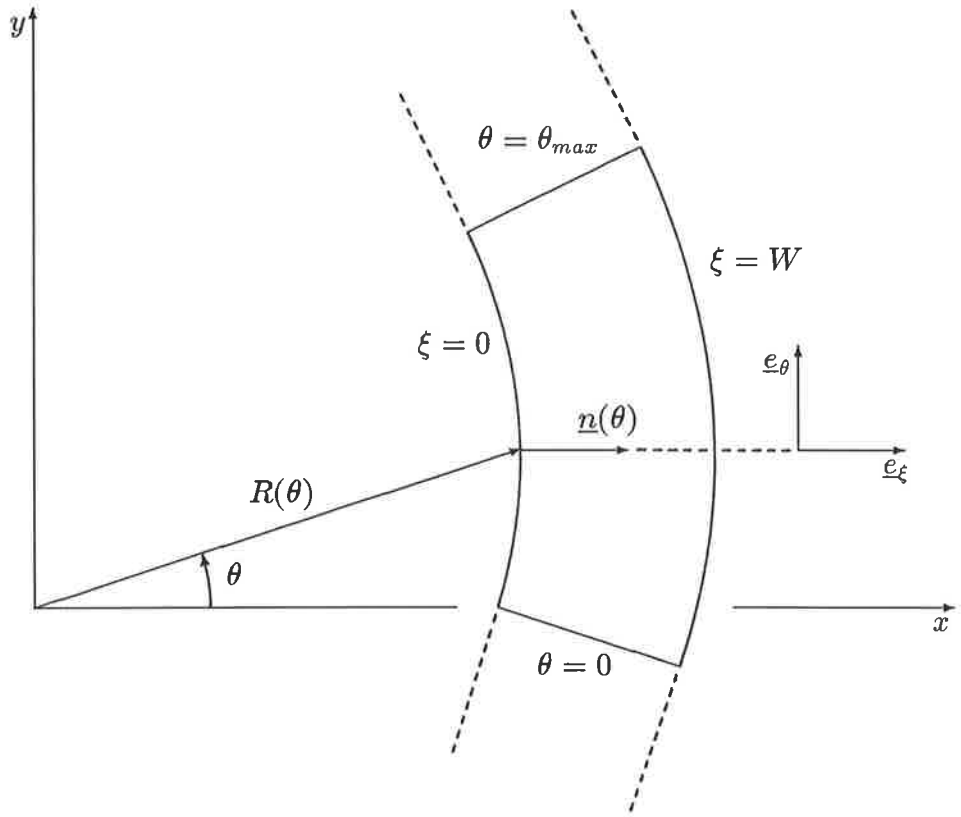

Figure 4.3: *Details of natural coordinates for the duct bend.*

and

$$y = R\sin(\theta) + \frac{\xi}{\sqrt{R^2 + R'^2}}\left[R\sin(\theta) - R'\cos(\theta)\right]. \tag{4.9}$$

Equations (4.8) and (4.9) define a coordinate transformation $(x, y) \rightarrow (\xi, \theta)$ which maps the walls of Σ_2 onto the lines $(\xi = 0, W)$ and $(\theta = 0, \theta_{max})$ in the (ξ, θ)-plane, as shown in Figure 4.3.

It can be shown (see Appendix A), that with respect to the (ξ, θ) coordinates,

$$\nabla\Phi = \frac{\partial\Phi}{\partial\xi}\underline{e}_\xi + \frac{1}{g}\frac{\partial\Phi}{\partial\theta}\underline{e}_\theta \tag{4.10}$$

and

$$\nabla^2\Phi = \frac{1}{g}\left[\frac{\partial}{\partial\xi}\left(g\frac{\partial\Phi}{\partial\xi}\right) + \frac{\partial}{\partial\theta}\left(\frac{1}{g}\frac{\partial\Phi}{\partial\theta}\right)\right], \tag{4.11}$$

where

$$g(\xi,\theta) = \xi\left[2 - \frac{R(R+R'')}{R^2+R'^2}\right] + \sqrt{R^2+R'^2}. \tag{4.12}$$

Hence, a solution Φ_2 to equations (1.1)–(1.3) which is valid within the curved region Σ_2 on the (x,y)-plane, must equivalently satisfy the equation

$$\frac{\partial}{\partial\xi}\left(g\frac{\partial\Phi}{\partial\xi}\right) + \frac{\partial}{\partial\theta}\left(\frac{1}{g}\frac{\partial\Phi}{\partial\theta}\right) + \lambda^2 g\Phi = 0 \tag{4.13}$$

within the rectangular region defined by the inequalities $(0 \leq \xi \leq W)$ and $(0 \leq \theta \leq \theta_{max})$ on the (ξ,θ)-plane, subject to the boundary conditions

$$\left[\frac{\partial\Phi}{\partial\xi}\right]_{\xi=0,W} = 0 \quad \text{for } N\text{-modes} \tag{4.14}$$

or

$$[\Phi]_{\xi=0,W} = 0 \quad \text{for } D\text{-modes.} \tag{4.15}$$

4.2.2 Continuity of the solution

Suppose that a general expression for $\Phi_2(\xi,\theta)$ has been found by solving equations (4.13)–(4.15). Then, similarly to the procedure adopted in section 3.2, a potential function which is valid throughout the duct is obtained by requiring that the general solutions Φ_1, Φ_2 and Φ_3 satisfy continuity conditions at the boundaries between the regions Σ_1, Σ_2 and Σ_3. These conditions are that Φ and the normal component of $\nabla\Phi$ should be continuous at the boundaries. Hence, the following four continuity equations must be satisfied. They are:

$$[\Phi_1]_{x'=\xi,y'=0} = [\Phi_2]_{\theta=0} \tag{4.16}$$

and

$$[\Phi_3]_{x''=\xi,y''=0} = [\Phi_2]_{\theta=\theta_{max}}, \tag{4.17}$$

ensuring continuity of Φ; and

$$\left[\frac{\partial\Phi_1}{\partial y'}\right]_{x'=\xi,y'=0} = \left[\frac{1}{g}\frac{\partial\Phi_2}{\partial\theta}\right]_{\theta=0} \tag{4.18}$$

and

$$\left[\frac{\partial \Phi_3}{\partial y''}\right]_{x''=\xi, y''=0} = \left[\frac{1}{g}\frac{\partial \Phi_2}{\partial \theta}\right]_{\theta=\theta_{max}}, \tag{4.19}$$

ensuring continuity of the normal component of $\nabla\Phi$.

4.2.3 The numerical solution

In this subsection, a general expression for $\Phi_2(\xi,\theta)$ is sought in the form of a finite functional series expansion. By then using this expression in conjunction with the continuity equations (4.16)–(4.19), the acoustic potential throughout the duct is approximately determined. Therefore, we start by letting

$$\Phi_2(\xi,\theta) \approx \Phi(\xi,\theta) = \sum_{i=1}^{I}\sum_{j=1}^{J} \alpha_{ij} f_{ij}(\xi,\theta). \tag{4.20}$$

The basis functions $f_{ij}(\xi,\theta)$ are chosen to be linearly independent, and to satisfy either of the boundary conditions (4.14) or (4.15) according to the type of mode solution required. Equations for determining the series coefficients α_{ij} are now derived by means of a formulation similar to that employed by Astley and Eversman [39], whereby the basic postulate of the Galerkin method is invoked. That is, the residual error produced by approximating the solution of equation (4.13) by $\Phi(\xi,\theta)$ is made orthogonal to each of the basis functions. This process yields the set of equations

$$\int_{\xi=0}^{W}\int_{\theta=0}^{\theta_{max}} f_{ij}\left[\frac{\partial}{\partial \xi}\left(g\frac{\partial \Phi}{\partial \xi}\right) + \frac{\partial}{\partial \theta}\left(\frac{1}{g}\frac{\partial \Phi}{\partial \theta}\right) + \lambda^2 g\Phi\right] d\xi\, d\theta = 0, \tag{4.21}$$

where $i = 1,\ldots I$ and $j = 1,\ldots J$. Integrating each of these equations by parts, the following weak formulation of the problem is obtained, namely:

$$\begin{aligned}&\int_{\xi=0}^{W}\int_{\theta=0}^{\theta_{max}}\left[g\frac{\partial f_{ij}}{\partial \xi}\frac{\partial \Phi}{\partial \xi} + \frac{1}{g}\frac{\partial f_{ij}}{\partial \theta}\frac{\partial \Phi}{\partial \theta} - \lambda^2 g f_{ij}\Phi\right] d\xi\, d\theta \\ &= \int_{\xi=0}^{W}\left[f_{ij}\frac{1}{g}\frac{\partial \Phi}{\partial \theta}\right]_{\theta=0}^{\theta_{max}} d\xi + \int_{\theta=0}^{\theta_{max}}\left[f_{ij} g\frac{\partial \Phi}{\partial \xi}\right]_{\xi=0}^{W} d\theta.\end{aligned} \tag{4.22}$$

The continuity equations (4.18) and (4.19) can be substituted into the integrand of the first integral appearing on the right hand side of equations (4.22). Also, as the basis functions satisfy the boundary conditions (4.14) or (4.15), the second integral appearing on the right hand side of equations (4.22) will be zero. Finally, the explicit series form for $\Phi(\xi,\theta)$ given by equation (4.20) can be substituted into the left hand side of equations (4.22) to yield

$$\begin{aligned}
&\sum_{k=1}^{I}\sum_{\ell=1}^{J}\alpha_{k\ell}\int_{\xi=0}^{W}\int_{\theta=0}^{\theta_{max}}\left[g\frac{\partial f_{ij}}{\partial\xi}\frac{\partial f_{k\ell}}{\partial\xi}+\frac{1}{g}\frac{\partial f_{ij}}{\partial\theta}\frac{\partial f_{k\ell}}{\partial\theta}-\lambda^2 g f_{ij}f_{k\ell}\right]d\xi\,d\theta \\
&= \sum_{m=1}^{M} i\mu_m\tau_m\int_{\xi=0}^{W} f_{ij}(\xi,\theta_{max})\phi_m(\xi)\,d\xi \\
&- \sum_{m=1}^{M} i\mu_m\left[\sigma_m-\rho_m\right]\int_{\xi=0}^{W} f_{ij}(\xi,0)\phi_m(\xi)\,d\xi. \qquad (4.23)
\end{aligned}$$

As the continuity equations (4.16) and (4.17) have not been included in the derivation of equations (4.23), they must be considered separately. Substituting equations (4.1), (4.2) and (4.20) into equations (4.16) and (4.17) yields

$$\sum_{i=1}^{I}\sum_{j=1}^{J}\alpha_{ij}f_{ij}(\xi,0)=\sum_{m=1}^{M}\left[\sigma_m+\rho_m\right]\phi_m(\xi) \qquad (4.24)$$

and

$$\sum_{i=1}^{I}\sum_{j=1}^{J}\alpha_{ij}f_{ij}(\xi,\theta_{max})=\sum_{m=1}^{M}\tau_m\phi_m(\xi). \qquad (4.25)$$

Now, assuming that the M incident modal coefficients σ_m are known, equations (4.23)–(4.25) specify $(IJ+2)$ equations from which the $(IJ+2M)$ complex constants α_{ij}, ρ_m and τ_m can be determined. So that these constants can be determined by algebraic means, we require that equations (4.24) and (4.25) be satisfied in a weighted average sense by multiplying through both of them by $\phi_n(\xi)$ $(n=1,\ldots M)$, and then integrating the resulting equations with respect to ξ over the interval $[0,W]$. Hence, the following coupled matrix equations are obtained from equations (4.23)–(4.25). They are:

$$\mathbf{A}\underline{\alpha}=\mathbf{DB}\underline{\tau}-\mathbf{CB}\left[\underline{\sigma}-\underline{\rho}\right], \qquad (4.26)$$

$$\mathbf{C}^T\underline{\alpha} = \mathbf{E}\left[\underline{\sigma} + \underline{\rho}\right] \tag{4.27}$$

and

$$\mathbf{D}^T\underline{\alpha} = \mathbf{E}\underline{\tau}. \tag{4.28}$$

Here the T superscript signifies the matrix operation of transpose; $\underline{\alpha}$, $\underline{\sigma}$, $\underline{\rho}$ and $\underline{\tau}$ are column vectors containing the series and modal coefficients; and the matrix elements are:

$$A_{(ij)(k\ell)} = \int_{\xi=0}^{W}\int_{\theta=0}^{\theta_{max}}\left[g\frac{\partial f_{ij}}{\partial\xi}\frac{\partial f_{k\ell}}{\partial\xi} + \frac{1}{g}\frac{\partial f_{ij}}{\partial\theta}\frac{\partial f_{k\ell}}{\partial\theta} - \lambda^2 g f_{ij}f_{k\ell}\right]d\xi\,d\theta, \tag{4.29}$$

$$B_{(m)(n)} = \begin{cases} i\mu_n & \text{if } m = n \\ 0 & \text{if } m \neq n, \end{cases} \tag{4.30}$$

$$C_{(ij)(n)} = \int_{\xi=0}^{W} f_{ij}(\xi,0)\phi_n(\xi)\,d\xi, \tag{4.31}$$

$$D_{(ij)(n)} = \int_{\xi=0}^{W} f_{ij}(\xi,\theta_{max})\phi_n(\xi)\,d\xi, \tag{4.32}$$

$$E_{(m)(n)} = \int_{\xi=0}^{W} \phi_m(\xi)\phi_n(\xi)\,d\xi; \tag{4.33}$$

where $i,k = 1,\ldots I$; $j,\ell = 1,\ldots J$ and $m,n = 1,\ldots M$. It should be noted that in equations (4.29)–(4.33), the indices in the first and second brackets indicate the row and column location of the matrix elements respectively.

Using equations (4.27) and (4.28) to eliminate $\underline{\rho}$ and $\underline{\tau}$ from equation (4.26) we have

$$\underline{\alpha} = \mathbf{Q}\underline{\sigma}, \tag{4.34}$$

where

$$\mathbf{Q} = 2\left[\mathbf{C}\mathbf{B}\mathbf{E}^{-1}\mathbf{C}^T + \mathbf{D}\mathbf{B}\mathbf{E}^{-1}\mathbf{D}^T - \mathbf{A}\right]^{-1}\mathbf{C}\mathbf{B}. \tag{4.35}$$

Substituting equation (4.34) back into equations (4.27) and (4.28) then yields

$$\underline{\rho} = \mathbf{R}\underline{\sigma} \tag{4.36}$$

and

$$\underline{\tau} = \mathbf{T}\underline{\sigma}, \tag{4.37}$$

where

$$\mathbf{R} = \mathbf{E}^{-1}\mathbf{C}^T\mathbf{Q} - \mathbf{I} \tag{4.38}$$

and

$$\mathbf{T} = \mathbf{E}^{-1}\mathbf{D}^T\mathbf{Q} \tag{4.39}$$

where $\mathbf{I}$ is the $(M \times M)$ identity matrix.

Once the matrices $\mathbf{Q}$, $\mathbf{R}$ and $\mathbf{T}$ are calculated, the vectors $\underline{\alpha}$, $\underline{\rho}$ and $\underline{\tau}$ can be specified for a given incident modal coefficient vector $\underline{\sigma}$ by using equations (4.34), (4.36) and (4.37). Hence, an approximate expression for the acoustic potential throughout the duct has been found. The $(M \times M)$ matrices $\mathbf{R}$ and $\mathbf{T}$ are recognised as being reflection and transmission matrices which specify how the incident straight duct modal coefficients will be scattered from the duct bend.

4.2.4 A spirally curved duct bend

Referring back to Figure 4.1, the preceding theory is applied to the analysis of a duct bend whose inner wall has the polar equation $r = R(\theta)$, where

$$R(\theta) = a\theta + b. \tag{4.40}$$

Differentiating equation (4.40) yields $R' = a$ and $R'' = 0$. Therefore, according to the theory presented in subsection 4.2.1, a solution to equations (4.13) and (4.14) or (4.15) must be found when

$$g(\xi, \theta) = \xi \left[1 + \frac{a^2}{R^2 + a^2}\right] + \sqrt{R^2 + a^2}. \tag{4.41}$$

The basis functions for the numerical solution are chosen to be

$$f_{ij}(\xi, \theta) = \phi_i(\xi) S_j(\theta). \tag{4.42}$$

Here, the $\phi_i(\xi)$ are as defined in equation (4.3) and $S_j(\theta)$ is the j^{th} cubic B-spline ([40], sect. 4.2), defined on the interval $[0, \theta_{max}]$ as follows:

$$S_j(\theta) = \begin{cases} [(\theta - \theta_{j-2})/h]^3 & \text{if } \theta\epsilon[\theta_{j-2}, \theta_{j-1}], \\ 1 + 3[(\theta - \theta_{j-1})/h] + 3[(\theta - \theta_{j-1})/h]^2 - 3[(\theta - \theta_{j-1})/h]^3 & \text{if } \theta\epsilon[\theta_{j-1}, \theta_j], \\ 1 + 3[(\theta_{j+1} - \theta)/h] + 3[(\theta_{j+1} - \theta)/h]^2 - 3[(\theta_{j+1} - \theta)/h]^3 & \text{if } \theta\epsilon[\theta_j, \theta_{j+1}], \\ [(\theta_{j+2} - \theta)/h]^3 & \text{if } \theta\epsilon[\theta_{j+1}, \theta_{j+2}], \\ 0 & \text{otherwise,} \end{cases} \tag{4.43}$$

where $h = \theta_{max}/(J-3)$ and $\theta_j = (j-2)h$.

As an example, results are presented which are relevant to the propagation of N-modes through a 90^0 bend whose inner wall spirals from $r = 1$ to $r = 5$. Here, all lengths are expressed as multiples of the wavelength χ. The values of the physical parameters used in the calculations are: $a = 8/\pi$, $b = 1$, $\theta_{max} = \pi/2$, $W = 2$ and $\lambda^2 = 3\pi^2$. Note that the value chosen for λ^2 can be used to describe acoustic waves in the duct when $H = 1$ and $n = 2$ in equation (2.33). Equation (4.4) shows that only four modes will propagate within a straight section of the duct under these conditions. $M = 6$ is taken when calculating the matrices $\mathbf{T}$ and $\mathbf{R}$ so that two evanescent modes are considered.

Tables 4.1 and 4.2 show absolute values of the elements of $\mathbf{T}$ and $\mathbf{R}$ when $I = 12$ and $J = 30, 50, 70, 80$. Looking down each block of numbers in these tables, the convergence of the matrix elements to constant values can be seen as the number of terms in the series approximation for Φ_2 increase.

As the duct's cross-section has a vertical line of symmetry, $\mathbf{T}$ and $\mathbf{R}$ matrices relevant to modes being incident upon the opposite end of the bend can be calculated by considering a bend whose inner wall spirals from $r = 5$ to $r = 1$. Redefining $a = -8/\pi$, $b = 5$ and repeating the above calculations yields the absolute values of the elements of $\mathbf{T}$ and $\mathbf{R}$ shown in Tables 4.3 and 4.4. Comparing the results presented in Tables

0.84117E+0	0.21852E+0	0.27180E+0	0.53795E−1	0.41350E−2	0.38088E−2
0.87379E+0	0.19267E+0	0.24670E+0	0.49639E−1	0.36340E−2	0.36385E−2
0.87423E+0	0.19234E+0	0.24630E+0	0.49570E−1	0.36259E−2	0.36354E−2
0.87426E+0	0.19232E+0	0.24627E+0	0.49566E−1	0.36255E−2	0.36352E−2
0.44348E+0	0.85068E+0	0.38454E+0	0.67555E−1	0.69456E−2	0.20729E−2
0.31220E+0	0.85677E+0	0.42123E+0	0.76462E−1	0.67615E−2	0.27098E−2
0.31008E+0	0.85678E+0	0.42181E+0	0.76615E−1	0.67579E−2	0.27203E−2
0.30995E+0	0.85678E+0	0.42185E+0	0.76624E−1	0.67577E−2	0.27210E−2
0.69471E+0	0.44308E+0	0.75274E+0	0.20532E+0	0.10423E−1	0.77054E−2
0.67971E+0	0.45914E+0	0.74990E+0	0.20578E+0	0.10889E−1	0.76644E−2
0.67944E+0	0.45947E+0	0.74982E+0	0.20579E+0	0.10897E−1	0.76633E−2
0.67942E+0	0.45949E+0	0.74982E+0	0.20579E+0	0.10898E−1	0.76633E−2
0.68069E−1	0.13185E+0	0.35892E+0	0.95431E+0	0.64868E−1	0.15417E−1
0.69465E−1	0.12838E+0	0.36227E+0	0.95375E+0	0.64900E−1	0.15424E−1
0.69513E−1	0.12831E+0	0.36233E+0	0.95374E+0	0.64901E−1	0.15424E−1
0.69516E−1	0.12830E+0	0.36234E+0	0.95374E+0	0.64901E−1	0.15424E−1
0.72901E−2	0.10428E−1	0.66467E−2	0.23433E−1	0.15671E−2	0.38316E−3
0.62026E−2	0.10657E−1	0.65642E−2	0.23472E−1	0.15770E−2	0.37905E−3
0.61860E−2	0.10660E−1	0.65640E−2	0.23472E−1	0.15771E−2	0.37899E−3
0.61851E−2	0.10660E−1	0.65640E−2	0.23472E−1	0.15771E−2	0.37898E−3
0.45417E−2	0.14317E−2	0.25270E−2	0.45899E−3	0.63156E−4	0.50615E−4
0.45194E−2	0.14499E−2	0.25263E−2	0.47821E−3	0.61551E−4	0.50715E−4
0.45186E−2	0.14511E−2	0.25260E−2	0.47863E−3	0.61533E−4	0.50712E−4
0.45186E−2	0.14512E−2	0.25260E−2	0.47865E−3	0.61532E−4	0.50712E−4

Table 4.1: *Absolute values of the* $\mathbf{T}$ *matrix elements for the* $r = 1 \rightarrow 5$ *spirally curved duct bend when* $M = 6$, $I = 12$ *and* $J = 30, 50, 70, 80$.

0.67596E−2	0.36629E−2	0.25442E−2	0.12913E−2	0.19343E−2	0.37341E−2
0.10980E−2	0.14207E−2	0.12692E−3	0.18326E−2	0.19816E−2	0.37108E−2
0.11135E−2	0.14109E−2	0.12847E−3	0.18348E−2	0.19818E−2	0.37109E−2
0.11141E−2	0.14103E−2	0.12893E−3	0.18349E−2	0.19818E−2	0.37109E−2
0.76515E−2	0.78103E−2	0.26068E−2	0.14877E−2	0.11446E−1	0.21164E−2
0.29677E−2	0.67830E−3	0.36603E−2	0.80626E−3	0.11444E−1	0.21485E−2
0.29474E−2	0.70596E−3	0.36597E−2	0.80163E−3	0.11444E−1	0.21484E−2
0.29460E−2	0.70652E−3	0.36596E−2	0.80136E−3	0.11444E−1	0.21484E−2
0.62319E−2	0.30568E−2	0.77903E−3	0.85302E−2	0.72505E−2	0.11299E−1
0.31089E−3	0.42921E−2	0.16346E−3	0.88372E−2	0.72805E−2	0.11284E−1
0.31470E−3	0.42914E−2	0.16277E−3	0.88391E−2	0.72806E−2	0.11284E−1
0.31582E−3	0.42912E−2	0.16294E−3	0.88392E−2	0.72806E−2	0.11284E−1
0.51652E−2	0.28488E−2	0.13930E−1	0.30934E−2	0.65019E−1	0.11726E−1
0.73304E−2	0.15439E−2	0.14431E−1	0.29161E−2	0.65005E−1	0.11733E−1
0.73392E−2	0.15350E−2	0.14434E−1	0.29146E−2	0.65005E−1	0.11733E−1
0.73395E−2	0.15345E−2	0.14434E−1	0.29145E−2	0.65005E−1	0.11733E−1
0.67005E−2	0.18980E−1	0.10254E−1	0.56308E−1	0.49945E−2	0.17923E−2
0.68645E−2	0.18978E−1	0.10296E−1	0.56296E−1	0.49918E−2	0.17685E−2
0.68652E−2	0.18977E−1	0.10296E−1	0.56296E−1	0.49916E−2	0.17676E−2
0.68652E−2	0.18977E−1	0.10296E−1	0.56296E−1	0.49916E−2	0.17675E−2
0.71752E−2	0.19468E−2	0.88634E−2	0.56328E−2	0.99418E−3	0.24290E−3
0.71305E−2	0.19764E−2	0.88515E−2	0.56365E−2	0.98101E−3	0.19943E−3
0.71307E−2	0.19763E−2	0.88516E−2	0.56365E−2	0.98046E−3	0.19859E−3
0.71307E−2	0.19763E−2	0.88516E−2	0.56365E−2	0.98042E−3	0.19853E−3

Table 4.2: *Absolute values of the* $\mathbf{R}$ *matrix elements for the* $r = 1 \rightarrow 5$ *spirally curved duct bend when* $M = 6$, $I = 12$ *and* $J = 30, 50, 70, 80$.

0.84117E+0	0.21230E+0	0.28361E+0	0.17017E−1	0.21045E−2	0.23636E−2
0.87379E+0	0.14945E+0	0.27749E+0	0.17366E−1	0.17905E−2	0.23520E−2
0.87423E+0	0.14844E+0	0.27738E+0	0.17378E−1	0.17858E−2	0.23516E−2
0.87426E+0	0.14838E+0	0.27737E+0	0.17379E−1	0.17855E−2	0.23515E−2
0.45648E+0	0.85068E+0	0.37786E+0	0.68858E−1	0.62884E−2	0.15564E−2
0.40247E+0	0.85677E+0	0.39155E+0	0.67042E−1	0.64267E−2	0.15762E−2
0.40178E+0	0.85678E+0	0.39184E+0	0.67007E−1	0.64283E−2	0.15776E−2
0.40174E+0	0.85678E+0	0.39186E+0	0.67005E−1	0.64284E−2	0.15776E−2
0.66578E+0	0.45091E+0	0.75274E+0	0.21980E+0	0.46999E−2	0.32213E−2
0.60429E+0	0.49394E+0	0.74990E+0	0.22184E+0	0.46416E−2	0.32204E−2
0.60330E+0	0.49462E+0	0.74982E+0	0.22188E+0	0.46414E−2	0.32201E−2
0.60325E+0	0.49466E+0	0.74982E+0	0.22188E+0	0.46414E−2	0.32200E−2
0.21518E+0	0.12936E+0	0.33528E+0	0.95431E+0	0.27059E−1	0.95546E−3
0.19855E+0	0.14641E+0	0.33604E+0	0.95375E+0	0.27103E−1	0.99548E−3
0.19828E+0	0.14671E+0	0.33605E+0	0.95374E+0	0.27104E−1	0.99634E−3
0.19826E+0	0.14672E+0	0.33605E+0	0.95374E+0	0.27104E−1	0.99639E−3
0.14324E−1	0.11518E−1	0.14741E−1	0.56177E−1	0.15671E−2	0.11386E−3
0.12589E−1	0.11213E−1	0.15399E−1	0.56205E−1	0.15770E−2	0.11096E−3
0.12561E−1	0.11207E−1	0.15411E−1	0.56206E−1	0.15771E−2	0.11093E−3
0.12559E−1	0.11206E−1	0.15412E−1	0.56206E−1	0.15771E−2	0.11093E−3
0.73188E−2	0.19068E−2	0.60446E−2	0.74063E−2	0.21254E−3	0.50615E−4
0.69915E−2	0.24927E−2	0.60125E−2	0.74096E−2	0.21026E−3	0.50715E−4
0.69856E−2	0.25024E−2	0.60116E−2	0.74097E−2	0.21022E−3	0.50712E−4
0.69852E−2	0.25029E−2	0.60116E−2	0.74097E−2	0.21022E−3	0.50712E−4

Table 4.3: *Absolute values of the* $\mathbf{T}$ *matrix elements for the* $r = 5 \rightarrow 1$ *spirally curved duct bend when* $M = 6$, $I = 12$ *and* $J = 30, 50, 70, 80$.

0.99332E−2	0.38056E−2	0.17520E−2	0.16391E−2	0.33408E−3	0.14889E−2
0.17170E−2	0.13056E−2	0.11579E−2	0.14231E−2	0.35355E−3	0.14828E−2
0.17393E−2	0.13025E−2	0.11567E−2	0.14210E−2	0.35372E−3	0.14828E−2
0.17390E−2	0.13021E−2	0.11566E−2	0.14209E−2	0.35373E−3	0.14828E−2
0.79497E−2	0.55967E−2	0.10862E−2	0.15655E−2	0.50632E−2	0.37543E−3
0.27273E−2	0.18534E−2	0.31932E−2	0.24242E−2	0.50725E−2	0.38492E−3
0.27209E−2	0.18346E−2	0.31925E−2	0.24339E−2	0.50722E−2	0.38490E−3
0.27200E−2	0.18343E−2	0.31926E−2	0.24345E−2	0.50722E−2	0.38490E−3
0.42914E−2	0.12737E−2	0.34578E−2	0.68834E−2	0.15540E−2	0.43322E−2
0.28363E−2	0.37443E−2	0.39672E−2	0.70515E−2	0.15714E−2	0.43250E−2
0.28334E−2	0.37436E−2	0.39669E−2	0.70513E−2	0.15714E−2	0.43250E−2
0.28330E−2	0.37437E−2	0.39672E−2	0.70513E−2	0.15714E−2	0.43250E−2
0.65564E−2	0.29978E−2	0.11241E−1	0.86107E−2	0.28532E−1	0.22511E−2
0.56925E−2	0.46421E−2	0.11515E−1	0.85859E−2	0.28524E−1	0.22543E−2
0.56840E−2	0.46605E−2	0.11515E−1	0.85864E−2	0.28524E−1	0.22543E−2
0.56835E−2	0.46616E−2	0.11515E−1	0.85865E−2	0.28524E−1	0.22542E−2
0.11573E−2	0.83963E−2	0.21977E−2	0.24709E−1	0.98606E−3	0.10139E−2
0.12247E−2	0.84118E−2	0.22222E−2	0.24702E−1	0.97013E−3	0.93240E−3
0.12253E−2	0.84113E−2	0.22223E−2	0.24702E−1	0.96950E−3	0.92898E−3
0.12254E−2	0.84113E−2	0.22224E−2	0.24702E−1	0.96945E−3	0.92870E−3
0.28610E−2	0.34534E−3	0.33985E−2	0.10814E−2	0.56241E−3	0.57998E−3
0.28493E−2	0.35407E−3	0.33928E−2	0.10829E−2	0.51720E−3	0.30351E−4
0.28493E−2	0.35405E−3	0.33928E−2	0.10829E−2	0.51531E−3	0.21603E−4
0.28493E−2	0.35405E−3	0.33928E−2	0.10829E−2	0.51515E−3	0.21875E−4

Table 4.4: *Absolute values of the* $\mathbf{R}$ *matrix elements for the* $r = 5 \rightarrow 1$ *spirally curved duct bend when* $M = 6$, $I = 12$ *and* $J = 30, 50, 70, 80$.

4.1 and 4.3, it is interesting to note that the diagonal elements in these tables are the same. This result is a verification of the reciprocity principle in duct acoustics [37], and implies that for a given incident mode, the proportion of energy transmitted through the bend to that same mode is independent of the direction of approach to the bend.

4.3 RECTANGULAR CROSS-SECTIONED DUCTS — A NUMERICAL SOLUTION WHICH USES A UNIFORMLY CURVED DUCT SEGMENT APPROXIMATION

Consider again the non-uniformly curved duct bend shown in Figure 4.1. By choosing $N+1$ values for θ, $(\theta_0 = 0, \theta_1, \ldots \theta_{N-1}, \theta_N = \theta_{max})$, such that the vectors $\underline{n}(\theta_1), \ldots \underline{n}(\theta_{N-1})$ subdivide the angle between the vectors $\underline{n}(\theta_0)$ and $\underline{n}(\theta_N)$ into N equal parts, a series of N duct segments can be defined. Figure 4.4 gives a geometrical description of the n^{th} segment. If the angle ε is defined by

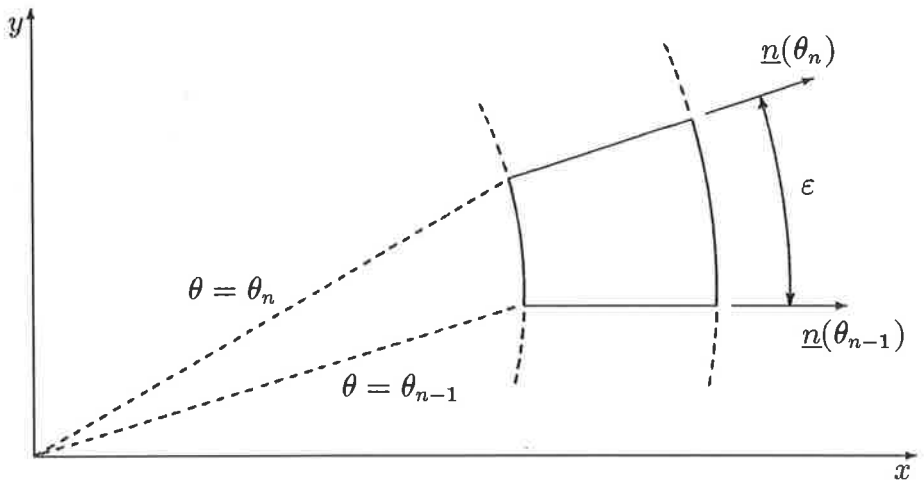

Figure 4.4: *Top view of* n^{th} *duct segment,* $(n = 1, \ldots N)$.

$$\varepsilon = \frac{1}{N} \arccos\left[\underline{n}(\theta_0) \bullet \underline{n}(\theta_N)\right], \tag{4.44}$$

then θ_n is the root of the equation

$$\arccos\left[\underline{n}(\theta_0) \bullet \underline{n}(\theta_n)\right] = n\varepsilon. \tag{4.45}$$

Also, using the fact that the radius of curvature of the curve $r = R(\theta)$ is given by

$$C(\theta) = \frac{\left(R^2 + R'^2\right)^{3/2}}{R^2 + 2R'^2 - RR''}, \tag{4.46}$$

one can approximately determine the mean radius of curvature of the n^{th} segment's inner wall from the expression

$$\overline{C}_n = \frac{1}{2}\left[C(\theta_{n-1}) + C(\theta_n)\right]. \tag{4.47}$$

A modal scattering matrix for the n^{th} segment can therefore be approximately calculated by taking the segment to have a constant inner wall radius of $\overline{C}_n$, and an angular extent of ε. In this manner, a scattering matrix cascade for the duct bend can be formed. The acoustic characteristics of the duct bend are then determined from this cascade with the aid of the algorithms presented in section 3.3.

4.3.1 A spirally curved duct bend

As in subsection 4.2.4, the propagation of N-modes through a spirally curved duct bend whose inner wall has the polar equation $r = a\theta + b$ is considered. The following values of the physical parameters used in the calculations are again assumed. They are: $a = 8/\pi$, $b = 1$, $W = 2$ and $\lambda^2 = 3\pi^2$. After subdividing the spiral duct bend into a series of uniformly curved segments, the submatrices of each $\mathbf{S}^{(n)}$ matrix are calculated using a 25-term approximation in the method presented by Tam[16]. $M = 12$ modes are then considered when using the iterative scattering matrix algorithm to calculate $\mathbf{S}^{(cas)}$, the modal scattering matrix of the duct bend.

Tables 4.5–4.8 show the absolute values of elements in the top-left (6×6) submatrices of $\mathbf{S}_{11}^{(cas)}$, $\mathbf{S}_{21}^{(cas)}$, $\mathbf{S}_{22}^{(cas)}$ and $\mathbf{S}_{12}^{(cas)}$ as the number of uniformly curved segments used in the approximation are increased in the manner $N = 20, 40, 60, 100$. Looking down a given block of numbers in these tables, one can see the convergence of the corresponding matrix element to its limiting value.

From the definition of $\mathbf{S}^{(cas)}$ in equation (3.40), it follows that the submatrices of this matrix are related to the transmission and reflection matrices presented in Tables 4.1–4.4 of subsection 4.2.4 in the manner: $\mathbf{S}_{11}^{(cas)} = \mathbf{T}(r = 1 \rightarrow 5)$, $\mathbf{S}_{21}^{(cas)} = \mathbf{R}(r = 1 \rightarrow 5)$, $\mathbf{S}_{22}^{(cas)} = \mathbf{T}(r = 5 \rightarrow 1)$, $\mathbf{S}_{12}^{(cas)} = \mathbf{R}(r = 5 \rightarrow 1)$. Making a comparison between the results presented in Tables 4.1–4.4 and 4.5–4.8, one can see that there is a good agreement between the limiting values of corresponding matrix elements in these tables (at least a 3 significant figure agreement in most cases). This serves as a verification that the acoustic characteristics of a non-uniformly curved duct bend can be accurately determined from the uniformly curved segment approximation.

An indication of the influence that evanescent modes have upon the accuracy of the uniformly curved duct segment approximation can be obtained by examining the absolute values of the elements of $\mathbf{S}^{(cas)}$ shown in Table 4.9. Here the spiral bend was subdivided into $N = 100$ segments, but only propagating modes were considered in the calculations (therefore $M = 4$). As one can see, the larger matrix elements are still determined with a reasonable accuracy. However, it is clear that if the values of the smaller elements are to be accurately determined, evanescent modes must be included in the calculations. In general, the accuracy of $\mathbf{S}^{(cas)}$ can be checked by increasing M (and N) until a further increase does not significantly alter the required matrix elements. While doing this, one should ensure that the submatrices of each $\mathbf{S}^{(n)}$ matrix are also being determined with sufficient accuracy.

0.87446E+0	0.19213E+0	0.24614E+0	0.49444E−1	0.36054E−2	0.36203E−2
0.87433E+0	0.19226E+0	0.24623E+0	0.49532E−1	0.36203E−2	0.36314E−2
0.87430E+0	0.19228E+0	0.24624E+0	0.49547E−1	0.36230E−2	0.36334E−2
0.87429E+0	0.19230E+0	0.24625E+0	0.49555E−1	0.36244E−2	0.36344E−2
0.30892E+0	0.85680E+0	0.42213E+0	0.76565E−1	0.67475E−2	0.27211E−2
0.30963E+0	0.85679E+0	0.42193E+0	0.76603E−1	0.67562E−2	0.27229E−2
0.30976E+0	0.85678E+0	0.42190E+0	0.76610E−1	0.67574E−2	0.27234E−2
0.30983E+0	0.85678E+0	0.42188E+0	0.76613E−1	0.67578E−2	0.27237E−2
0.67934E+0	0.45966E+0	0.74967E+0	0.20599E+0	0.10916E−1	0.76338E−2
0.67939E+0	0.45953E+0	0.74978E+0	0.20585E+0	0.10904E−1	0.76552E−2
0.67939E+0	0.45951E+0	0.74980E+0	0.20582E+0	0.10902E−1	0.76581E−2
0.67939E+0	0.45950E+0	0.74982E+0	0.20581E+0	0.10901E−1	0.76589E−2
0.69312E−1	0.12808E+0	0.36258E+0	0.95370E+0	0.64729E−1	0.15355E−1
0.69470E−1	0.12827E+0	0.36240E+0	0.95373E+0	0.64857E−1	0.15405E−1
0.69499E−1	0.12830E+0	0.36236E+0	0.95374E+0	0.64880E−1	0.15413E−1
0.69512E−1	0.12831E+0	0.36234E+0	0.95374E+0	0.64890E−1	0.15415E−1
0.62112E−2	0.10770E−1	0.66143E−2	0.23649E−1	0.15853E−2	0.38008E−3
0.61883E−2	0.10684E−1	0.65786E−2	0.23514E−1	0.15791E−2	0.37917E−3
0.61858E−2	0.10671E−1	0.65705E−2	0.23491E−1	0.15779E−2	0.37897E−3
0.61845E−2	0.10664E−1	0.65660E−2	0.23479E−1	0.15774E−2	0.37883E−3
0.45784E−2	0.14708E−2	0.25579E−2	0.48626E−3	0.62268E−4	0.51176E−4
0.45337E−2	0.14563E−2	0.25341E−2	0.48097E−3	0.61726E−4	0.50828E−4
0.45252E−2	0.14537E−2	0.25295E−2	0.47967E−3	0.61609E−4	0.50754E−4
0.45209E−2	0.14521E−2	0.25271E−2	0.47891E−3	0.61538E−4	0.50710E−4

Table 4.5: *Absolute values of elements in the top-left* (6×6) *submatrix of* $\mathbf{S}_{11}^{(cas)}$ *for the spirally curved duct bend when* $M = 12$ *and* $N = 20, 40, 60, 100$.

0.13725E−2	0.14039E−2	0.17140E−3	0.18828E−2	0.19829E−2	0.36976E−2
0.11148E−2	0.14205E−2	0.12546E−3	0.18396E−2	0.19805E−2	0.37072E−2
0.11139E−2	0.14139E−2	0.12554E−3	0.18338E−2	0.19804E−2	0.37089E−2
0.11134E−2	0.14110E−2	0.12562E−3	0.18312E−2	0.19802E−2	0.37095E−2
0.29327E−2	0.10498E−2	0.36484E−2	0.75968E−3	0.11410E−1	0.21419E−2
0.29674E−2	0.72960E−3	0.36628E−2	0.77479E−3	0.11435E−1	0.21466E−2
0.29535E−2	0.72288E−3	0.36573E−2	0.77667E−3	0.11439E−1	0.21465E−2
0.29475E−2	0.71969E−3	0.36551E−2	0.77772E−3	0.11440E−1	0.21457E−2
0.41985E−3	0.42781E−2	0.12294E−3	0.89264E−2	0.72645E−2	0.11239E−1
0.30732E−3	0.42950E−2	0.13468E−3	0.88413E−2	0.72742E−2	0.11271E−1
0.30751E−3	0.42885E−2	0.14755E−3	0.88330E−2	0.72760E−2	0.11277E−1
0.30771E−3	0.42859E−2	0.15382E−3	0.88293E−2	0.72765E−2	0.11279E−1
0.75313E−2	0.14547E−2	0.14577E−1	0.27005E−2	0.64833E−1	0.11683E−1
0.73582E−2	0.14836E−2	0.14438E−1	0.28309E−2	0.64960E−1	0.11718E−1
0.73350E−2	0.14872E−2	0.14424E−1	0.28451E−2	0.64981E−1	0.11724E−1
0.73246E−2	0.14892E−2	0.14418E−1	0.28521E−2	0.64992E−1	0.11725E−1
0.68689E−2	0.18922E−1	0.10274E−1	0.56147E−1	0.49646E−2	0.17628E−2
0.68606E−2	0.18963E−1	0.10287E−1	0.56257E−1	0.49824E−2	0.17699E−2
0.68604E−2	0.18969E−1	0.10290E−1	0.56276E−1	0.49854E−2	0.17716E−2
0.68597E−2	0.18972E−1	0.10291E−1	0.56285E−1	0.49867E−2	0.17728E−2
0.71051E−2	0.19702E−2	0.88168E−2	0.56123E−2	0.97781E−3	0.19567E−3
0.71236E−2	0.19746E−2	0.88420E−2	0.56292E−2	0.98176E−3	0.19671E−3
0.71267E−2	0.19745E−2	0.88461E−2	0.56318E−2	0.98272E−3	0.19679E−3
0.71279E−2	0.19738E−2	0.88478E−2	0.56326E−2	0.98336E−3	0.19673E−3

Table 4.6: *Absolute values of elements in the top-left* (6×6) *submatrix of* $\mathbf{S}_{21}^{(cas)}$ *for the spirally curved duct bend when* $M = 12$ *and* $N = 20, 40, 60, 100$.

0.87446E+0	0.14789E+0	0.27734E+0	0.17328E−1	0.17930E−2	0.23826E−2
0.87433E+0	0.14822E+0	0.27736E+0	0.17367E−1	0.17864E−2	0.23594E−2
0.87430E+0	0.14829E+0	0.27736E+0	0.17375E−1	0.17857E−2	0.23550E−2
0.87429E+0	0.14832E+0	0.27736E+0	0.17378E−1	0.17853E−2	0.23527E−2
0.40136E+0	0.85680E+0	0.39200E+0	0.66888E−1	0.64944E−2	0.15989E−2
0.40162E+0	0.85679E+0	0.39189E+0	0.66985E−1	0.64427E−2	0.15832E−2
0.40167E+0	0.85678E+0	0.39187E+0	0.67002E−1	0.64348E−2	0.15803E−2
0.40169E+0	0.85678E+0	0.39186E+0	0.67009E−1	0.64309E−2	0.15787E−2
0.60292E+0	0.49499E+0	0.74967E+0	0.22203E+0	0.46770E−2	0.32607E−2
0.60313E+0	0.49476E+0	0.74978E+0	0.22192E+0	0.46518E−2	0.32304E−2
0.60316E+0	0.49472E+0	0.74980E+0	0.22190E+0	0.46460E−2	0.32244E−2
0.60318E+0	0.49470E+0	0.74982E+0	0.22189E+0	0.46429E−2	0.32214E−2
0.19778E+0	0.14661E+0	0.33638E+0	0.95370E+0	0.27307E−1	0.10122E−2
0.19813E+0	0.14668E+0	0.33615E+0	0.95373E+0	0.27152E−1	0.10012E−2
0.19819E+0	0.14670E+0	0.33611E+0	0.95374E+0	0.27125E−1	0.99852E−3
0.19822E+0	0.14670E+0	0.33608E+0	0.95374E+0	0.27111E−1	0.99693E−3
0.12489E−1	0.11189E−1	0.15438E−1	0.56057E−1	0.15853E−2	0.11226E−3
0.12541E−1	0.11204E−1	0.15421E−1	0.56168E−1	0.15791E−2	0.11128E−3
0.12550E−1	0.11206E−1	0.15418E−1	0.56188E−1	0.15779E−2	0.11107E−3
0.12555E−1	0.11207E−1	0.15417E−1	0.56197E−1	0.15774E−2	0.11094E−3
0.69565E−2	0.25031E−2	0.59885E−2	0.73763E−2	0.21083E−3	0.51176E−4
0.69780E−2	0.25047E−2	0.60052E−2	0.74003E−2	0.21033E−3	0.50828E−4
0.69817E−2	0.25051E−2	0.60075E−2	0.74040E−2	0.21022E−3	0.50754E−4
0.69836E−2	0.25055E−2	0.60081E−2	0.74052E−2	0.21014E−3	0.50710E−4

Table 4.7: *Absolute values of elements in the top-left* (6×6) *submatrix of* $\mathbf{S}_{22}^{(cas)}$ *for the spirally curved duct bend when* $M = 12$ *and* $N = 20, 40, 60, 100$.

0.20513E−2	0.13177E−2	0.10911E−2	0.14253E−2	0.35886E−3	0.15041E−2
0.17404E−2	0.13116E−2	0.11573E−2	0.14234E−2	0.35486E−3	0.14880E−2
0.17410E−2	0.13067E−2	0.11576E−2	0.14223E−2	0.35422E−3	0.14850E−2
0.17412E−2	0.13046E−2	0.11578E−2	0.14218E−2	0.35385E−3	0.14836E−2
0.27526E−2	0.15585E−2	0.33064E−2	0.24726E−2	0.51242E−2	0.39224E−3
0.27398E−2	0.18303E−2	0.32199E−2	0.24395E−2	0.50822E−2	0.38669E−3
0.27297E−2	0.18299E−2	0.32102E−2	0.24392E−2	0.50765E−2	0.38589E−3
0.27253E−2	0.18298E−2	0.32058E−2	0.24392E−2	0.50738E−2	0.38533E−3
0.26726E−2	0.38771E−2	0.40507E−2	0.71456E−2	0.15921E−2	0.43812E−2
0.28347E−2	0.37757E−2	0.39603E−2	0.70546E−2	0.15755E−2	0.43396E−2
0.28356E−2	0.37643E−2	0.39581E−2	0.70427E−2	0.15731E−2	0.43314E−2
0.28360E−2	0.37591E−2	0.39573E−2	0.70374E−2	0.15718E−2	0.43272E−2
0.57013E−2	0.47347E−2	0.11669E−1	0.85144E−2	0.28739E−1	0.22853E−2
0.56938E−2	0.46713E−2	0.11520E−1	0.85313E−2	0.28574E−1	0.22620E−2
0.56891E−2	0.46708E−2	0.11501E−1	0.85340E−2	0.28545E−1	0.22577E−2
0.56872E−2	0.46707E−2	0.11492E−1	0.85359E−2	0.28530E−1	0.22552E−2
0.12431E−2	0.84975E−2	0.22515E−2	0.24889E−1	0.98214E−3	0.94164E−3
0.12293E−2	0.84279E−2	0.22281E−2	0.24746E−1	0.97247E−3	0.93289E−3
0.12270E−2	0.84184E−2	0.22246E−2	0.24721E−1	0.97060E−3	0.93074E−3
0.12258E−2	0.84139E−2	0.22228E−2	0.24708E−1	0.96960E−3	0.92956E−3
0.28901E−2	0.36081E−3	0.34369E−2	0.10978E−2	0.52233E−3	0.23061E−4
0.28593E−2	0.35570E−3	0.34043E−2	0.10866E−2	0.51747E−3	0.22609E−4
0.28536E−2	0.35497E−3	0.33978E−2	0.10846E−2	0.51628E−3	0.22531E−4
0.28508E−2	0.35445E−3	0.33946E−2	0.10834E−2	0.51563E−3	0.22510E−4

Table 4.8: *Absolute values of elements in the top-left* (6×6) *submatrix of* $\mathbf{S}_{12}^{(cas)}$ *for the spirally curved duct bend when* $M = 12$ *and* $N = 20, 40, 60, 100$.

0.874E+0	0.193E+0	0.246E+0	0.500E−1	0.176E−2	0.133E−2	0.114E−2	0.147E−2
0.313E+0	0.857E+0	0.420E+0	0.777E−1	0.277E−2	0.192E−2	0.313E−2	0.237E−2
0.678E+0	0.458E+0	0.751E+0	0.206E+0	0.279E−2	0.367E−2	0.385E−2	0.686E−2
0.730E−1	0.132E+0	0.362E+0	0.953E+0	0.588E−2	0.454E−2	0.112E−1	0.114E−1
0.114E−2	0.144E−2	0.180E−3	0.193E−2	0.874E+0	0.150E+0	0.277E+0	0.182E−1
0.300E−2	0.512E−3	0.379E−2	0.111E−2	0.402E+0	0.857E+0	0.391E+0	0.689E−1
0.441E−3	0.444E−2	0.427E−3	0.924E−2	0.603E+0	0.493E+0	0.751E+0	0.222E+0
0.770E−2	0.212E−2	0.151E−1	0.482E−2	0.200E+0	0.149E+0	0.336E+0	0.953E+0

Table 4.9: *Absolute values of the elements of* $\mathbf{S}^{(cas)}$ *for the spirally curved duct bend which were calculated using propagating modes only (therefore* $M = 4$*).* $N = 100$ *segments were used in the approximation.*

4.4 DUCTS OF ARBITRARY CROSS-SECTION

Clearly, the method presented in section 4.3 can be readily applied to the analysis of non-uniformly curved bends in ducts of arbitrary cross-section. This is shown in the following subsection, where analyses of parabolic bends in elliptic and circular ducts are presented.

4.4.1 Parabolic bends in elliptic and circular cross-sectioned ducts

Consider the two parabolically curved duct bends shown in Figure 4.5. The centreline of bend I is defined by the equation

$$y = ax^2, \quad -x_{max} \leq x \leq x_{max}. \tag{4.48}$$

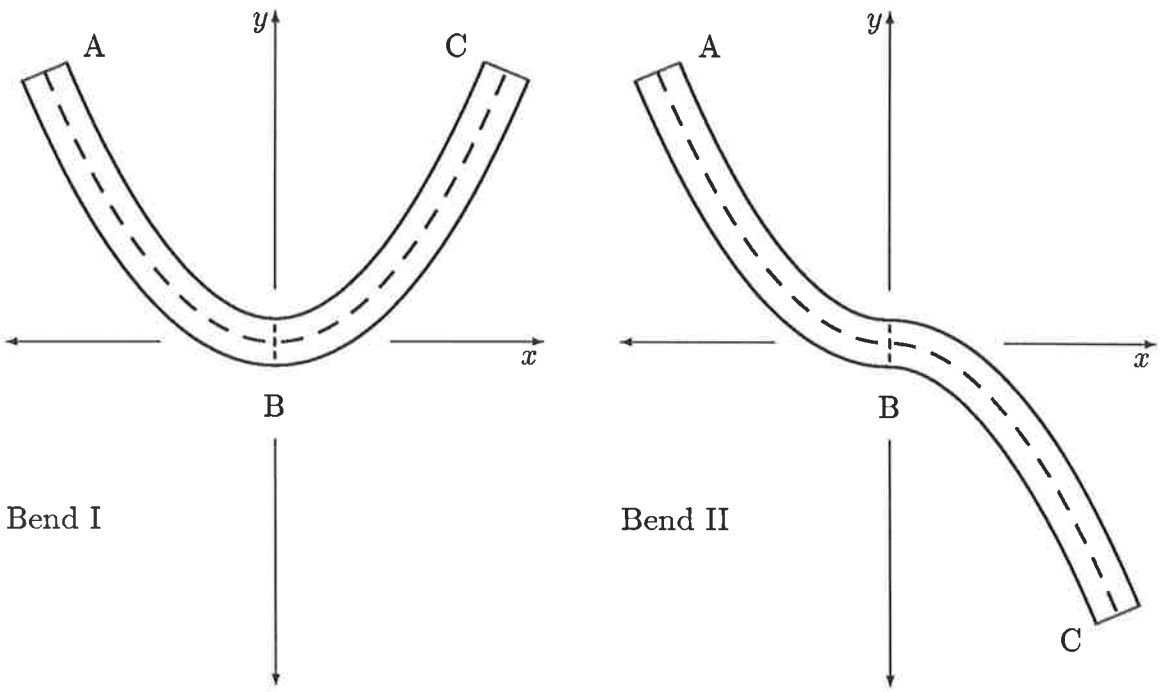

Figure 4.5: *Top views of two parabolically curved duct bends.*

The centreline of bend II is defined by the equation

$$y = \begin{cases} ax^2, & -x_{max} \leq x < 0 \\ -ax^2, & 0 \leq x \leq x_{max}. \end{cases} \tag{4.49}$$

It can be seen from the symmetries involved that one only needs to subdivide bend I from B to C in order to obtain all of the $\mathbf{S}^{(n)}$ matrices required. So, considering this section of duct in particular, a unit outward normal vector to the centreline is

$$\underline{n}(x) = \frac{1}{\sqrt{1+4a^2x^2}} \begin{bmatrix} 2ax \\ -1 \end{bmatrix}, \tag{4.50}$$

and its radius of curvature is

$$C(x) = \frac{(1+4a^2x^2)^{3/2}}{2a}. \tag{4.51}$$

Proceeding in an analogous manner to that described in section 4.3, one can choose $N+1$ values for x, $(x_0 = 0, x_1, \ldots x_{N-1}, x_N = x_{max})$, such that the duct section is subdivided into N equi-angular segments. The modal scattering matrix of each segment is approximately calculated by taking the segment to have a constant centreline radius of $\overline{C}_n$, and an angular extent of ε. Here, $\overline{C}_n$ and ε satisfy equations of the same form as equations (4.44), (4.45) and (4.47), with θ_n being replaced by x_n.

In the following calculations, the duct is assumed to have an elliptic cross-section, with width W in the plane of the duct centreline, height H in a direction normal to the plane of the duct centreline, and where W and H are the major and minor axis dimensions of the ellipse. The submatrices of each $\mathbf{S}^{(n)}$ matrix can therefore be calculated in the manner shown in subsection 3.2.1. Expressing all lengths as multiples of the free-space wavelength χ, let $W = 1.6$, $H = 1.0$, $a = 0.2$ and $x_{max} = 5.0$, with the analysis being restricted to N-modes which are even about the plane of the duct centreline. Only 4 modes will propagate within a straight section of the duct under these conditions. Tables 4.10–4.13 show the absolute values of elements of $\mathbf{S}_{11}^{(cas)}$, $\mathbf{S}_{21}^{(cas)}$, $\mathbf{S}_{22}^{(cas)}$ and $\mathbf{S}_{12}^{(cas)}$ for the section of bend I from B–C as the number of segments used in the analysis are increased in the manner $N = 20, 40, 60, 80$. Here, a 144-term ($I = J = 12$) double series approximation and $K^2 = 36$ modes were used to calculate each $\mathbf{S}^{(n)}$ matrix. $M = 12$ modes were then considered when using the iterative scattering matrix algorithm to determine $\mathbf{S}^{(cas)}$. Looking down a given block of numbers in these tables, one can see the convergence of the corresponding matrix element to its limiting value.

Now let $W = 1.2502$, $H = 1.2500$, $a = 0.2$ and $x_{max} = 6.0$. These values for W and H define a duct which has essentially a circular cross-section. Again, the analysis is restricted to N-modes which are even about the plane of the duct centreline, and only 4 modes will propagate within a straight section of the duct under these conditions. After

0.76839E+0	0.57709E+0	0.19045E+0	0.22360E−1	0.20875E−2	0.38990E−2
0.76990E+0	0.57496E+0	0.19096E+0	0.22631E−1	0.20784E−2	0.38650E−2
0.77019E+0	0.57455E+0	0.19105E+0	0.22710E−1	0.20765E−2	0.38638E−2
0.77029E+0	0.57441E+0	0.19108E+0	0.22735E−1	0.20759E−2	0.38637E−2
0.53944E+0	0.52608E+0	0.59306E+0	0.59545E−1	0.26652E−2	0.22603E−2
0.53734E+0	0.53074E+0	0.59121E+0	0.59320E−1	0.26947E−2	0.22463E−2
0.53696E+0	0.53159E+0	0.59087E+0	0.59278E−1	0.26999E−2	0.22452E−2
0.53682E+0	0.53189E+0	0.59075E+0	0.59263E−1	0.27017E−2	0.22450E−2
0.43131E+0	0.67169E+0	0.67408E+0	0.13208E+0	0.46051E−2	0.92011E−2
0.43100E+0	0.66986E+0	0.67638E+0	0.13060E+0	0.45881E−2	0.91154E−2
0.43094E+0	0.66953E+0	0.67679E+0	0.13040E+0	0.45852E−2	0.91042E−2
0.43091E+0	0.66941E+0	0.67693E+0	0.13034E+0	0.45841E−2	0.91003E−2
0.74237E−1	0.12257E+0	0.38247E+0	0.96838E+0	0.39657E−2	0.72578E−1
0.72770E−1	0.11805E+0	0.37995E+0	0.96890E+0	0.40015E−2	0.72694E−1
0.72535E−1	0.11740E+0	0.37967E+0	0.96898E+0	0.40076E−2	0.72711E−1
0.72453E−1	0.11719E+0	0.37956E+0	0.96900E+0	0.40098E−2	0.72716E−1
0.57250E−3	0.56292E−3	0.56230E−3	0.33202E−3	0.20074E−5	0.24614E−4
0.52716E−3	0.52715E−3	0.50925E−3	0.31741E−3	0.19656E−5	0.23112E−4
0.50948E−3	0.50993E−3	0.48716E−3	0.31437E−3	0.19365E−5	0.22737E−4
0.50509E−3	0.50575E−3	0.48081E−3	0.31353E−3	0.19391E−5	0.22602E−4
0.24329E−3	0.26867E−3	0.15108E−2	0.27001E−2	0.10816E−4	0.20657E−3
0.23348E−3	0.28498E−3	0.14029E−2	0.25335E−2	0.99708E−5	0.19420E−3
0.22668E−3	0.28369E−3	0.13693E−2	0.24873E−2	0.97483E−5	0.19067E−3
0.22466E−3	0.28423E−3	0.13561E−2	0.24691E−2	0.96557E−5	0.18928E−3

Table 4.10: *Absolute values of elements in the top-left* (6×6) *submatrix of* $\mathbf{S}_{11}^{(cas)}$ *for bend I from B–C when* $W = 1.6$, $H = 1.0$, $a = 0.2$, $x_{max} = 5.0$, $M = 12$ *and* $N = 20, 40, 60, 80$.

0.39956E−3	0.24365E−2	0.13279E−2	0.40552E−2	0.75933E−3	0.56762E−3
0.48465E−3	0.29904E−2	0.14789E−2	0.45870E−2	0.76118E−3	0.52955E−3
0.71266E−3	0.30713E−2	0.14870E−2	0.45597E−2	0.76142E−3	0.53216E−3
0.69179E−3	0.30690E−2	0.14811E−2	0.45556E−2	0.76151E−3	0.53220E−3
0.26240E−2	0.82881E−3	0.68449E−2	0.36782E−2	0.50171E−2	0.56774E−2
0.32203E−2	0.11281E−2	0.68760E−2	0.38286E−2	0.50214E−2	0.56448E−2
0.33073E−2	0.11090E−2	0.68815E−2	0.36809E−2	0.50226E−2	0.56436E−2
0.33047E−2	0.11473E−2	0.68518E−2	0.36501E−2	0.50233E−2	0.56445E−2
0.17926E−2	0.85794E−2	0.69691E−2	0.22435E−1	0.87065E−3	0.39979E−2
0.19965E−2	0.86190E−2	0.74270E−2	0.23090E−1	0.87042E−3	0.40231E−2
0.20074E−2	0.86262E−2	0.70525E−2	0.23044E−1	0.87022E−3	0.40197E−2
0.19994E−2	0.85891E−2	0.70767E−2	0.23022E−1	0.87019E−3	0.40198E−2
0.14724E−1	0.12400E−1	0.60350E−1	0.86619E−2	0.47298E−2	0.72662E−1
0.16655E−1	0.12907E−1	0.62110E−1	0.82148E−2	0.47205E−2	0.72758E−1
0.16556E−1	0.12409E−1	0.61985E−1	0.82833E−2	0.47243E−2	0.72764E−1
0.16540E−1	0.12305E−1	0.61925E−1	0.83048E−2	0.47255E−2	0.72766E−1
0.16903E−2	0.10369E−1	0.14358E−2	0.28996E−2	0.11648E−3	0.59979E−4
0.16944E−2	0.10378E−1	0.14355E−2	0.28939E−2	0.11683E−3	0.59503E−4
0.16950E−2	0.10381E−1	0.14352E−2	0.28962E−2	0.11692E−3	0.59492E−4
0.16952E−2	0.10382E−1	0.14351E−2	0.28969E−2	0.11696E−3	0.59487E−4
0.76827E−3	0.71398E−2	0.40117E−2	0.27107E−1	0.36499E−4	0.23311E−2
0.71655E−3	0.70979E−2	0.40367E−2	0.27142E−1	0.36211E−4	0.23350E−2
0.72002E−3	0.70960E−2	0.40332E−2	0.27144E−1	0.36205E−4	0.23346E−2
0.72003E−3	0.70969E−2	0.40332E−2	0.27144E−1	0.36202E−4	0.23342E−2

Table 4.11: *Absolute values of elements in the top-left* (6×6) *submatrix of* $\mathbf{S}_{21}^{(cas)}$ *for bend I from B–C when* $W = 1.6$, $H = 1.0$, $a = 0.2$, $x_{max} = 5.0$, $M = 12$ *and* $N = 20, 40, 60, 80$.

0.76839E+0	0.50086E+0	0.31953E+0	0.20444E−1	0.25718E−3	0.17960E−3
0.76990E+0	0.49891E+0	0.31929E+0	0.20040E−1	0.23681E−3	0.17236E−3
0.77018E+0	0.49855E+0	0.31925E+0	0.19975E−1	0.22887E−3	0.16734E−3
0.77028E+0	0.49843E+0	0.31923E+0	0.19952E−1	0.22690E−3	0.16584E−3
0.62154E+0	0.52608E+0	0.53593E+0	0.36355E−1	0.27236E−3	0.21361E−3
0.61925E+0	0.53074E+0	0.53448E+0	0.35015E−1	0.25505E−3	0.22658E−3
0.61882E+0	0.53159E+0	0.53421E+0	0.34822E−1	0.24672E−3	0.22555E−3
0.61867E+0	0.53189E+0	0.53411E+0	0.34758E−1	0.24470E−3	0.22598E−3
0.25708E+0	0.74329E+0	0.67408E+0	0.14218E+0	0.34097E−3	0.15054E−2
0.25776E+0	0.74097E+0	0.67638E+0	0.14124E+0	0.30881E−3	0.13979E−2
0.25789E+0	0.74054E+0	0.67679E+0	0.14114E+0	0.29541E−3	0.13644E−2
0.25793E+0	0.74039E+0	0.67693E+0	0.14110E+0	0.29156E−3	0.13512E−2
0.81194E−1	0.20075E+0	0.35530E+0	0.96838E+0	0.54160E−3	0.72374E−2
0.82179E−1	0.19999E+0	0.35133E+0	0.96890E+0	0.51777E−3	0.67911E−2
0.82464E−1	0.19985E+0	0.35080E+0	0.96898E+0	0.51281E−3	0.66671E−2
0.82558E−1	0.19980E+0	0.35062E+0	0.96900E+0	0.51143E−3	0.66184E−2
0.46468E−2	0.55084E−2	0.75942E−2	0.24312E−2	0.20075E−5	0.17773E−4
0.46265E−2	0.55694E−2	0.75662E−2	0.24531E−2	0.19657E−5	0.16384E−4
0.46224E−2	0.55802E−2	0.75614E−2	0.24569E−2	0.19366E−5	0.16019E−4
0.46209E−2	0.55839E−2	0.75597E−2	0.24582E−2	0.19392E−5	0.15867E−4
0.52812E−2	0.28417E−2	0.92342E−2	0.27075E−1	0.14978E−4	0.20655E−3
0.52344E−2	0.28234E−2	0.91481E−2	0.27118E−1	0.14063E−4	0.19419E−3
0.52324E−2	0.28216E−2	0.91369E−2	0.27124E−1	0.13835E−4	0.19065E−3
0.52321E−2	0.28211E−2	0.91330E−2	0.27126E−1	0.13753E−4	0.18926E−3

Table 4.12: *Absolute values of elements in the top-left* (6×6) *submatrix of* $\mathbf{S}_{22}^{(cas)}$ *for bend I from B–C when* $W = 1.6$, $H = 1.0$, $a = 0.2$, $x_{max} = 5.0$, $M = 12$ *and* $N = 20, 40, 60, 80$.

0.36129E−2	0.39317E−2	0.29270E−2	0.46301E−2	0.85393E−5	0.29751E−4
0.39323E−2	0.37174E−2	0.27736E−2	0.48585E−2	0.58719E−5	0.28574E−4
0.38921E−2	0.38819E−2	0.27510E−2	0.48951E−2	0.53252E−5	0.27950E−4
0.38894E−2	0.38411E−2	0.27529E−2	0.49087E−2	0.51597E−5	0.27665E−4
0.42346E−2	0.45341E−2	0.37425E−2	0.83435E−2	0.49427E−3	0.68573E−3
0.40037E−2	0.43136E−2	0.39753E−2	0.85182E−2	0.45878E−3	0.64508E−3
0.41808E−2	0.43916E−2	0.42091E−2	0.85137E−2	0.44330E−3	0.62624E−3
0.41369E−2	0.43847E−2	0.41891E−2	0.85127E−2	0.43947E−3	0.61925E−3
0.39515E−2	0.46910E−2	0.38904E−2	0.17761E−1	0.58658E−5	0.82165E−4
0.37448E−2	0.49832E−2	0.42029E−2	0.18672E−1	0.87847E−5	0.83614E−4
0.37146E−2	0.52764E−2	0.42188E−2	0.18509E−1	0.93927E−5	0.81724E−4
0.37173E−2	0.52515E−2	0.42285E−2	0.18472E−1	0.95934E−5	0.81155E−4
0.16812E−1	0.28129E−1	0.47776E−1	0.26750E−1	0.50576E−3	0.77797E−2
0.17640E−1	0.28717E−1	0.50225E−1	0.26638E−1	0.48008E−3	0.73065E−2
0.17773E−1	0.28701E−1	0.49785E−1	0.26627E−1	0.47465E−3	0.71726E−2
0.17822E−1	0.28698E−1	0.49686E−1	0.26625E−1	0.47278E−3	0.71200E−2
0.19009E−4	0.10216E−2	0.96725E−5	0.31005E−3	0.12484E−5	0.68319E−6
0.13071E−4	0.94821E−3	0.14485E−4	0.29431E−3	0.11168E−5	0.63814E−6
0.11855E−4	0.91622E−3	0.15488E−4	0.29098E−3	0.10633E−5	0.60536E−6
0.11486E−4	0.90831E−3	0.15819E−4	0.28983E−3	0.10452E−5	0.59433E−6
0.40301E−4	0.86249E−3	0.82451E−4	0.29023E−2	0.41576E−6	0.25881E−4
0.38704E−4	0.81136E−3	0.83904E−4	0.27258E−2	0.38834E−6	0.22830E−4
0.37858E−4	0.78767E−3	0.82006E−4	0.26759E−2	0.36839E−6	0.22012E−4
0.37470E−4	0.77887E−3	0.81435E−4	0.26563E−2	0.36168E−6	0.21692E−4

Table 4.13: *Absolute values of elements in the top-left* (6×6) *submatrix of* $\mathbf{S}_{12}^{(cas)}$ *for bend I from B–C when* $W = 1.6$, $H = 1.0$, $a = 0.2$, $x_{max} = 5.0$, $M = 12$ *and* $N = 20, 40, 60, 80$.

subdividing the section of bend I from B to C into $N = 80$ segments, each $\mathbf{S}^{(n)}$ matrix was calculated using a 144-term ($I = J = 12$) double series approximation and $K^2 = 36$ modes. These $\mathbf{S}^{(n)}$ matrices were then appropriately ordered in cascades so that bends I and II were each modelled by 160 uniformly curved segments. When modelling bend II, an $\mathbf{S}^{(apr)}(\pi)$ matrix (subsect. 3.3.4) was also inserted at two points in the cascade. Its location was such that it would operate on the modal coefficient vectors at points B and C on the bend — the one at point B being used to simulate the $\gamma = \pi$ bend, and the one at point C being used to reorientate Φ to its original sense. In terms of the formulation presented in subsections 2.3.1 and 3.2.1, the elements of the matrix $\mathbf{H}$ which were used to evaluate this $\mathbf{S}^{(apr)}(\pi)$ matrix are

$$H_{mn} = 2 \int_{\xi=0}^{\xi_{max}} \int_{\eta=0}^{\pi} \phi_m(\xi,\eta)\phi_n(\xi,\eta-\pi)g^2(\xi,\eta)\,d\xi\,d\eta, \tag{4.52}$$

where $\phi_m(\xi,\eta)$ is the m^{th} dominant eigenfunction. Having formed the scattering matrix cascades used to model ducts I and II, $M = 12$ modes were then considered when using the iterative scattering matrix algorithm to determine $\mathbf{S}^{(cas)}$ for each cascade.

Due to their symmetrical form, bends I and II will transmit and reflect modes in an identical manner from either end. Hence, $\mathbf{S}_{11}^{(cas)} = \mathbf{S}_{22}^{(cas)} = \mathbf{T}^{(cas)}$ and $\mathbf{S}_{21}^{(cas)} = \mathbf{S}_{12}^{(cas)} = \mathbf{R}^{(cas)}$. Tables 4.14–4.17 show the absolute values of elements in the top-left (6×6) submatrices of $\mathbf{T}^{(cas)}$ and $\mathbf{R}^{(cas)}$ for bends I and II. Looking at the elements in Tables 4.14 and 4.15, one can see that modes incident upon bend I generate virtually no reflected modes, and remain largely uncoupled after transmission through the duct. Thus, even though the centreline curvature becomes quite large ($C = 2.5$ at point B), because this curvature varies in a smooth manner, bend I has quite good modal transmission characteristics. In contrast, the elements in Tables 4.16 and 4.17 show that modes incident upon bend II generate reflected modes of larger amplitude, and become coupled to a greater extent upon transmission through the bend. For example, one can see from the elements in the first column of Table 4.16 that if a wave comprised only of the dominant plane-wave mode is incident upon bend II, then the transmitted wave

0.996E+00	0.833E−01	0.203E−01	0.797E−04	0.487E−04	0.247E−06
0.944E−01	0.977E+00	0.162E+00	0.227E−02	0.382E−03	0.191E−05
0.323E−01	0.227E+00	0.981E+00	0.681E−02	0.233E−02	0.113E−04
0.368E−03	0.928E−02	0.198E−01	0.100E+01	0.470E−04	0.228E−06
0.127E−03	0.882E−03	0.382E−02	0.266E−04	0.907E−05	0.439E−07
0.269E−06	0.184E−05	0.773E−05	0.537E−07	0.184E−07	0.890E−10

Table 4.14: *Absolute values of elements in the top-left* (6×6) *submatrix of* $\mathbf{T}^{(cas)}$ *for bend I when* $W = 1.2502$, $H = 1.2500$, $a = 0.2$, $x_{max} = 6.0$, $M = 12$ *and* $N = 160$.

0.606E−04	0.637E−04	0.668E−04	0.684E−04	0.283E−06	0.114E−08
0.721E−04	0.223E−03	0.677E−03	0.141E−02	0.103E−04	0.157E−06
0.106E−03	0.952E−03	0.164E−03	0.199E−03	0.237E−02	0.115E−04
0.316E−03	0.575E−02	0.577E−03	0.168E−02	0.106E−05	0.566E−08
0.739E−06	0.237E−04	0.389E−02	0.597E−06	0.196E−04	0.179E−03
0.124E−08	0.152E−06	0.789E−05	0.134E−08	0.747E−04	0.177E−05

Table 4.15: *Absolute values of elements in the top-left* (6×6) *submatrix of* $\mathbf{R}^{(cas)}$ *for bend I when* $W = 1.2502$, $H = 1.2500$, $a = 0.2$, $x_{max} = 6.0$, $M = 12$ *and* $N = 160$.

0.923E−01	0.808E+00	0.383E+00	0.616E−01	0.900E−03	0.428E−05
0.915E+00	0.194E+00	0.384E+00	0.607E−01	0.912E−03	0.445E−05
0.609E+00	0.539E+00	0.745E+00	0.408E−01	0.177E−02	0.865E−05
0.284E+00	0.247E+00	0.118E+00	0.979E+00	0.279E−03	0.133E−05
0.235E−02	0.210E−02	0.291E−02	0.158E−03	0.692E−05	0.338E−07
0.467E−05	0.428E−05	0.593E−05	0.313E−06	0.141E−07	0.689E−10

Table 4.16: *Absolute values of elements in the top-left* (6×6) *submatrix of* $\mathbf{T}^{(cas)}$ *for bend II when* $W = 1.2502$, $H = 1.2500$, $a = 0.2$, $x_{max} = 6.0$, $M = 12$ *and* $N = 162$.

0.164E−01	0.902E−02	0.309E−02	0.186E−01	0.758E−05	0.374E−07
0.102E−01	0.426E−02	0.709E−02	0.185E−01	0.258E−04	0.232E−06
0.492E−02	0.996E−02	0.112E−01	0.132E−01	0.238E−02	0.114E−04
0.857E−01	0.755E−01	0.382E−01	0.128E−01	0.901E−04	0.430E−06
0.198E−04	0.595E−04	0.390E−02	0.510E−04	0.195E−04	0.179E−03
0.408E−07	0.223E−06	0.782E−05	0.102E−06	0.747E−04	0.177E−05

Table 4.17: *Absolute values of elements in the top-left* (6×6) *submatrix of* $\mathbf{R}^{(cas)}$ *for bend II when* $W = 1.2502$, $H = 1.2500$, $a = 0.2$, $x_{max} = 6.0$, $M = 12$ *and* $N = 162$.

will contain only a small component of this mode, and will be comprised predominantly of the second mode. These effects are due to the "sign change" discontinuity in the centreline curvature of bend II at point B.

A further description of the mode coupling effects referred to above can be given with the aid of Figures 4.6 and 4.7. In these figures, the real part of the acoustic potential Φ is plotted as it varies along the centreline of bends I and II. A plane-wave was taken to be incident at end A of each bend by setting $\underline{a}_0^T = [1\,0\ldots0]$, and both bends were anechoically terminated at end C. Φ was determined throughout the bends in the manner described in subsection 3.3.3. Looking at Figure 4.6, one can see that the wave propagating through bend I maintains its unimodal characteristics. The decrease in amplitude observed in the vicinity of point B is due to the fact that Φ is biased radially outwards in this region of high curvature (as would occur to the dominant mode if the bend was uniformly curved). The matrix elements in the first column of Table 4.14 confirm the observation that the wave returns to what is essentially its original form at end C of bend I. Now looking at Figure 4.7, one can see clearly the effects of higher order mode generation at junction B in bend II. From A to B, Φ results from the superposition of the incident wave and a wave reflected from the junction at B. The elements in the first column of Table 4.17 suggest that the reflected wave is comprised mainly of the fourth mode. This observation is consistent with Figure 4.7 as the straight duct propagation constant associated with that mode has a value of 1.36, therefore yielding the wavelength of $2\pi/1.36 = 4.62$ seen superposed onto the incident wave. From B to C, Φ results from a forward propagating wave which has, according to the elements in the first column of Table 4.16, a predominantly higher order mode content. A physical explanation of why these higher order modes are excited can be given if one considers the radial biasing of modes in the vicinity of junction B. As noted in Chapter 2, the dominant mode in a uniformly curved bend will be biased away from the centre of curvature of the bend, with this bias being progressively reversed

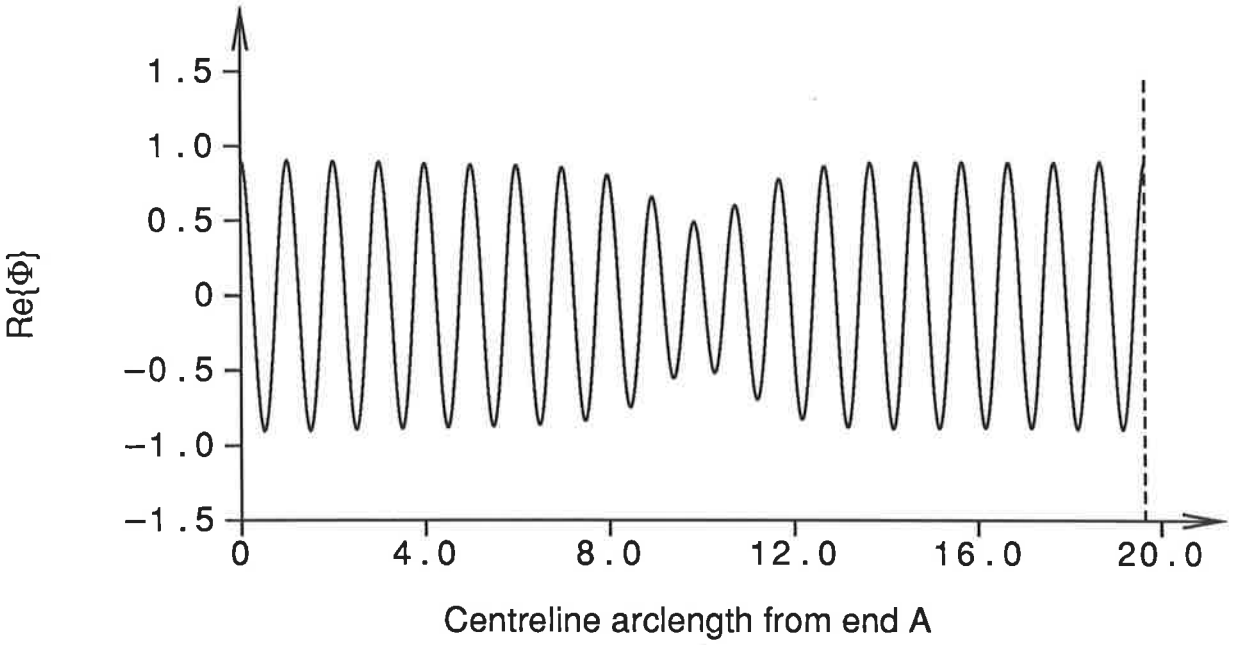

Figure 4.6: *Plot of Re{Φ} along the centreline of bend I from end A to end C. A plane wave is incident at end A, and the bend is anechoically terminated at end C.*

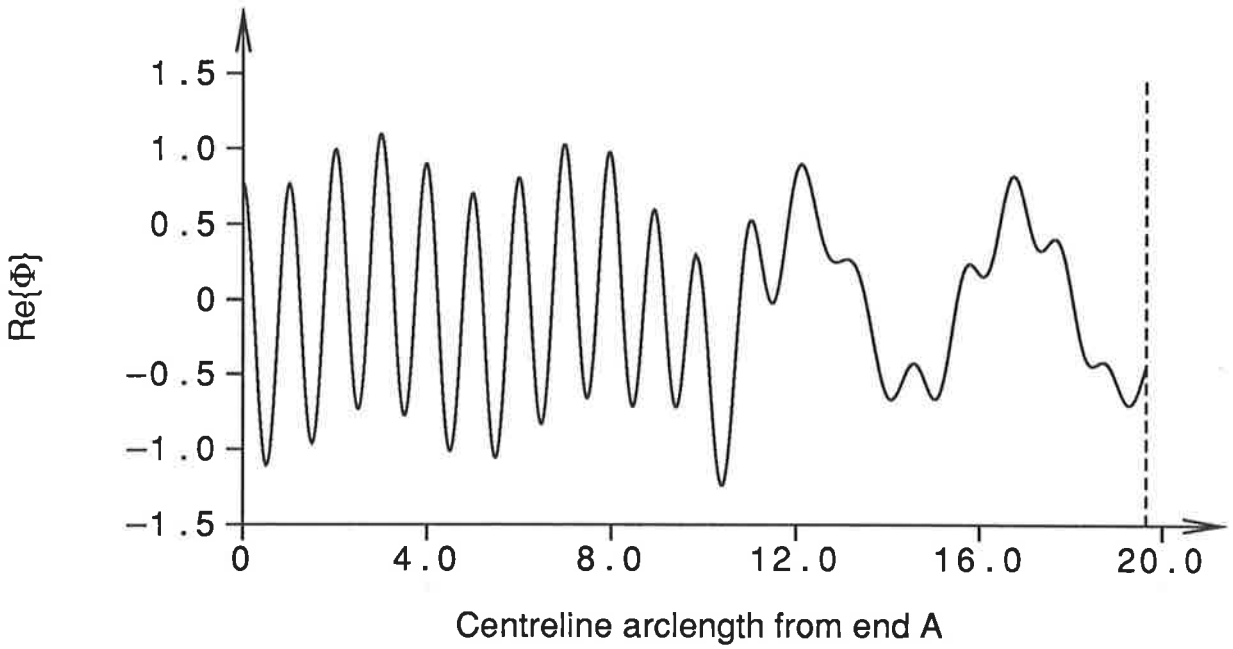

Figure 4.7: *Plot of Re{Φ} along the centreline of bend II from end A to end C. A plane wave is incident at end A, and the bend is anechoically terminated at end C.*

for the higher order modes. Hence, to the left of junction B, the incident wave (which will behave like the dominant mode in a uniformly curved bend) will be biased in the $-y$ direction. To the right of junction B, the dominant mode will be biased in the $+y$ direction, with only the higher order modes being biased more towards the $-y$ direction. Hence, as the acoustic field must be continuous when crossing junction B, there will be a tendancy for higher order modes to be excited as the incident wave is transmitted through the junction. It is believed that the excitation of higher order modes in this manner is a general characteristic associated with "S-bends", and forms the basis behind the design of the ventilation duct attenuation unit presented in Appendix B.

Upon finishing this section, it should be made clear that in general, one may not be able to interpret acoustic wave propagation within non-uniformly curved duct bends in the simple manner just presented. For example, modes that propagate within a straight duct will not necessarily propagate within each uniformly curved segment when near cut-off. Hence, a mode which is propagating within a non-uniformly curved duct may suddenly cease to propagate. Also, one cannot strictly refer to the existence of modes within non-uniformly curved bends in the classical sense due to the non-separable nature of equation (1.1). However, it is felt that the descriptions presented above are justified as they enable one to usefully rationalise the complicated acoustic processes which occur within these bends.

4.5 SUMMARY

The task of determining solutions to equations (1.1)–(1.3) within non-uniformly curved duct bends was initially undertaken by two different methods in this chapter. To reduce the complexity of the task when presenting these methods, rectangular cross-sectioned ducts were considered.

The first of these methods was presented in section 4.2. This method combined a generalised coordinate transformation technique with the Galerkin method to yield an approximate solution in the form of a finite functional series. The method was applied to the analysis of a spirally curved duct bend, and the solution was shown to converge as the Galerkin discretisation was refined.

The second method was presented in section 4.3. In this method, the duct bend was geometrically approximated by a series of uniformly curved duct segments. Modal scattering matrices for each of these segments were then calculated. Finally, the acoustic characteristics of the duct bend were obtained from the resulting scattering matrix cascade via the algorithms presented in section 3.3. The method was applied to the analysis of the same spirally curved duct bend considered earlier, and the solution was shown to converge as the number of uniformly curved segments used in the approximation was increased. A good agreement was noted between the results produced by this method and those produced by the method presented in section 4.2.

In section 4.4, the adaptation of the method presented in section 4.3 to the analysis of non-uniformly curved bends in ducts of arbitrary cross-section was illustrated. This was done by using the method to study the propagation of acoustic waves through parabolic bends in elliptic and circular cross-sectioned ducts. Here, some interesting results were presented which showed that acoustic waves within non-uniformly curved bends have quasi-modal characteristics, with most of the mode coupling effects occurring within the bends being caused by the presence of centreline curvature discontinuities.

The method used in sections 4.3 and 4.4 is highly recommended for the analysis of non-uniformly curved duct bends in general. This recommendation is made because the method possesses a number of characteristics which make it well suited to this type of problem. These characteristics are:

1. *Simplicity and flexibility.*

   - The task of subdividing a bend into a series of uniformly curved segments is not a difficult one, and leaves one with considerable freedom to use physical intuition when deciding how the approximation should be implemented. For example, in the analyses presented, an equi-angular subdivision was chosen as this would tend to concentrate more segments in regions of high curvature.
   - Computer programs which use the method need only be altered in a superficial way when considering a variety of different bend curvatures. One need not be concerned with how the alterations will affect the workings of a coordinate transformation, or the suitability of basis functions, etc., whose details may be deeply embedded in the structure of the program code.

2. *Efficiency.*

   - By subdividing the bend into a series of uniformly curved segments, good use is made of a natural reduction in the dimensionality of the problem. As a result, the solution is obtained from a series of two-dimensional analyses.
   - As each segment can be analysed individually, and because of the iterative nature of the algorithms used in the calculations, the method can be implemented without making excessive demands on computer memory.

3. *Others.*

   - The nature of the method allows it to be directly incorporated into a general program (based upon the theory presented in Chapters 2 and 3) for analysing multi-bend ducting systems which contain both uniformly and non-uniformly curved bends.
   - The method enables one to utilise some of the convenient aspects of classical modal wave propagation theory within non-uniformly curved bends. For

example, suppose one wishes to determine how long it would take a given mode to "propagate" through a non-uniformly curved bend. As the mode has an angular and temporal coordinate dependence of the form $\exp[i(\nu_n\theta - \omega t)]$ within the n^{th} segment, a propagation time through this segment will be $T_n = \varepsilon_n\nu_n/\omega$, where ε_n is the angular extent of the segment. The required propagation time is therefore obtained by summing the T_n $\{n = 1, \ldots N\}$.

CHAPTER 5

— ◇ —

CONCLUSION

5.1 REVIEW OF THESIS

In Chapter 1, the principal aim of this thesis was stated as being "to develop numerical methods for accurately determining the acoustic characteristics of curved ducting systems in a computationally efficient manner". A literature survey showed that the major portion of previous research in this area was directed towards the analysis of single bends in rectangular cross-sectioned ducts. In most of these cases, the bends were assumed to have uniform curvature. Analyses of single, uniformly curved bends in circular cross-sectioned ducts were also cited. However, the few more general analyses of the single bend problem were characterised by the use of asymptotic and perturbation methods, which produced solutions under conditions which are too restrictive for many engineering applications. The only analyses of multi-bend ducting systems cited dealt with rectangular cross-sectioned ducts which contained bends of uniform curvature.

The characteristics of acoustic waves within straight and uniformly curved ducts were studied in Chapter 2. Here it was shown that a general expression for the acoustic potential takes the form of a superposition of exponentially modulated modes. Analytic expressions for the modes and modulation parameters (in general, the eigenvalues and eigenfunctions of equations (2.3)–(2.5) and (2.9)–(2.11)) within rectangular cross-sectioned ducts were presented. A numerical solution procedure based upon the Rayleigh-Ritz method was then proposed so that these modes and modulation param-

eters could be determined within ducts of more general cross-section. In a series of illustrative examples, elliptic cross-sectioned ducts were considered, and the characteristics of the modes and modulation parameters within these ducts were discussed. These characteristics were seen to be similar to those in rectangular cross-sectioned ducts. A general observation which was made was that curved duct modes can be approximately considered to be radially biased versions of straight duct modes. This bias was noted to be away from the centre of curvature of the bend for propagating modes, and towards the centre of curvature of the bend for evanescent (non-propagating) modes. The degree of bias was seen to be greater the further a mode was from cut-off, and was enhanced by an increase in duct curvature. From these observations, it was concluded that sound propagating within curved ducts has an affinity for the outer wall of the duct — especially at high frequencies and within strongly curved ducts.

The scattering of modes within multi-bend ducting systems was considered in Chapter 3. The chapter began with the presentation of a general method for calculating modal transmission and reflection matrices for a single, uniformly curved bend. The method utilised the numerical solution procedure of Chapter 2, and in an example, a 90^0 bend in an elliptic cross-sectioned duct was considered. In the results presented, the matrix elements were shown to converge as the discretisation used in the numerical solution procedure was refined. Modal scattering matrices for sections of straight and uniformly curved duct were then defined in terms of the modal transmission and reflection matrices for these sections. For a straight duct section, the modal scattering matrix was found to be a diagonal matrix, which applied an appropriate phase shift to modes propagating through it. For a uniformly curved duct section, the required modal transmission and reflection matrices could be calculated by the general method just presented. Having introduced the concept of a modal scattering matrix, it was then proposed that a multi-bend ducting system should be analysed by subdividing it into a series of purely straight and uniformly curved sections, calculating a modal scattering

matrix for each section, and then considering the system to be a cascade of modal scatterers. Algorithms for calculating the modal scattering matrix of such a cascade were presented, together with a method for determining the acoustic potential within any duct section. Finally, the effects of out-of-plane and serpentine bends upon scattered modes were accounted for. Hence, in Chapter 3, the necessary methods were developed for analysing a wide variety of uniformly curved, multi-bend ducting systems.

In Chapter 4, two methods were initially proposed for the analysis of non-uniformly curved duct bends. For simplicity, the methods were introduced via analyses of rectangular cross-sectioned ducts. In the first method, a classic approach to the problem was taken. This approach involved the use of a coordinate transformation to map the interior region of the bend onto that of a straight duct section. The resulting simplification of the problem's boundary conditions then enabled a solution to be obtained in the form of a finite functional series via the Galerkin method. The method was successfully used to determine modal transmission and reflection matrices for a spirally curved duct bend. In the second method, the duct bend was geometrically approximated by a series of uniformly curved duct segments. This enabled the bend to be interpreted as being a "multi-bend ducting system" of the type considered in Chapter 3. Hence, the algorithms presented in that chapter could be used to determine the acoustic characteristics of the bend. The method was used to analyse the same spirally curved duct bend considered earlier, and a good agreement between the results produced by the two methods was noted. In a final application, the second method was used to study the propagation of acoustic waves through parabolic bends in elliptic and circular cross-sectioned ducts. By comparing a bend whose curvature became large, but varied in a smooth manner, with an "S-bend", whose curvature was the same except for a sign change discontinuity, it was shown that centreline curvature discontinuities are a major cause of mode coupling effects within curved ducting systems. The second method was highly recommended for the analysis of non-uniformly curved bends in general because it possessed a number

of characteristics which made it well suited for such problems. These characteristics included the method's simplicity, flexibility and efficiency.

5.2 ACHIEVEMENTS OF THESIS

The research conducted in this thesis has resulted in the development of a series of numerical methods which, when combined, enable one to accurately and efficiently determine the acoustic characteristics of any configuration of straight and curved duct sections likely to be encountered in an engineering situation. A number of the methods presented in this thesis have not been previously used in the field of curved duct acoustics. Also, in many of the illustrative examples, solutions are presented to problems which have not been previously considered in the literature. The following list presents the main achievements of this thesis, highlighting the original aspects of the work.

1. A general numerical procedure for determining the acoustic characteristics of uniformly curved duct bends was presented in Chapters 2 and 3. The procedure is based upon the Rayleigh-Ritz method, and has not been previously used. In Chapter 2, the procedure enabled the acoustic modes within the straight and uniformly curved sections of a duct to be expressed as series expansions using a chosen set of basis functions. Determining the modes in this form then enabled general expressions for the modal transmission and reflection matrices of a single duct bend to be derived in Chapter 3. In a series of examples, the procedure was used to analyse uniformly curved bends in elliptic cross-sectioned ducts. Such bends have not been previously considered in the literature. From the examination of mode contour plots, a number of important original observations were made about the "radial biasing" of modes within curved ducts. The research described here has been presented in the recent publication [41].

2. In Chapter 3, a series of numerical algorithms were presented for determining the acoustic characteristics of multi-bend ducting systems. In the approach adopted, the multi-bend ducting system was considered to be a cascade of modal scatterers. A similar approach has been previously used with great success by researchers for analysing electromagnetic waveguiding systems which contain stepped (and tapered) filters and horns [42–44]. However, an adaptation of this approach to the analysis of curved ducting systems has not been previously accomplished. The significance of this achievement is better appreciated when one considers that problems such as the determination of Φ throughout the ducting system and the treatment of out-of-plane and serpentine bends have been successfully dealt with. The details of the above approach to the analysis of curved ducting systems have been presented in the recent publication [45].

3. In section 4.2, an original method was presented for determining the acoustic characteristics of non-uniformly curved bends in rectangular cross-sectioned ducts. The principal advantage of the method is that, by means of a generalised coordinate transformation, it can be used to analyse any continuously curved bend. The acoustic potential within the bend is obtained as a functional series via the Galerkin method. Hence, the method does not require that the bend be geometrically subdivided. In an example, the method was used to determine the modal scattering matrix for a spirally curved bend. Such bends have not been previously considered in the literature. The details of this method have been presented in the recent publication [46].

4. In sections 4.3 and 4.4, a powerful method for analysing non-uniformly curved duct bends was presented. The method requires that the bend be geometrically subdivided into a series of uniformly curved segments. This has the effect of reducing the difficult non-uniformly curved duct bend problem to a simpler, uniformly curved, multi-bend problem. The idea of geometrically subdividing non-uniformly

curved duct bends in this manner is not original. For example, Bahar [24] proposed a semi-analytic analysis in which the segments were assumed to be of differential angular extent. However, the idea has not been previously amalgamated with a theory of the type presented in Chapter 3, and it is suggested that the idea is best utilised when used in this context. The validity of the method was first checked by using it to analyse the same spirally curved duct bend considered in section 4.2, and comparing results. The method was then used to determine the acoustic characteristics of parabolic bends in elliptic and circular cross-sectioned ducts. It should be noted that there has not been any previous presentation of numerical results for this class of problem (i.e. a non-uniformly curved bend in a non-rectangular cross-sectioned duct). The results presented show that acoustic waves within non-uniformly curved duct bends have quasi-modal characteristics, with higher order mode coupling effects being mainly caused by duct bend curvature discontinuities. The research described above has been presented in the recent publications [45, 47].

5.3 SUGGESTIONS FOR FUTURE RESEARCH

In the following list, a number of suggestions for future research are made. Some of these suggestions deal with alternative applications of the methods presented in this thesis. Other suggestions outline alterations which could be made to these methods so that they may be used to solve a broader class of problems. In all cases, the basic principles behind the methods remain as they were presented in this thesis. Hence, the work presented in this thesis can be considered to form the basis of a quite general approach to duct acoustics problems.

1. It was mentioned in item 2 of the list in section 5.2 that the scattering cascade approach adopted in this thesis has been used in a similar context by researchers to study the propagation of electromagnetic waves through sections of tapered waveguide. Various duct termination problems have also been considered by these researchers [48, 49]. Hence, by combining the techniques used in those analyses with the methods presented in this thesis, one would be able to formulate a numerical procedure for determining the acoustic characteristics of ducting systems which are terminated in a variety of ways, and contain both curved and tapered sections.

2. As shown in section 4.2, the single duct bend problem can be more readily solved by conventional techniques if one uses an appropriate coordinate transformation to map the interior region of the bend onto that of a section of straight duct. However, although the transformation has the effect of simplifying the problem's boundary conditions, the form of equation (1.1) will be altered in the process. Physically, the modified form of equation (1.1) can be interpreted as describing the acoustic potential within a section of straight duct which is filled with an inhomogeneous fluid (as effectively done by Heiblum and Harris [50] when studying uniformly curved, optical waveguide bends). Hence, every homogeneously filled, curved duct problem can be considered to be equivalent to a corresponding inhomogeneously filled, straight duct problem. Now, in sections 4.3 and 4.4, a very good method for solving the homogeneously filled, curved duct problem was presented. As a result, a procedure which is opposite to that normally practised is proposed. That is, researchers studying the propagation of acoustic waves within certain inhomogeneously filled ducts should obtain their solutions from an equivalent, homogeneously filled, curved duct problem. An area of research where this type of approach may be beneficial is in the field of underwater acoustics.

3. In Chapter 2, a numerical solution procedure was presented for determining the acoustic modes within straight and uniformly curved ducts. The procedure utilised a variational formulation of the problem, and was based upon the Rayleigh-Ritz method. When using the procedure to determine the modes within elliptic cross-sectioned ducts, a coordinate transformation was used to map the duct cross-section onto a rectangular region. This gave one greater flexibility when choosing the set of basis functions to be used in the procedure. Such an approach is important as the choice of basis functions has a great effect upon the success of the Rayleigh-Ritz method. For ducts having a complicated cross-sectional geometry (for which a suitable coordinate transformation mapping does not exist), problems will be encountered as it is likely that one will not be able to choose a good set of basis functions. For such cases, it is suggested that the numerical solution procedure be modified to incorporate the principles of the Finite Element method [32, 51]. This modification should not be too difficult as the Finite Element method is a natural extension of the Rayleigh-Ritz method.

4. Another point worth discussing is the possibility of modifying the numerical solution procedure presented in Chapter 2, so that duct bends whose walls are locally reacting can be analysed. Theoretically, it is not difficult to make the required modifications. Assuming that the duct walls have a specific acoustic admittance ζ, the required modes will determine the stationary values of the functional

$$J^{(c)}(\psi) = I^{(c)}(\psi) - ik \int_{\Gamma} r\zeta\psi^2 \, d\Gamma, \tag{5.1}$$

where $I^{(c)}(\psi)$ is as defined in equation(2.24). Applying the Rayleigh-Ritz method will yield an algebraic eigenvalue equation, the eigenvalues and eigenvectors now being complex in general. The extension seems to be fairly routine, however there is a drawback, namely a greater difficulty in the choice of suitable basis functions. One possibility is to map the cross-section of the duct onto a rectangular region, and then choose basis functions so that the approximate eigenfunctions

take the form of complex Fourier series. An alternative means of determining the modes within an acoustically lined bend is via the Boundary Element method [52]. This method is worth investigating as it has the advantages that it reduces the dimensionality of the problem, and can be readily adapted to complicated duct wall geometries.

5. A problem which poses a significant challenge to the ingenuity of future researchers is the development of numerical methods for determining the acoustic characteristics of curved ducting systems which contain a mean fluid flow. The principal difficulties associated with this problem are related to the determination and description of a suitable fluid flow field. Perhaps a simple, one-dimensional flow field could be assumed within each duct segment? The effects of the fluid flow could then be incorporated into the existing formulation by modifying each mode's associated propagation constant (and therefore the segment's modal scattering matrix). Some previous research which is relevant to this problem appears in the references [53–59].

APPENDIX A

The following is a derivation of the gradient and Laplacian operators for the natural coordinates presented in subsection 4.2.1.

Let $M(\theta) = (R^2 + R'^2)^{-\frac{1}{2}}$. Then consider the equations

$$x = R\cos(\theta) + \xi M\left[R\cos(\theta) + R'\sin(\theta)\right] \tag{A.1}$$

and

$$y = R\sin(\theta) + \xi M\left[R\sin(\theta) - R'\cos(\theta)\right], \tag{A.2}$$

which define the coordinate transformation $(x, y) \rightarrow (\xi, \theta)$. Differentiating equations (A.1) and (A.2) and grouping terms with a common factor of $\cos(\theta)$ or $\sin(\theta)$ yields

$$\begin{aligned} \frac{\partial x}{\partial \xi} &= A\cos(\theta) + B\sin(\theta), & \frac{\partial x}{\partial \theta} &= C\cos(\theta) - D\sin(\theta), \\ \frac{\partial y}{\partial \xi} &= -B\cos(\theta) + A\sin(\theta), & \frac{\partial y}{\partial \theta} &= D\cos(\theta) + C\sin(\theta), \end{aligned} \tag{A.3}$$

where

$$\begin{aligned} A &= MR, \quad B = MR', \\ C &= \xi M'R + (1 + 2\xi M)R', \\ D &= (1 + \xi M)R - \xi M'R' - \xi MR''. \end{aligned} \tag{A.4}$$

Now, the elements of the metric tensor g_{ij} $\{i, j = 1, 2\}$ can be calculated as follows (see [60], Chapter 6). Firstly

$$\begin{aligned} g_{11} &= \left(\frac{\partial x}{\partial \xi}\right)^2 + \left(\frac{\partial y}{\partial \xi}\right)^2 \\ &= A^2 + B^2 \\ &= 1. \end{aligned} \tag{A.5}$$

Also

$$\begin{aligned} g_{12} = g_{21} &= \left(\frac{\partial x}{\partial \xi}\right)\left(\frac{\partial x}{\partial \theta}\right) + \left(\frac{\partial y}{\partial \xi}\right)\left(\frac{\partial y}{\partial \theta}\right) \\ &= AC - BD \\ &= \xi M\left[MR'(R+R'') + M'(R^2+R'^2)\right] \\ &= 0. \end{aligned} \tag{A.6}$$

Finally

$$\begin{aligned} g_{22} &= \left(\frac{\partial x}{\partial \theta}\right)^2 + \left(\frac{\partial y}{\partial \theta}\right)^2 \\ &= C^2 + D^2. \end{aligned} \tag{A.7}$$

But as $A^2 + B^2 = 1$ and $AC - BD = 0$, so

$$\begin{aligned} g_{22} &= \left\{\frac{C}{B}\right\}^2 \\ &= \left\{\xi\left[2 - \frac{R(R+R'')}{R^2+R'^2}\right] + \sqrt{R^2+R'^2}\right\}^2 \\ &= g^2 \quad \text{say.} \end{aligned} \tag{A.8}$$

The fact that $g_{12} = g_{21} = 0$ indicates that the coordinates (ξ, θ) are orthogonal. This simplifies general expressions for the gradient and Laplacian of a function Φ of these coordinates to

$$\nabla\Phi = \frac{1}{\sqrt{g_{11}}}\frac{\partial \Phi}{\partial \xi}\underline{e}_\xi + \frac{1}{\sqrt{g_{22}}}\frac{\partial \Phi}{\partial \theta}\underline{e}_\theta \tag{A.9}$$

and

$$\nabla^2\Phi = \frac{1}{\sqrt{g_{11}g_{22}}}\left[\frac{\partial}{\partial \xi}\left(\sqrt{\frac{g_{22}}{g_{11}}}\frac{\partial \Phi}{\partial \xi}\right) + \frac{\partial}{\partial \theta}\left(\sqrt{\frac{g_{11}}{g_{22}}}\frac{\partial \Phi}{\partial \theta}\right)\right]. \tag{A.10}$$

Therefore, as $g_{11} = 1$ and $g_{22} = g^2(\xi, \theta)$, equations (4.10) and (4.11) are obtained.

APPENDIX B

In this appendix, the numerical methods presented in the thesis are used to determine the modal transmission characteristics of the "S-bend" in a proposed ventilation duct attenuation unit. A view showing details of the attenuation unit is given in Figure B.1, where the duct is assumed to have a rectangular cross-section, and when unlined, to be perfectly rigid. Figure B.1 shows that the attenuation unit is comprised of three basic

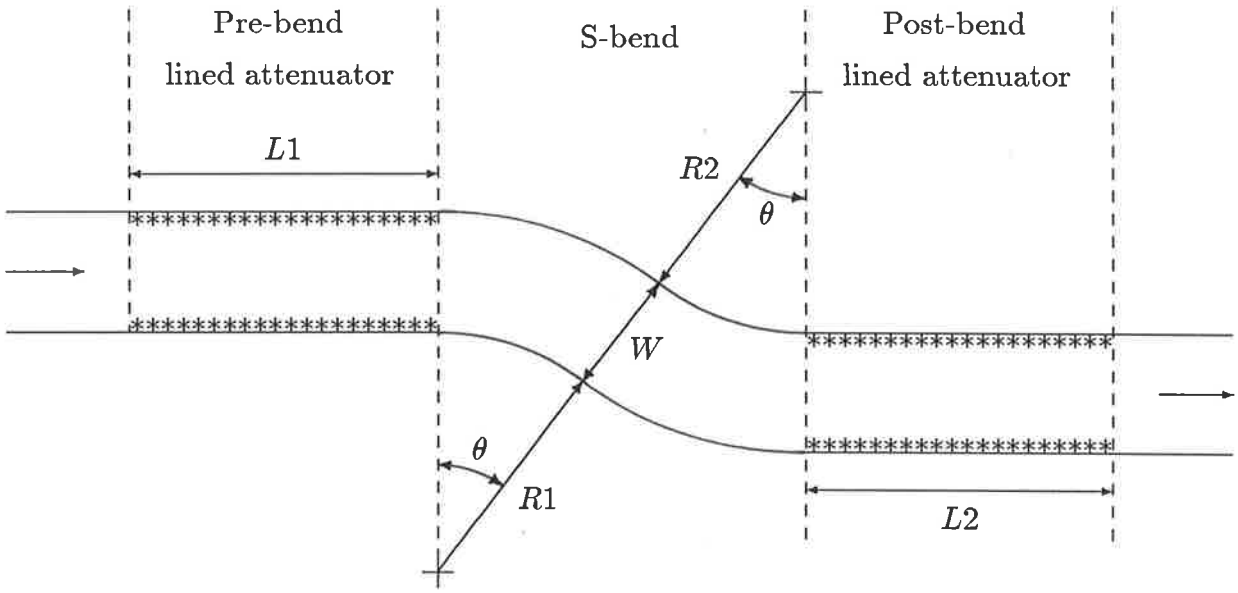

Figure B.1: *Details of the attenuation unit.*

components: a pre-bend lined attenuator, an S-bend, and a post-bend lined attenuator. A short description of how these components combine to attenuate incident duct noise can be given as follows. Firstly, the pre-bend lined attenuator ensures that only plane waves will be incident upon the S-bend. For frequencies such that $kW > \pi$ (where k is the wavenumber and W the duct width), the S-bend then acts as a mode converter and transfers a significant proportion of the energy in the plane waves to higher order

"cross-modes". Finally, these cross-modes are rapidly attenuated by the post-bend lined attenuator. Hence, the effectiveness of the attenuation unit is based upon the fact that cross-modes are more rapidly attenuated by duct liners than plane waves. The net result is a more efficient utilisation of the duct liner.

From the description given, one can see that the attenuation unit is designed to work most efficiently in the wavenumber range $kW > \pi$. In terms of the acoustic frequency f, this range is equivalently specified by the inequality $f > v/(2W)$. Hence, if $W = 250mm$ and $v = 340ms^{-1}$, one obtains the frequency range for efficient attenuation: $f > 680Hz$. When considering wider ducts, the units can be mounted in parallel, as shown in Figure B.2. Note that in Figure B.2, the units are mounted in a manner which does not reduce the cross-sectional area of the duct.

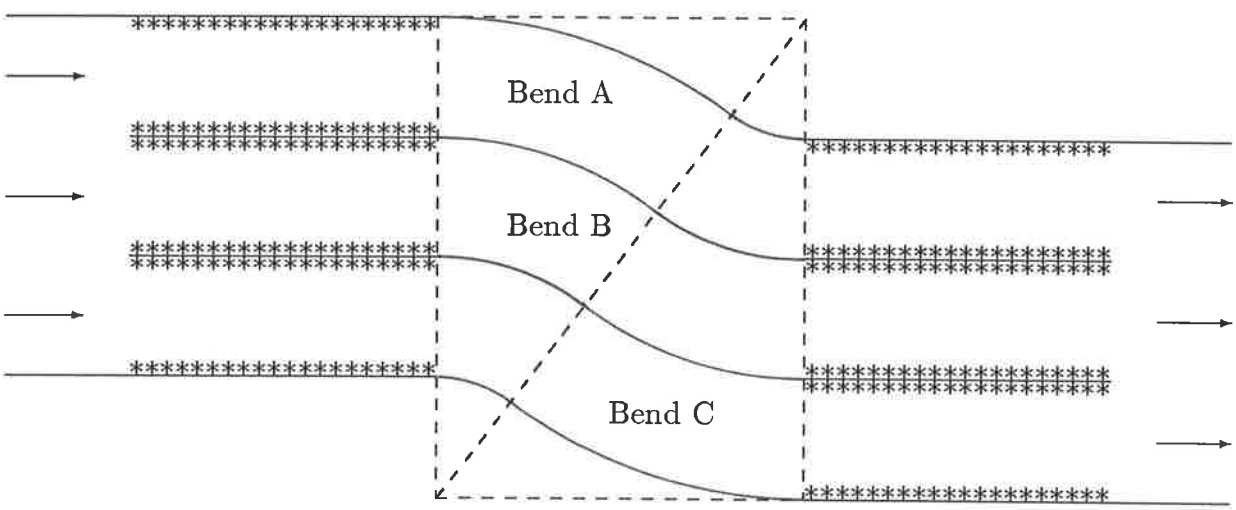

Figure B.2: *An attenuation unit for wider ducts.*

The fact that S-bends actually do act as mode converters is now illustrated by means of the following numerical calculations. In these calculations, plane waves are assumed to be incident upon bends A, B and C in Figure B.2. Comparing Figures B.1 and B.2,

one can see that if all lengths are expressed as multiples of the duct width W, then for bend A: $R1 = 3$ and $R2 = 1$; for bend B: $R1 = R2 = 2$; and for bend C: $R1 = 1$ and $R2 = 3$; where $\theta = \arctan(3/4)$ for all bends. Following an analysis similar to that presented in sections 4.3 and 4.4, the modal scattering matrix of each circularly curved section in the S-bends is calculated using a 25-term approximation in the method presented by Tam [16]. An $\mathbf{S}^{(apr)}(\pi)$ matrix is then located in positions two and four of the four segment cascade used to model each S-bend. The elements of the matrix $\mathbf{H}$ used to evaluate the $\mathbf{S}^{(apr)}(\pi)$ matrix are

$$H_{mn} = c_m c_n \int_{r'=R2}^{R2+W} \cos\left[\tfrac{(m-1)\pi(r'-R2)}{W}\right] \cos\left[\tfrac{(n-1)\pi(r'-R2-W)}{W}\right] \, dr', \tag{B.1}$$

where the normalisation constants are

$$c_m = \begin{cases} \frac{1}{\sqrt{W}} & m = 1 \\ \sqrt{\frac{2}{W}} & m = 2, 3, \ldots \end{cases} \tag{B.2}$$

Hence,

$$H_{mn} = \begin{cases} (-1)^{n+1} & m = n \\ 0 & m \neq n. \end{cases} \tag{B.3}$$

Finally, $M = 12$ modes are considered when using the iterative scattering matrix algorithm to determine the modal scattering matrix $\mathbf{S}^{(cas)}$, of each S-bend. The elements in the first column of $\mathbf{S}_{11}^{(cas)}$ give the relative complex amplitudes of the required transmitted modes.

Using a presentation which is similar to that of Shepherd and Cabelli [38], Figures B.3–B.5 show plots of $|\mathbf{S}_{11}^{(cas)}(m,1)|$ $\{m = 1,2,3\}$ vs. kW for bends A–C respectively. In these plots, $|\mathbf{S}_{11}^{(cas)}(m,1)|$ is referred to as the Amplitude Transmission Coefficient (A.T.C.) of the m^{th} mode. Also, the vertical dashed lines are at $kW = \pi, 2\pi, 3\pi$; where $kW = \pi$ specifies the cut-on frequency for the first cross-mode ($m = 2$), $kW = 2\pi$ specifies the cut-on frequency for the second cross-mode ($m = 3$), and so on. One can see from the plots that in all three bends, the A.T.C.'s of the cross-modes dominate in the wavenumber range $kW > \pi$.

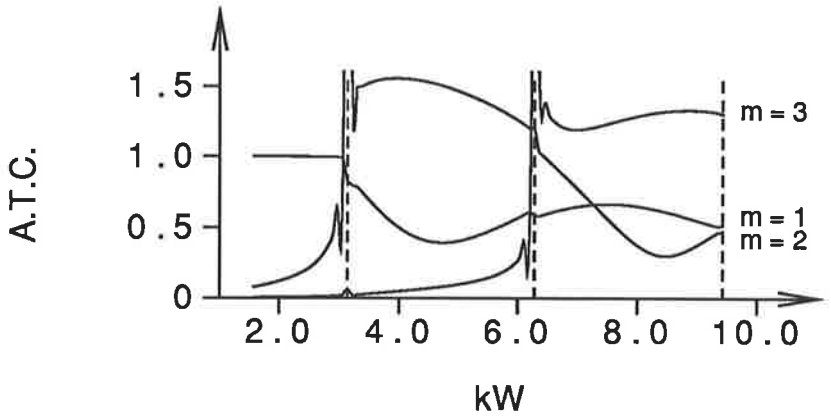

Figure B.3: *Plots of the A.T.C. for m = 1,2,3 modes; bend A.*

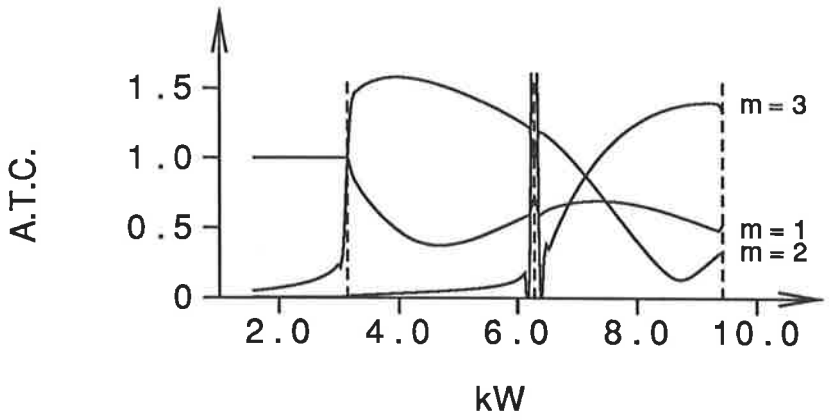

Figure B.4: *Plots of the A.T.C. for m = 1,2,3 modes; bend B.*

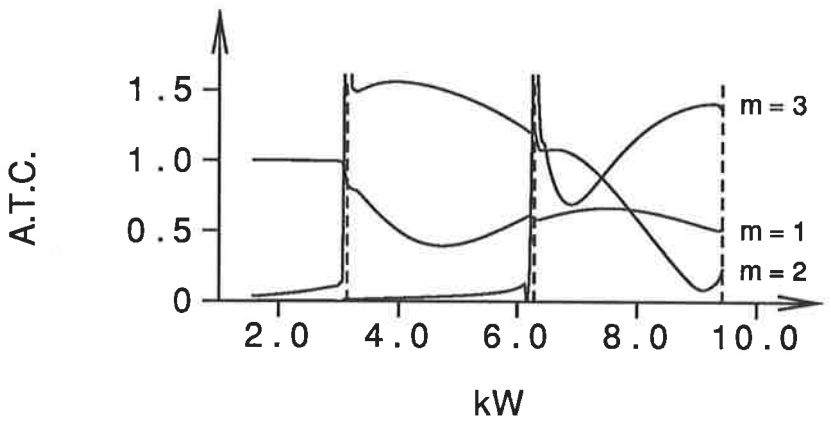

Figure B.5: *Plots of the A.T.C. for m = 1,2,3 modes; bend C.*

A further illustration of the mode converting characteristics of bends A–C is obtained by examining the Energy Transmission Coefficient (E.T.C.) of each transmitted mode. Following Shepherd and Cabelli ([38], sect. 3.2), the E.T.C. of the m^{th} transmitted mode is defined to be

$$\begin{cases} |p_1|^2 & m = 1 \\ \frac{1}{2}\left(\frac{\mu_{m1}}{k}\right)|p_m|^2 & m = 2, 3, \ldots \end{cases} \tag{B.4}$$

where μ_{m1} is as defined in equation (2.28), and p_m is the complex amplitude of the corresponding *pressure* mode. It follows from equations (1.5) and (2.21) that the E.T.C. of a mode specifies the relative proportion of the total mean transmitted power associated with that mode. Figures B.6–B.8 show E.T.C. vs. kW plots of transmitted modes for bends A–C. In these plots, it is assumed that

$$p_m = \mathbf{S}_{11}^{(cas)}(m, 1). \tag{B.5}$$

That is, $\mathbf{S}^{(cas)}$ is interpreted as specifying the scattering of pressure modes from the S-bend. This interpretation is valid as the acoustic pressure satisfies equations (1.1) and (1.2). Hence, the data presented in Figures B.6–B.8 can be directly compared with the results produced by experimental procedures such as the one presented in reference [38], where measurements of the pressure modes are made. An examination of the plots in Figures B.6–B.8 shows that in the wavenumber range $kW > \pi$, most of the transmitted power is carried by the cross-modes.

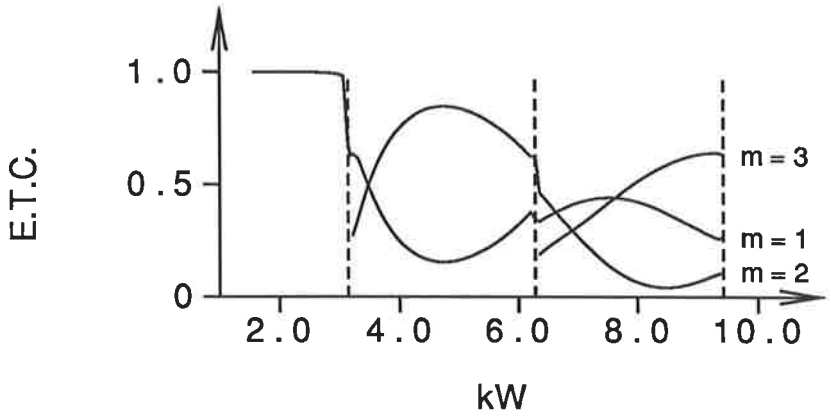

Figure B.6: *Plots of the E.T.C. for m = 1,2,3 modes; bend A.*

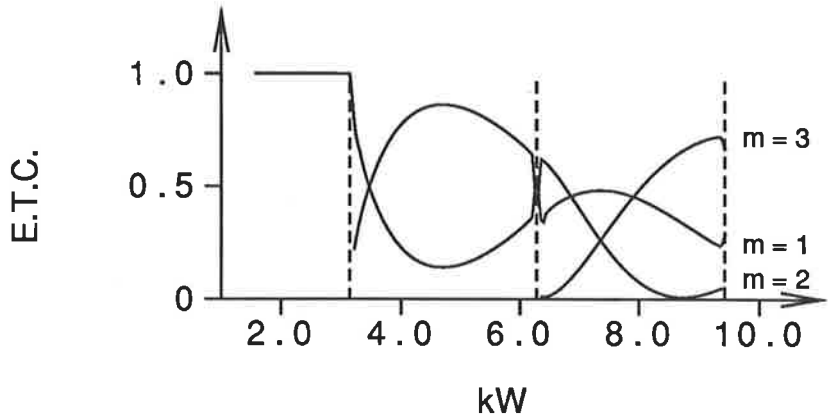

Figure B.7: *Plots of the E.T.C. for m = 1,2,3 modes; bend B.*

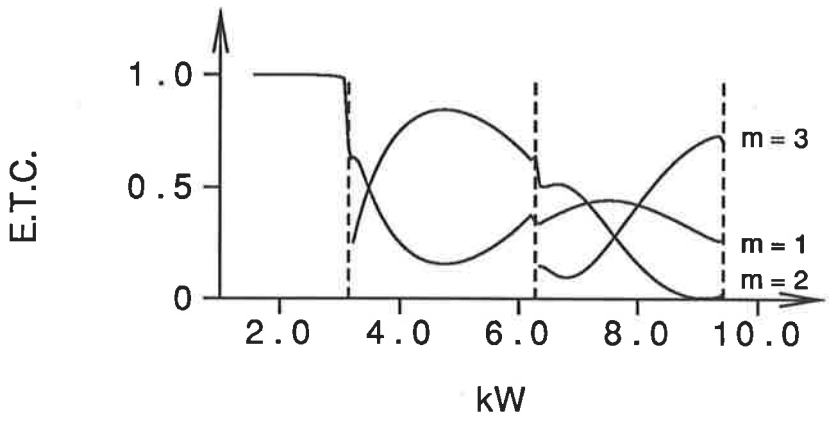

Figure B.8: *Plots of the E.T.C. for m = 1,2,3 modes; bend C.*

BIBLIOGRAPHY

1. Lord Rayleigh (J.W. Strutt) 1878 *Theory of Sound.* London: Macmillan.

2. H. Buchholz 1939 *Elektrisch. Nachrichten-Technik* **16**, 73–85. Der Einfluss der Krümmung von rechteckigen Hohleitern auf das Phasenmass ultrakurzer Wellen [Effect of the curvature of rectangular hollow waveguides on the phase of ultrashort waves].

3. F.E. Grigor'yan 1969 *Soviet Physics-Acoustics* **14**, 315–321. Theory of sound wave propagation in curvilinear waveguides.

4. W.C. Osborne 1974 *Journal of Sound and Vibration* **37**, 65–77. Calculation of the angular propagation constant for a bend.

5. W. Rostafinski 1976 *Journal of the Acoustical Society of America* **60**, 23–28. Acoustic systems containing curved duct sections.

6. S.H. Ko 1979 *Journal of Sound and Vibration* **66**, 165–179. Three-dimensional acoustic waves propagating in acoustically lined cylindrically curved ducts without fluid flow.

7. C.P. Bates 1969 *Bell System Technical Journal* **48**, 2259–2280. Intermodal coupling at the junction between straight and curved waveguides.

8. S.O. Rice 1948 *Bell System Technical Journal* **27**, 305–349. Reflections from circular bends in rectangular waveguides — matrix theory.

9. L. Lewin, D.C. Chang and E.F. Kuester 1977 *IEE Electromagnetic Waves Series 2 — Electromagnetic Waves and Curved Structures.* Stevenage, Herts: P. Peregrinus.

10. J.A. Cochran and R.G. Pecina 1966 *Radio Science* **1**, 679–696. Mode propagation in continuously curved waveguides.

11. W. Rostafinski 1982 *Journal of the Acoustical Society of America* **71**, 36–41. Propagation of long waves in acoustically treated, curved ducts.

12. W. Rostafinski 1974 *Journal of the Acoustical Society of America* **56**, 11–15. Analysis of propagation of waves of acoustic frequencies in curved ducts.

13. A. Cummings 1974 *Journal of Sound and Vibration* **35**, 451–477. Sound transmission in curved duct bends.

14. W.C. Osborne 1976 *Journal of Sound and Vibration* **45**, 39–52. Higher mode propagation in short curved bends of rectangular cross-section.

15. C.R. Fuller and D.A. Bies 1978 *Journal of the Acoustical Society of America* **63**, 681–686. Propagation of sound in a curved bend containing a curved axial partition.

16. C.K.W. Tam 1976 *Journal of Sound and Vibration* **45**, 91–104. A study of sound transmission in curved duct bends by the Galerkin method.
Note: For important additional information which is relevant to this paper see — G.D. Furnell 1989 *Journal of Sound and Vibration* (provisionally scheduled

for vol. 129, no. 1 as a letter to the editor). Corrections to "A study of sound transmission in curved duct bends by the Galerkin method".

17. A. Cabelli 1980 *Journal of Sound and Vibration* **68**, 369–388. The acoustic characteristics of duct bends.

18. A. Cabelli and I.C. Shepherd 1981 *Journal of Sound and Vibration* **78**, 119–129. The influence of geometry on the acoustic characteristics of duct bends for higher order modes.

19. V.Yu. Prikhod'ko and V.V. Tvutekin 1982 *Soviet Physics-Acoustics* **28**, 422. Natural modes of curved waveguides.

20. D.H. Keefe and A.H. Benade 1983 *Journal of the Acoustical Society of America* **74**, 320–332. Wave propagation in strongly curved ducts.

21. M. El-Raheb and P. Wagner 1982 *Journal of the Acoustical Society of America* **71**, 1335–1346. Acoustic propagation in a rigid torus.

22. D. Firth and F.J. Fahy 1984 *Journal of Sound and Vibration* **97**, 287–303. Acoustic characteristics of circular bends in pipes.

23. J.P. Quine 1965 *IEEE Transactions on Microwave Theory and Techniques* **13**, 54–63. E and H-plane bends for high-power oversized rectangular waveguide.

24. E. Bahar 1969 *IEEE Transactions on Microwave Theory and Techniques* **17**, 210–217. Fields in waveguide bends expressed in terms of coupled local annular waveguide modes.

25. E. Bahar and G. Govindarajan 1973 *IEEE Transactions on Microwave Theory and Techniques* **21**, 819–824. Rectangular and annular modal analyses of multimode waveguide bends.

26. D.S. Ahluwalia, J.B. Keller and B.J. Matkowsky 1974 *Journal of the Acoustical Society of America* **55**, 7–12. Asymptotic theory of propagation in curved and nonuniform waveguides.

27. L. Ting and M.J. Miksis 1983 *Journal of the Acoustical Society of America* **74**, 631–639. Wave propagation through a slender curved tube.

28. M. El-Raheb 1980 *Journal of the Acoustical Society of America* **67**, 1924–1930. Acoustic propagation in rigid three-dimensional waveguides.

29. M. El-Raheb 1981 *Journal of Sound and Vibration* **78**, 39–67. Vibrations of three-dimensional pipe systems with acoustic coupling.

30. M. El-Raheb and P. Wagner 1983 *Journal of Sound and Vibration* **88**, 151–162. Acoustic loading in planar networks.

31. L.V. Kantorovich and V.I. Krylov 1958 *Approximate Methods of Higher Analysis.* Groningen: Noordhoff.

32. K.J. Bathe 1982 *Finite Element Procedures in Engineering Analysis.* Englewood Cliffs, New Jersey: Prentice-Hall.

33. M.V. Lowson and S. Baskaran 1975 *Journal of Sound and Vibration* **38**, 185–194. Propagation of sound in elliptic ducts.

34. R.E. Collin 1966 *Foundations for Microwave Engineering.* New York: McGraw-Hill.

35. W. Möhring 1978 *Journal of the Acoustical Society of America* **64**, 1186–1189. Acoustic energy flux in nonhomogeneous ducts.

36. W. Eversman 1976 *Journal of Sound and Vibration* **47**, 515–521. A reciprocity relationship for transmission in non-uniform hard walled ducts without flow.

37. Y. Cho 1980 *Journal of the Acoustical Society of America* **67**, 1421–1426. Reciprocity principle in duct acoustics.

38. I.C. Shepherd and A. Cabelli 1981 *Journal of Sound and Vibration* **77**, 495–511. Transmission and reflection of higher order acoustic modes in a mitred duct bend.

39. R.J. Astley and W. Eversman 1978 *Journal of Sound and Vibration* **57**, 367–388. A finite element method for transmission in non-uniform ducts without flow: comparison with the method of weighted residuals.

40. P.M. Prenter 1975 *Splines and variational methods.* New York: Wiley.

41. G.D. Furnell and D.A. Bies 1989 *Journal of Sound and Vibration* (provisionally scheduled for vol. 129, no. 2). Characteristics of modal wave propagation within longitudinally curved acoustic waveguides.

42. F. Arndt, A. Frye, M. Wellnitz and R. Wirsing 1985 *I.E.E.E. Transactions on Microwave Theory and Techniques* **33**, 373–381. Double dielectric-slab-filled waveguide phase shifter.

43. A.S. Omar and K. Schünemann 1985 *I.E.E.E. Transactions on Microwave Theory and Techniques* **33**, 765–770. Transmission matrix representation of finline discontinuities.

44. J.A. Encinar and J.M. Rebollar 1986 *I.E.E.E. Transactions on Antennas and Propagation* **34**, 961–968. A hybrid technique for analysing corrugated and non-corrugated rectangular horns.

45. G.D. Furnell and D.A. Bies 1989 *Journal of Sound and Vibration* (provisionally scheduled for vol. 131, no. 2). Matrix analysis of acoustic wave propagation within curved ducting systems.

46. G.D. Furnell 1989 *Wave Motion* (accepted but yet to be scheduled) Transmission and reflection characteristics of a curved waveguide junction.

47. G.D. Furnell 1988 in *Computational Techniques and Applications: CTAC-87.* J. Noye and C. Fletcher, Editors. 227–238. Wave propagation in longitudinally curved waveguides. North-Holland, Amsterdam: Elsevier Science.

48. J.M. Rebollar 1986 *I.E.E.E. Transactions on Microwave Theory and Techniques* **34**, 175–178. Response of waveguides terminated in a tapered metallic wall.

49. J.A. Encinar and J.M. Rebollar 1986 *I.E.E.E. Transactions on Microwave Theory and Techniques* **34**, 809–814. Convergence of numerical solutions of open-ended waveguide by modal analysis and hybrid modal-spectral techniques.

50. M. Heiblum and J.H. Harris 1975 *I.E.E.E. Journal of Quantum Electronics* **11**, 75–83. Analysis of curved optical waveguides by conformal transformation.

51. O.C. Zienkiewicz 1977 *The Finite Element Method.* London: McGraw-Hill.

52. C.A. Brebbia, J.C.F. Telles and L.C. Wrobel 1984 *Boundary Element Techniques — Theory and Applications in Engineering.* Berlin: Springer-Verlag.

53. C.R. Fuller and D.A. Bies 1979 *Journal of Sound and Vibration* **62**, 73–92. The effects of flow on the performance of a reactive acoustic attenuator.

54. W. Eversman and R.J. Astley 1981 *Journal of Sound and Vibration* **74**, 89–101. Acoustic transmission in non-uniform ducts with mean flow, Part I: The method of weighted residuals.

55. R.J. Astley and W. Eversman 1981 *Journal of Sound and Vibration* **74**, 103–121. Acoustic transmission in non-uniform ducts with mean flow, Part II: The finite element method.

56. K.J. Baumeister 1981 *Transactions of the A.S.M.E.* **103**, 270–281. Numerical techniques in linear duct acoustics — a status report.

57. A. Cabelli 1982 *Journal of Sound and Vibration* **82**, 131–149. The influence of flow on the acoustic characteristics of a duct bend for higher order modes — a numerical study.

58. K.E. Heinig 1983 *A.I.A.A. Journal* **21**, 98–105. Sound propagation in multistage axial flow turbomachines.

59. K. Uenishi and M.K. Myers 1984 *A.I.A.A. Journal* **22**, 1242–1248.
Two-dimensional acoustic field in a nonuniform duct carrying compressible flow.

60. G.A. Korn and T.M. Korn 1968 *Mathematical Handbook for Scientists and Engineers.* New York: McGraw-Hill.